In situ preparation and properties of rubber/inorganic oxide nanocomposites

by

THABANG HENDRICA MOKHOTHU (M.Sc.)

Submitted in accordance with the requirements for the degree of

Philosophiae Doctor (Ph.D.) in Polymer Science

Department of Chemistry

Faculty of Natural and Agricultural Sciences

at the

UNIVERSITY OF THE FREE STATE (QWAQWA CAMPUS)

SUPERVISOR: PROF A.S. LUYT

CO-SUPERVISOR: PROF M. MESSORI

January 2014

DECLARATION

I declare that the dissertation hereby submitted by me for the degree Philosophiae Doctor at the University of the Free State is my own independent work and has not previously been submitted by me at another university/faculty. I furthermore cede copyright of the dissertation in favour of the University of the Free State.

_____

T.H. Mokhothu

DEDICATIONS

This work is dedicated to the entire Mokhothu family for their love and support. To Matlholi Jerminah (mom), Constance Motlalepule (grandmother), Tshepiso (sister), and a special gratitude to Bokamoso Elizabeth and her mom Nthabiseng Mirriam.

To Tebogo Weer and Mpho Mongale: "*Perseverance is the mother of success"*

To the following families; Sepeng, Manana, Molele and Moremi.

To the members of the Shield of Love Ministries: for their day to day prayers, love and support. May the Almighty God continually pour out his blessing to all you. To all the young people in the church "*The beginning of wisdom is the fear of the Lord"*.

"TO GOD BE ALL THE GLORY"

ACKNOWLEDGEMENTS

- Above all, special thanks are extended to the **Lord Jesus Christ** my Saviour for providing me with the strength and heart to stand throughout this project. For the knowledge, wisdom and understanding that He grants to us when we ask in His name. "*I can do all things through Christ who strengthens me*" Philippians 4:13

- My gratitude and appreciation to my supervisor **Prof A.S. Luyt**, for his consistent supervision, guidance, encouragement and patience during all the stages of this project. His overly enthusiasm and integral view on research and his mission for providing 'only high-quality work and not less', has made a deep impression on me.

- I am also grateful to my co-supervisor **Prof M. Messori**, at University of Modena and Reggio Emilia, Italy, for following up the progress of the project and providing technical guidance and valuable contributions throughout the research programme.

- To new friendships I've made, Davide Morselli and Katia Paderni, at the University of Modena and Reggio Emilia, Italy. Thank you for the collaboration and exchanging ideas and knowledge, may God continually bless you.

- I acknowledge the financial support from the NRF and the University of the Free State.

- Special thanks to Jeremia Shale Sefadi, who has been more a brother than a friend. For his support, advice, encouragement and most for being there in times of troubles through the course of this project.

- I am grateful to the faculty, staff and colleagues in the Department of Chemistry for their assistance in every aspect of my project. To the entire polymer research team (Post Doctorate, Ph.D., M.Sc. and Honours). Special thanks to Dr Dusko Dudic, Jonas Mochane, Teboho Mokhena, Teboho Motsoeneng, Motshabi Sibeko, Puseletso Mofokeng, Tladi Mofokeng, Cherylann Clarke, Thandi Gumede, Patricia Molaba, Lerato Mollo, Tyson Mosoabisane, Thollwana Makhetha, James Moreane, Chale Maboya, for their support throughout this project.

- To all the Chemistry lectures, Mrs M. Madimabe, Mrs N.F. Molefe, Mr. R. Moji and Mr. T. Tsotetsi. Thank you for the support and encouragements.

- To Mrs M Jackson, the Faculty secretary. Thank you for all the appointments you set for me and the assistance you gave throughout the duration of my studies.

- To Mfiso Mngomezulu and Dr. Tshwafo Motaung. Thanks guys for your support and encouragement.

- To my Family: Matlholi Jerminah Mokhothu (mother), Tshepiso Mokhothu (sister), Motlalepule Mokhothu (grandmother), Stephen Moremi (Uncle), Masene Mokhothu (Rakgadi), and Abuti Thabo Moloi,for their support, wisdom and encouragement to further my studies. To Tladi Mokhothu, Dr. Joyce Moloi, Bernard Motshoko, Peter Motshoko and Nkgono Masima (mama) for their day to day support. To Tebogo Weer, and Mpho Mongale, Tebogo Sepeng, Tsholofelo Mongale, Paballo Moremi, the pathway to achieve beyond is already open when you are dedicated and have faith in God. Special gratitude to Nthabiseng Molaba (wife) and Bokamoso Elizabeth (Daughter), for being always excused among them for my Ph.D. degree studies, their patience, support and love.

- To the Shield of Love ministry, for their everyday prayers, love and support. May the Almighty God continually pour out His blessings to you all and your families.

- I am also grateful to my many friends for their support, motivation towards my studies: Setumo Motloung, Thami Koao, Maqaleng Mbule, Khamohelo Tshabalala, Teboho Mofokeng, Ditaba Radebe, Khulekani Vilakazi, Papi Tshabalala, Bethuel Mokhele, Paleho Lepota, Edward Sikhosana, Thabiso Skosana, Sello Mokgoko, Sthembiso Khumalo, Karedi Motsau, Sidney Khuduga, Malefetsane Mokwatle, Junior Besane, Tiisetso Nonyana, Pheello Mokoena, and Lerato Mofokeng, . “Ayobaness Gents”. To Keke Makhado, Palesa Karedi, and Jeanette Morake “Ayoba ladies”.

- Selina Makhele, and Dr Philemon Matabola, for their support, guidance and encouragement through tough times during this project.

ABSTRACT

Silica and titania particles were prepared *in situ* in an ethylene propylene diene monomer (EPDM) rubber by means of hydrolytic and non-hydrolytic sol-gel routes. For the hydrolytic sol-gel (HSG) process tetraethoxysilane (TEOS) was used as precursor in toluene in the absence and presence of bis-[-3-(triethoxysilyl)-propyl]-tetrasulfide (TESPT) as coupling agent. In the non-hydrolytic sol-gel (NHSG) synthesis the EPDM-silica composites were prepared with silicone tetrachloride ($SiCl_4$) as precursor and *tert*-butanol as an oxygen donor. The morphology, as well as mechanical properties and thermal stability, of these nanocomposites were determined and the influence of the filler content, preparation route and the presence of a coupling agent on the morphology and properties of EPDM/silica nanocomposites were investigated.

For silica filled composites prepared at long and short reaction times by the HSG route, the silica particles were homogeneously dispersed in the EPDM matrix with the presence of agglomeration at higher filler contents. The transparency progressively decreased by increasing the filler content, and the swelling ratio of the EPDM-silica filled composites increased with increasing filler content while the gel content decreased. This indicated a hindering effect on the presence of *in situ* generated silica on the vulcanization process which reduced the crosslinking degree of the rubber matrix. With longer reaction times a more extensive crosslinked network was formed when grafted and/or unreacted fractions of TEOS reacted further to form more crosslinks between the rubber chains. This observation correlated well with the high modulus values obtained for the composites prepared at long reaction times.

EPDM filled with silica particles in the presence of a coupling agent showed significantly improved properties. The composites showed both large and small particles at higher silica contents in the composites, and some particles were fully imbedded in the EPDM matrix, which indicated good particle-matrix interactions. The presence of the silica particles reduced the crosslink density of the rubber matrix, but the networks were still extensive enough to maintain a high gel content. The composites showed good thermal stability as a result of better interactions between the silica particles and EPDM. There was a good correlation between the storage modulus and Young's modulus values, and their values increased significantly with increasing filler content. A Nielsen's model fit to the Young's modulus values indicated improved dispersion and reduced size of the silica aggregates in the EPDM

matrix. The increased stiffness and thermal stability were confirmed by the filler effectiveness factor values, and the damping reduction values confirmed the reduction in the polymer chain mobility.

The NHSG route was also investigated as a new preparation route to reinforce the EPDM rubber with an inorganic metal oxide. Silica and titania filled composites showed similar decreases in the swelling ratio and gel content, which indicates the hindering effect of the metal oxide on the vulcanization of the rubber matrix. The thermal stabilities of both the silica and titania filled EPDM composites were reduced by the presence of metal oxides prepared according to this route. The EPDM-silica composites prepared in the absence and presence of a coupling agent showed a mass loss in the range 100-400 °C caused by the evaporation of t-butyl chloride and other acid chlorides present in the composites, as well as the evaporation of TESPT that settled on the interface between the silica particles and EPDM for composites prepared in the presence of TESPT. In the case of EPDM-titania composites, a strong decrease in thermal stability of the composites compared with the pristine EPDM was observed due to a metal oxide-catalyzed oxidative decomposition mechanism. The mechanical properties improved significantly due to better filler-matrix interactions. In the case of the silica nanocomposites the filler particles were smaller and better dispersed.

It is clear from this research that the type and amount of filler, the method used for the *in situ* sol-gel preparation of the composites, the type of precursor used, and whether a coupling agent was used, to a large extent determines the thermal and mechanical properties of the EPDM nanocomposites. The way these variables are combined will also significantly influence these properties.

TABLE OF CONTENTS

LIST OF TABLES

LIST OF FIGURES

Page

LIST OF SYMBOLS AND ABBREVIATIONS

A	related to the Einstein coefficient
APTS	3-aminipropyltriethoxysilane
BTOS	*iso*-butyltriethoxysilane
C_{EPDM}	weight fraction of EPDM present in the composites
DCP	dicumyl peroxide
DMA	dynamic mechanical analysis
DR	damping reduction
DSC	differential scanning calorimetry
E''	loss modulus
E	modulus of composites
E'	storage modulus
$E'_{T=50°C}$, $E'_{T= -80°C}$, $E'_{T=20°C}$	storage modulus at 50 °C, -80 °C and 20 °C
E_1	modulus of the matrix
E_2	modulus of the filler
E'_g	storage modulus at glassy region
EPDM	ethylene propylene diene monomer
E'_r	storage modulus at rubbery region
EtOH	ethanol
ETOS	ethyltriethoxysilane
f	absolute extractable fraction
Factor C	filler effectiveness
FTIR	Fourier-transform infrared
HSG	hydrolytic sol-gel
m_0	mass of sample before immersion
m_d	dried mass
m_{EPDM}	mass of EPDM without silica
m_s	swollen mass
$M_{T300\ °C}$	mass loss at 300 °C
NHSG	non-hydrolytic sol-gel
q	absolute swelling ratio
q_{EPDM} and f_{EPDM}	normalized to the actual EPDM weight

RE	reinforcing efficiency
SEM	scanning electron microscopy
$T_{50\%}$,$T_{60\%}$, $T_{30\%}$	temperature at 50%, 60%, and 30% weight loss
tanδ	damping coefficient
t-BuOH	*tert*-Butanol
TEM	transmission electron microscopy
TEOS	tetraethyl orthosilicate
TESPD	bis-(3-(triethoxysilyl-propyl)-disulfide
TESPT	bis-[-3-(triethoxysilyl)-propyl]-tetrasulfide
T_g	glass transition temperature
TGA	thermogravimetric analysis
TMTSPM	(3-mercaptopropyl)-trimethoxysilane
Tonset	temperature taken at the onset
VTOS	vinyltriethoxysilane
$\%wt_{EPDM}$	weight percentage of EPDM
XRD	X-ray diffraction
ε_b	elongation at break
ρ	density
σ_b	stress at break
ϕ	volume fraction
ϕ_m	maximum packing fraction

Chapter 1

Introduction and overview

1.1 Introduction

Reinforcement of rubber materials with inorganic fillers is a very important aspect of rubber science and technology and has drawn considerable attention in recent years [1-7]. It has also generated tremendous interest in the rubber industry owing to decreased industrial cost and enhancements in a variety of mechanical and thermal performances. Carbon black has been the most widely used reinforcing filler in the rubber industry for rubbers prepared by conventional methods (melt mixing) [5,6]. Inorganic metal oxides (silica, titania, zirconia and more) have also been receiving more attention because of better reduction in heat build-up, tear strength and ageing resistance. They also impart to the tyre treads lower rolling, as well as better wear and abrasion resistance than carbon black [3,6]. The main disadvantage of the use of metal oxides, compounded by conventional methods such as melt mixing, is their tendency to form agglomerates inside the rubber matrix, often resulting in poor particle dispersion and high viscosities during mixing. An example is the very strong interaction between silica particles caused by the hydrogen bonding of the silanol groups to the silica surface [1,2]. This interaction prevents the filler from uniformly dispersing in the matrix and therefore results in the formation of silica aggregates. Another important disadvantage of reinforcement with inorganic fillers is their incompatibility with the rubber matrix, which ultimately gives rise to the formation of large aggregates in the matrix.

Growing of *in situ* derived inorganic metal oxides (silica, titania, zirconia) is a promising route for producing rubber matrices filled with uniformly dispersed particles [5-15]. However, among the different synthetic procedures, sol-gel chemistry represents one of the preferred ways for the preparation of organic-inorganic hybrids owing to its mild conditions particularly suited for thermally unstable organic polymers. It also allows fine control of particle size and distribution. The sol-gel process is a chemical method used to prepare inorganic materials, and was initially employed to synthesize high purity inorganic networks such as glasses and ceramics. The sol-gel process is divided into two routes, namely hydrolytic and non-hydrolytic, and apart from being used to synthesize inorganic filler, they

can be also employed for the *in situ* generation of inorganic fillers as reinforcement of rubber matrices.

The most widely used process is hydrolytic sol-gel (HSG), which involves hydrolysis and condensation of the precursors (metal oxide) to form oxide networks. The HSG process is generally divided into two steps: the first step is hydrolysis, which produces hydroxyl groups, and the second step is condensation, which involves the polycondensation of the hydroxyl groups and residual alkoxyl groups to form a three-dimensional network. The inorganic oxide can be directly grown in the organic matrix, leading to the formation of organic-inorganic hybrid structures composed of metal oxide and organic phases intimately mixed with each other. This application of the sol–gel process in rubber chemistry is related to the use of silane coupling agents and of moisture or silane curing, and it has already been carried out on natural rubber (NR), as well as styrene-butadiene, ethylene propylene diene monomer(EPDM) and butadiene rubbers [8-11,15-17]. The main drawback of the hydrolytic route is the low miscibility of the sol-gel aqueous system, which limits the dispersion of the filler in the polymer [18-20]. The inorganic oxide prepared in the hydrolytic sol-gel way also has low purity and crystallinity.

Another method to prepare organic-inorganic material is the non-hydrolytic sol-gel (NHSG) process, which can be used to produce metal oxides of high purity and crystallinity. This route features different reactions and reaction conditions, which significantly affect the texture, homogeneity and surface chemistry of the resulting oxide [21-23]. In the past 20 years several non-hydrolytic synthesis methods of oxides and mixed oxides have been described, involving the reaction of precursors (alkoxides, chlorides, acetylacetonates) with oxygen donors (ethers, alcohols, ketones) [21-25]. The main non-hydrolytic routes involve the reaction of a metal chloride with either a metal alkoxide or organic ether, which acts as oxygen donors [23-26]. It is recognized that the NHSG process is potentially solvent-free, without problems with hydrophobic substances, and it is particularly suitable for water-sensitive species [27]. On the other hand, the formation of alkyl halide and/or alkyl ethers as by-products and the potential incompatibility with oxygen-containing species have to be taken into account. However, the use of the NHSG processes to prepare filled polymers is not widely reported in literature, and most reports are limited to rigid thermoplastics [18,19] and thermosets [20].

1.2 Overview

The preparation of rubber based nanocomposites with metal oxides prepared by means of a conventional melt mixing method is one of the most used methods for introducing reinforcing filler in the rubber industry [3,13,28-35]. The preparation of these materials requires several mixing steps to disperse the silica aggregates in the rubber matrix, and the biggest problem in this technique is the constant agglomeration of the filler in the rubber which gives rise to poorer mechanical properties of the rubber/filler nanocomposites. The sol–gel approach has been applied to several types of rubber to prepare reinforced vulcanized and unvulcanized rubbers. Several synthetic procedures were used, while the most investigated filler is silica obtained by hydrolysis and condensation of tetraethoxysilane (TEOS). The sol-gel reaction allows growth of the silica particles directly into the rubber matrix, possibly with a different surface chemistry. It is believed to result in improved rubber-silica interactions and thus improved mechanical properties of the rubber/silica nanocomposites [1-17,34]

1.2.1 Properties of inorganic metal oxide

Inorganic metal-oxide nanoparticles can be used to enhance the stiffness, toughness, and probably the service life of polymers. Characterization of the nano- and microstructure, as well as dispersion, of the particles is necessary to optimize the structure-property relationships. However, there are various factors which could affect the performance of the oxide nanoparticles for specific applications. These factors include the chemical composition, physical, electrical, mechanical and thermal properties, and the synthesis route [28-31]. The nature of the oxide, as well as the surface modification, determines the final properties of the nanoparticles. Titanium dioxide (TiO_2), and silicon dioxide (SiO_2) nanoparticles are amongst the oxides that attracted a lot of attention due to their ease of synthesis and abundance.

1.2.1.2 Silicon dioxide (SiO_2)

Silicon dioxide, also known as silica, is the most common mineral in the earth’s crust. Silica is most commonly found in nature as quartz, as well as in various living organisms, and it is one of the most complex and most abundant families of materials. It naturally exists as several minerals, but can also be produced synthetically. The sol-gel and microemulsion methods are two methods developed for the formation of silica nanoparticles [36,37].

Commercial silica nanoparticles usually exist in the form of powders or colloids, mainly produced by fuming and precipitation methods in industry. Fumed silica is manufactured by a hydrothermal process from silicon tetrachloride ($SiCl_4$) (Equation 1.1). The precursor material is purified by multiple distillation and introduced as an aerosol in an oxygen-hydrogen flame under a controlled atmosphere at temperatures between 600 and 1200 °C [36,37].

$$SiCl_4 + 2H_2 + O_2 \rightarrow SiO_2 + 4HCl \qquad (1.1)$$

Silica is an amorphous material, consisting of silicon and oxygen atoms connected in a non-regular 3D network of Si-O-Si bonds with silanol groups (Si-OH) present inside and on the surface. It consists of three different types of silanol groups which can be distinguished on the silica surface: (i) geminal silanol where two hydroxyl groups are linked to one silicon atom ($Si-(OH)_2$, (ii) isolated silanol that has only one hydroxyl group (Si-OH) and (iii) vicinal silanol that contains hydroxyl groups close enough to develop hydrogen interactions (H-bonded single silanols, H-bonded geminals and their H-bonded combinations) as shown in Figure 1.1 [33,36]. The silanol groups are directly responsible for the high polarity of the silica and the strong affinity to absorb water on its surface (~6% for precipitated silica). The silanol groups have a strong tendency to form hydrogen bonds with the silanol groups from the neighbouring particles, resulting in aggregates with various sizes [1-3].

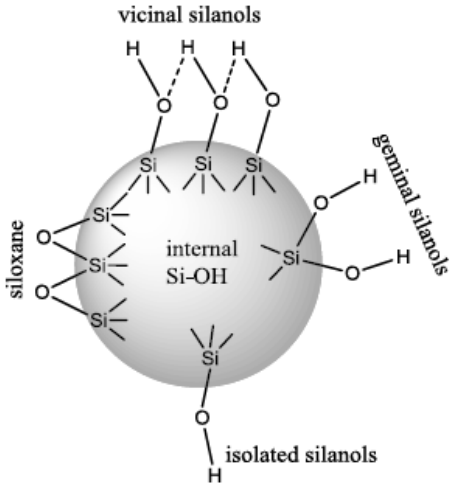

Figure 1.1 Structure of amorphous silica containing three types of silanol (Si-OH) groups

Three structures of silica at different length scales are distinguished, such as primary particles (10-50 nm), aggregates (primary particles fused together *via* hydrogen bonding: 100-500 nm) and agglomerates (aggregates held together with van der Waals forces: > 1 μm) (Figure 1.2) [36].

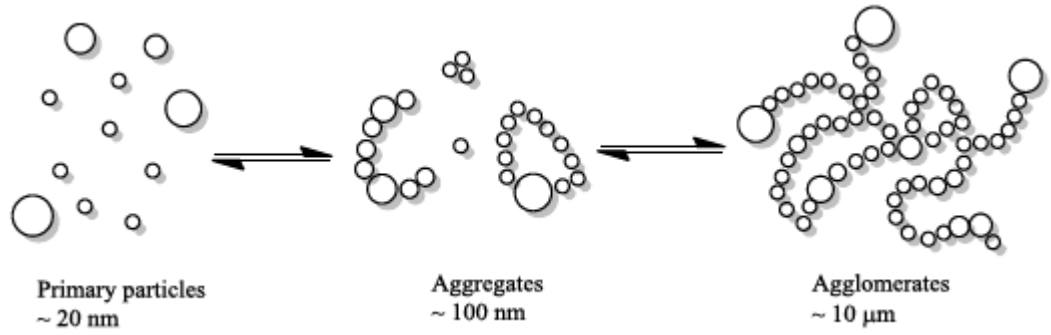

Figure 1.2 Different silica structures

Silica is also used in shoe soles for improving the wear and tear resistance, as well as to improve the tear strength and heat ageing resistance in a wide variety of manufactured rubber goods, including conveyor and power transmission belts, hoses, motor and dock mounts, bumper pads and rubber rolls. Silica further imparts to tyre treads a lower rolling resistance and at the same time better wear resistance and wet grip, and better reduction in heat build-up, tear strength and ageing resistance.

The sol-gel method is a very interesting method for the formation of silica nanoparticles. The sol-gel process involves the generation of ceramic-type materials by hydrolysis and condensation reactions of organometallic compounds such as metal oxides. The most used reaction to form silica is the hydrolysis and condensation of tetraethoxysilane (TEOS) according to the reaction in Equation 1.2.

$$Si(OC_2H_5) + 2H_2O \rightarrow SiO_2 + 4C_2H_5OH \qquad (1.2)$$

The advantage of the sol-gel method is that it provides an alternative and interesting approach to reinforce polymer matrices with silica nanoparticles *via in situ* synthesis. *In situ* generation of silica and other metal oxides inside polymers provides optical, physical and mechanical properties of the nanocomposites that are strongly dependent not only on the individual properties of each component, but also on important aspects of the chemistry involved such as uniformity, phase continuity, domain size and molecular mixing at the phase boundaries [13].

Investigation of polymers filled with silica nanoparticles and other metal oxides prepared by melt mixing reported that the dispersion of the nanoparticles could not be controlled and as a result the silica nanoparticles agglomerate in the matrix which often results to high viscosities during mixing [3,36,38]. The poor dispersion of the oxide nanoparticles results in poor mechanical and other physical properties. Studies on metal oxides prepared by the hydrolysis and condensation of TEOS have shown that the properties of the nanoparticles could be controlled by varying the ratio of water to ethanol and the reaction time of the sol-gel process [1-13,39-41].

The combination of silica with coupling agents for reinforcement of polymers through a sol-gel process gives materials with better properties than the same materials filled with carbon black. This is because nano-silica provides a better reinforcing effect which allows the use of less filler in the rubber reducing the negative effects on the mechanical properties. This improves the elasticity of the rubber/silica nanocomposites, resulting in a reduction of the rolling resistance. Moreover, the chemical bonds between the silica and the rubber results in a more stable silica-rubber network which results in a lower degree of breaking and reforming of the silica-rubber network during cyclic deformation of the nanocomposite, giving rise to a lower loss modulus and consequently lower tan δ values which additionally reduces the rolling resistance [1,10,36].

1.2.1.3 Titanium dioxide (TiO_2)

Titanium dioxide, also known as titanium(IV)oxide or titania, is a naturally occurring oxide of titanium. Titania mainly exists in nature as three polymorphs, namely brookite, anatase and rutile. These three forms can be obtained quasi selectively from a soluble precursor such as titanium tetrachloride ($TiCl_4$), in well controlled conditions in which different mechanisms are used [42]. Titanium dioxide has a wide range of applications and has attracted much attention in the fields of environmental purification, solar energy cells, photo-catalysts, gas sensors, photo-electrodes and electronic devices [43,44].

Preparation of nano-sized titanium dioxide by a sol-gel method has proven to be useful to obtain pure TiO_2 crystalized in the anatase phase. Non-hydrolytic (or non-aqueous) sol-gel routes were found to be particularly versatile and cost-effective methods for the synthesis of metal oxide nanoparticles with various structures, sizes and shapes. Many investigations have

been conducted on the non-hydrolytic synthesis of titania anatase nano-crystals by reaction of titanium(IV)isopropoxide ($Ti(OiPr)_4$) with titanium(IV)chloride ($TiCl_4$) in the presence of trioctylphosphine oxide, while a lot of effort went into finding new synthetic routes to synthesis TiO_2 nanoparticles [25,42-44].

In current research studies the focus of synthesising TiO_2 nanoparticles has shifted to the use of alcohols such as benzyl-, ethyl-, and tert-butyl alcohol. In the use of $TiCl_4$ as a precursor for producing TiO_2 nanoparticles in the presence of an alcohol, the alcohols can be used as oxygen donors, solvents and stabilizing agents. This "solvent-controlled" route was also extended to the synthesis of a large variety of other metal oxide nanoparticles [22,45]. Non-hydrolytic sol-gel routes have been found particularly useful to address several drawbacks of hydrolytic sol-gel, such as high and different hydrolysis-condensation rates of metal alkoxides, particle agglomeration and poor crystallinity of the crude precipitates.

1.2.2 General properties of EPDM rubber

Ethylene propylene diene monomer (EPDM) rubber (Figure 1.3) is a synthetic rubber synthesized mostly *via* solution polymerization using Ziegler-Natta catalysts which mainly contain vanadium compounds, such as $VOCl_3$ or $VO(OR)_3$, co-catalyzed by alkylaluminum chloride in the presence of organic halogen promoters. It is commercially attractive because it displays excellent resistance to weathering and ageing at both at high and low temperatures, due to their stable saturated polymer backbone structure [30,35]. Amorphous or low crystalline grades of EPDM have excellent low temperature flexibility with glass transition points at approximately -60°C. Heat ageing resistance up to 130°C can be obtained with properly selected sulphur acceleration systems, and heat resistance up to 160°C can be obtained with peroxide cured compounds. Compression set resistance is good, particularly at high temperatures, if sulphur donor or peroxide cure systems are used. These polymers respond well to high filler and plasticizer loading, providing economical compounds. They can develop high tensile and tear properties, excellent abrasion resistance, as well as improved oil swell resistance and flame retardance [33,34].

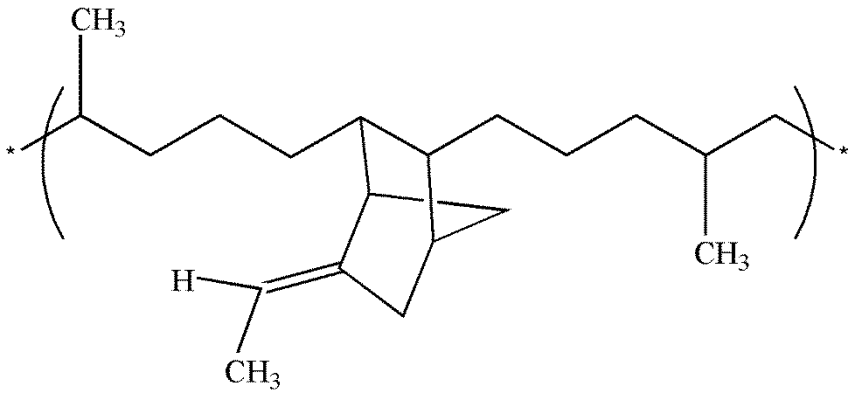

Figure 1.3 Chemical structure of EPDM rubber

The properties of EPDM strongly depend on several characteristics such as the ratio of the ethylene and propylene monomers, the distribution of these monomers in the main chain, and the amount and type of the diene monomer. These characteristics are determined by the catalyst structure and polymerization conditions. The ethylene/propylene ratio in commercial products generally ranges from 45:55 to 80:20 (w/w). At higher propylene contents the thermal and oxidative stability of the polymer are negatively affected. At higher ethylene contents the polymer becomes too crystalline and loses its rubbery properties. Some crystallinity is beneficial because it gives EPDM a higher strength; making the polymer easier to handle in the un-vulcanized state and giving it better tensile properties in the crosslinked state. On the other hand, a low level of un-saturation gives rise to a low crosslink density and slow vulcanization. EPDM is mostly used for automotive sealing systems, roof membrane linings and extruded window gaskets.

As a non-polar hydrocarbon elastomer, EPDM has excellent insulating properties. It is widely used in many products including hoses, moulded parts for automobile applications, cable insulation, connectors in the electrical industry, and sheet goods [33,46]. EPDM is also blended with other elastomers to modify many properties in a particular way. The development of blends of natural rubber (NR) with EPDM, with the aim of combining the excellent physical properties of NR with the ozone resistance of EPDM, has received much attention over the past three decades [46]. Blends of other polar and unsaturated rubbers with EPDM have been developed to achieve better thermal stability and wettability. For example, synthetic polyisoprene rubber (IR) blends with EPDM exhibit better thermal stability than natural rubber. Different types of inorganic oxide (silica, titania, alumina) have also been introduced in the blends of EPDM with natural rubber, with the aim to use the excellent

physical properties of oxides in to improve mechanical and thermomechanical, thermal and electrical properties, as well as conductivity [13,46,47].

1.2.3 In-situ rubber/silica composites *via* hydrolytic sol-gel (HSG) reaction

1.2.3.1 Morphology

A study of the morphology of the *in situ* silica particles in the matrix is important, because the filler content, particle size and dispersion of the silica particles significantly influence the properties of the composite elastomers. In most cases scanning electron microscopy (SEM) and transmission electron microscopy (TEM) were used to characterize the morphology of these composites. Several studies were conducted on the *in situ* sol-gel of TEOS with different catalysts (*n*-hexylamine and *n*-butylamine) in the presence natural rubber (NR) under different preparation conditions [2,48,49]. There is good agreement of the results of these studies, with the silica particles homogeneously dispersed with only some aggregates, and with the particle size in the nano-scale range (50-60 nm). In a study where isoprene rubber (IR) was filled with *in situ* generated silica particles, a significant increase in particle size was observed with increasing filler content [12]. The increase in the particle diameter was attributed to an increase in the coalescence of the growing silica particles when increasing the amount of *in situ* formed dispersed phase. The silica particles may also have agglomerated in the suspension, because the hydrophilic silica particles have a tendency to associate *via* hydrogen bonding. When IR/silica composites were prepared in the presence of a coupling agent (octyltriethoxysilane (OTES)), the coupling agent seemed to stabilize the surfaces of the growing particles and reduced their average dimensions. However, in other studies on *in situ* generated silica prepared with different rubber matrices (EPDM, IR, NR, epoxidized SBR) and different coupling agents (TESPT, APTS, TESPD, TMTSPM, VTOS, ETOS and BTOS), the tendency of silica particles to form aggregates or agglomerates was still observed [4,5,23,24,50].

1.2.3.2 Equilibrium swelling ratio

Equilibrium swelling of rubber matrices reinforced with *in situ* generated inorganic metal oxides is widely studied in the sol-gel chemistry of rubber composites. Swelling experiments are used as direct indication of the crosslinking degree of the rubber obtained after

vulcanization in the presence of metal oxides. Investigation on *in situ* generated silica and alkylated silica in natural rubber latex reported on the swelling ratio of the vulcanized composites [4]. The swelling of silica-filled NR vulcanizates was significantly lower than that of the neat vulcanizate. This was attributed to restriction of rubber chain motions by silica in the silica-filled network. Melt-mixed NR/silica composites were found to have high swelling degrees, which was attributed to larger silica particles. In other studies the swelling ratio was found to significantly increase with increasing silica content for vulcanized silica-filled IR matrix [6]. The decrease in the crosslinking degree was ascribed to a hindering effect of the silica particles on the vulcanization process, which limited the extent of crosslinking of the IR phase. A similar explanation was given for NR/silica composites [17].

1.2.3.3 Thermal properties

The thermal properties of rubber matrices containing metal oxides were studied by a number of researchers using thermogravimetric analysis (TGA). The thermal stability of *in situ* silica filled NR vulcanizates was improved as a result of delayed decomposition upon heating [48]. The composites showed two degradation steps, the first at 250 °C to 450 °C as a result of the decomposition of NR, and the second 450-570 °C associated with carbonaceous residues from the rubber. Furthermore, the residual weight of silica was equal to the initially silica concentration. In other studies the thermal stability of silica-filled rubber matrices was found to be similar to that of the neat rubber matrix [50].

1.2.3.4 Mechanical and viscoelastic properties

Dynamic mechanical analysis (DMA) and tensile testing were mostly used to get information on the thermomechanical and mechanical properties of *in situ* silica-filled rubber nanocomposites [5,16,48,50,51]. The presence the nanosized silica particles in the rubber matrices generally showed a significant increase in the Young's modulus, storage modulus, loss modulus and tan δ for both low and high silica contents. Interestingly the storage moduli at high temperatures increased and the tan δ decreased with increasing silica content. The reason was attributed to good adhesion between the filler and the matrix, which resulted in a restriction of the mobility of the rubber chains in the composite. The tensile properties such as the stress and elongation at break also improved. However, there are some investigations which showed reduced mechanical properties, especially at high silica loadings [52]. The

differences in the influence of these nanoparticles on the mechanical properties were mainly attributed to the filler agglomeration in the rubber matrix. The presence of aggregates in the composite results in dewetting or crazing in which the adhesion between the filler and matrix phase is destroyed, and this result in a decline in the mechanical properties.

The reinforcing effect of particles in rubber materials was extensively investigated by using several different theoretical and semi-empirical models to predict the mechanical reinforcement of *in situ* generated silicas in elastomers [52-57]. In some studies the Young's modulus fit well with the theoretical models, while in other cases there was little correlation.

1.2.4 In-situ PMMA/titania composites *via* non-hydrolytic sol-gel (NHSG) reaction

The use of the NHSG processes to prepare filled polymers is not widely reported in literature. Most of the reported studies were limited to rigid thermoplastics [18,19] and thermosets [20]. In the mentioned studies benzyl alcohol was used as an oxygen donor and $TiCl_4$ as a precursor. In both cases improvements in the mechanical and functional properties were observed, independent of the chosen polymer matrix. This was due to the improved interfacial interactions between the organic and inorganic phase brought about by the non-hydrolytic sol-gel route. It was also found that the *in situ* generated titania did not have any negative effect on the PMMA molecular weight and thermal stability, and that there was a significant stiffening effect.

1.3 References

1. M. Messori, F. Bignotti, R. De Santis, R. Taurino. Modification of isoprene rubber by *in situ* silica generation. Polymer International 2009; 58:880-887. DOI: 10.1002/pi.2606
2. Y. Ikeda, Y. Kemeda. Preparation of "green" composites by the sol-gel process: *In situ* filled natural rubber. Journal of Sol-Gel Science and Technology 2004; 31:137-142. DOI: 10.1023/B:JSST.0000047975.48812.1b
3. S. Prasertsri, N. Tattanasom. Mechanical and damping properties of silica/natural rubber composites prepared from latex system. Polymer Testing 2011; 30:515-526. DOI: 10.1016/j.polymertesting.2011.04.001

4. J. Siramanont, V. Tangpasuthadol, A. Intasiri, N. Na-Ranong, S. Kiatkamjornwon. Sol-gel process of alkyltriethoxysilane in latex for alkylated silica formation in natural rubber. Polymer Engineering and Science 2009; 49:1099-1106.
DOI 10.1002/pen.21363
5. A. Das, R. Jurk, K.W. Stöckelhuber, G. Heinrich. Silica-ethylene propylene diene monomer rubber networking by *in situ* sol-gel method. Journal of Macromolecular Science, Part A: Pure and Applied Chemistry 2008; 45:101-106.
DOI: 10.1080/10601320701683447
6. M. Messori, M. Fiorini. Isoprene rubber filled with silica generated *in situ*. Journal of Applied Polymer Science 2011; 119:3422-3428.
DOI: 10.1002/app.32992
7. Q. Ji, X. Wang, Y. Zhang, Q. Kong, Y. Xia. Characterization of poly(ethylene terephthalate)/SiO_2 nanocomposites prepared by sol-gel method. Composites: Part A 2009; 40:878-882.
DOI: 10.1016/j.compositesa.2009.04.010
8. Y. Ikeda, A. Tanaka, S. Kohjiyab. Effect of catalyst on in situ silica reinforcement of styrene–butadiene rubber vulcanizate by the sol-gel reaction of tetraethoxysilane. Journal of Materials Chemistry1997; 7:455-458.
9. K. Murakami, S. Iio, Y. Ikeda, H. Ito, M. Tosaka, S. Kohjiya. Effect of silane-coupling agent on natural rubber filled with silica generated in situ. Journal of Materials Science2003; 38:1447-1455.
DOI: 10.1023/A:1022908211748
10. S. Kohjiya, Y. Ikeda. In situ formation of particulate silica in natural rubber matrix by the sol-gel reaction. Journal of Sol-Gel Science and Technology 2003; 26:495-498.
DOI: 10.1023/A:1020743214628
11. Y. Ikeda, S. Kohjiya. In situ formed silica particles in rubber vulcanizate by the sol-gel method. Polymer 1997; 38:4417-4423.
12. M. Messori. In situ synthesis of rubber nanocomposites. Advanced Structured Materials 2011; 9:57-85.
DOI: 10.1007/978-3-642-15787-5_2
13. T.E. Motaung, A.S. Luyt, S. Thomas. Morphology and properties of NR/EPDM rubber blends filled with small amounts of titania nanoparticles. Polymer Composites 2011; 32:1289-1296.
DOI:10.1002/pc.21150

14. D. Fragiadakis, L. Bokobza, P. Pissis. Dynamics near the filler surface in natural rubber-silica nanocomposites. Polymer 2011; 52:3175-3182.
DOI:10.1016/j.polymer.2011.04.045

15. R. Scotti, L. Wahba, M. Crippa, M. D'Arienzo, R. Donetti, N. Santod, F. Morazzoni. Rubber–silica nanocomposites obtained by in situ sol–gel method: Particle shape influence on the filler-filler and filler-rubber interactions. Soft Matter 2012; 8:2131-2143.
DOI: 10.1039/c1sm06716h

16. V. Tangpasuthadol, A. Intasiri, D. Nuntivanich, N. Niyompanich, S. Kiatkamjornwong. Silica-reinforced natural rubber prepared by the sol-gel process of ethoxysilanes in rubber latex. Journal of Applied Polymer Science 2008; 109:424-433.
DOI: 10.1002/app.28120

17. L. Bokobza, J.-P. Chauvin. Reinforcement of natural rubber: Use of *in situ* generated silicas and nanofibres of sepiolite. Polymer 2005; 46:4144-4151.
DOI: 10.1016/j.polymer.2005.02.048

18. D. Morselli, F. Bondioli, M. Fiorini, M. Messori. Poly(methyl methacrylate)-TiO_2 nanocomposites obtained by non-hydrolytic sol-gel synthesis: The innovative tert–butyl alcohol route. Journal of Materials Science 2012; 47:7003-7012.
DOI: 10.1007/s10853-012-6651-4

19. D. Morselli, M. Messori, F. Bondioli. Poly(methyl methacrylate)-TiO_2 nanocomposite obtained by non-hydrolytic sol-gel synthesis. Journal of Materials Science 2011; 46:6609-6617.
DOI:10.1007/s10853-011-5610-9

20. D. Morselli, F. Bondioli, M. Sangermano, M. Messori. Photo-cured epoxy networks reinforced with TiO_2 in-situ generated by means of non-hydrolytic sol-gel process. Polymer 2012; 53:283-290.
DOI: 10.1016/j.polymer.2011.12.006

21. P.H. Mutin, A. Vioux. Nonhydrolytic processing of oxide-based materials: Simple routes to control homogeneity, morphology, and nanostructure. Chemistry of Materials 2009; 21:582-596.
DOI: 10.1021/cm802348c

22. D.P. Debecker, P.H. Mutin. Non-hydrolytic sol–gel routes to heterogeneous catalysts. Chemical Society Reviews 2012; 41:3624-3650.
DOI: 10.1039/C2CS15330K

23. V. Lafond, P.H. Mutin, A. Vioux. Non-hydrolytic sol–gel routes based on alkyl halide elimination: Toward better mixed oxide catalysts and new supports: Application to the preparation of a SiO_2-TiO_2 epoxidation catalyst. Journal of Molecular Catalysis A: Chemical 2002; 182-183:81-88.
DOI: S1381-1169(01)00487-3
24. M. Niederberger. Nonaqueous sol-gel routes to metal oxide nanoparticles. Accounts of Chemical Research 2007; 40:793-800.
DOI: 10.1021/ar600035e
25. C. Lind, S.D. Gates, N.M. Pedoussaut, T.I. Baiz. Novel materials through non-hydrolytic sol-gel processing: Negative thermal expansion oxides and beyond. Materials 2010; 3:2567-2587.
DOI:10.3390/ma3042567
26. P. Arnal, R.J.P. Corriu, D. Leclercq, P.H. Mutin, A. Vioux. A solution chemistry study of non-hydrolytic sol-gel routes to titania. Chemistry of Materials 1997; 9:694-698.
DOI:10.1021/cm960337t
27. J.N. Hay, H.M. Raval. Synthesis of organic-inorganic hybrids via the non-hydrolytic sol-gel process. Chemistry of Materials 2001; 13:3396-3403.
28. B.P. Panda, S. Mohanty, S.K. Nayak, S. Pandit. Fracture study of modified TiO_2 reinforced PP/EPDM composite: mechanical behavior and effect of compatibilization. International Journal of Plastics Technology 2012; 16:89-100.
DOI 10.1007/s12588-012-9032-6
29. Z. Wang, Y. Lu, J. Liu, Z. Dang, L. Zhang, W. Wang. Preparation of nano-zinc oxide/EPDM composites with both good thermal conductivity and mechanical properties. Journal of Applied Polymer Science 2011; 119:1144-1155.
DOI 10.1002/app.32736
30. V. Jovanović, S. Samaržija-Jovanović, J. Budinski-Simendić, G. Marković, M. Marinović-Cincović. Composites based on carbon black reinforced NBR/EPDM rubber blends. Composites: Part B 2013; 45:333-340.
DOI: 10.1016/j.compositesb.2012.05.020
31. Q. Wang, W. Gao, L. Zhang. Research of styrene-butadiene rubber/silicon-aluminum oxides nanotube binary nanocomposites. Journal of Applied Polymer Science 2011; 120:3196–3203.
DOI 10.1002/app.33245

32. M. Jarnthong, C. Nakason. Influence of incorporation sequence of silica nanoparticles on morphology, crystallization behavior, mechanical properties, and thermal resistance of melt blended thermoplastic natural rubber. Polymer Composites 2012; 33:1911-1920. DOI: 10.1002/pc.22331
33. E. Miloskovska. Structure-property of rubber/silica nanocomposites via sol-gel process. http://alexandra.tue.nl/extra2/739216.pdf (Accessed on 05October 2013).
34. http://en.wikipedia.org/wiki/EPDM_rubber (Accessed on 05October 2013).
35. S. Haitao, C. Juqing, Z. Qiang, Z. Wei, H. Qihui, H. Baixing, S. Jian. Preparation and properties of EPDM/TiO_2 composites. Journal of Applied Polymer Science 2007; 106:314-319.
DOI 10.1002/app.26614
36. K. Chrissafis, D. Bikiaris. Can nanoparticles really enhance thermal stability of polymers? Part I: An overview on thermal decomposition of addition polymers. Thermochimica Acta 2011; 523:1-24.
DOI: 10.1016/j.tca.2011.06.010
37. http://en.wikipedia.org/wiki/Silicone_dioxide (Accessed on the 05 November 2013)
38. J. Móczó, B. Pukánszky. Polymer micro and nanocomposites: Structure, interactions, properties. Journal of Industrial and Engineering Chemistry 2008; 14:535-563.
DOI: 10.1016/j.jiec.2008.06.011
39. H.L. Castricum, A. Sah, J.A.J. Geenevasen, R. Kreiter, D.H.A. Blank, J.F. Vente, J.E. Elshof. Structure of hybrid organic–inorganic sols for the preparation of hydrothermally stable membranes. Journal of Sol-Gel Science and Technology 2008; 48:11–17.
DOI: 10.1007/s10971-008-1742-z
40. S. Choi, B. Chu, S.G. Lee, S.W. Lee, S.S. Im, S.H. Kim, J.K. Park. Titania-doped silica fibers prepared by electrospinning and sol-gel process. Journal of Sol-Gel Science and Technology 2004; 30:215-221.
DOI: 10.1023/B:JSST.0000039530.09380.bc
41. G. Debora, G. Yoshitaka, M. Celso, C. Tania, B. Edilson. The effects of temperature of condensation on the thermal stability and morphology of 1,4-phenylenediamine-1-propylsilica xerogels. Journal of Sol-Gel Science and Technology 2005; 34:189-195.
DOI: 10.1007/s10971-005-1365-6
42. J.-P. Jolivet, S. Cassaignon, C. Chanéac, D. Chiche, O. Durupthy, D. Portehault. Design of metal oxide nanoparticles: Control of size, shape, crystalline structure and functionalization by aqueous chemistry. Comptes Rendus Chimie 2010; 13:40-51.

DOI:10.1016/j.crci.2009.09.012

43. A. Karami. Synthesis of TiO_2 nano powder by the sol-gel method and its use as a photocatalyst. Journal of the Iranian Chemical Society 2010; 7:S154-S160.
44. A. Aboulaich, B. Boury, P.H. Mutin. Reactive and organosoluble anatase nanoparticles by a surfactant-free nonhydrolytic synthesis. Chemistry of Materials 2010; 22:4519-4521.
DOI:10.1021/cm101191a
45. Y. Zhu, L. Zhang, C. Gao, L. Cao. The synthesis of nanosized TiO_2 powder using a sol-gel method with $TiCl_4$ as a precursor. Journal of Materials Science 2000; 35:4049-4054.
DOI:10.1023/A:1004882120249
46. C. Gamlin, M.G. Markovic, N.K. Dutta, N.R. Choudhury, J.G. Matisons. Structural effects on the decomposition kinetics of EPDM elastomers by high-resolution TGA and modulated TGA. Journal of Thermal Analysis and Calorimetry 2000; 59:319-336.
DOI: 10.1023/A:1010164702571
47. C. Scott, H. Ishida, F.H.J. Maurer. Characterization of polyethylene/EPDM/silicon dioxide multicomponent composites by solid-state dynamic mechanical spectroscopy. Journal of Materials Science 1991; 26:5708-5716.
48. B. Chaichua,P. Prasassarakich, S. Poompradub. In situ silica reinforcement of natural rubber by sol-gel process via rubber solution. Journal of Sol-Gel Science and Technology 2009; 52:219-227.
DOI 10.1007/s10971-009-2019-x
49. Y. Ikeda, S. Poompradub, Y. Morita, S. Kohjiya. Preparation of high performance nanocomposite elastomer: Effect of reaction conditions on in situ silica generation of high content in natural rubber. Journal of Sol-Gel Science and Technology 2008; 45:299-306.
DOI 10.1007/s10971-008-1682-7
50. M.A. de Luca, M.M. Jacobi, L.F. Orlandini. Synthesis and characterisation of elastomeric composites prepared from epoxidised styrene butadiene rubber, 3-aminopropyltriethoxysilane and tetraethoxysilane. Journal of Sol-Gel Science and Technology 2009; 49:150-158.
DOI 10.1007/s10971-008-1851-8
51. Y. Ikeda, A. Tanaka, S. Kohjiya. Reinforcement of styrene–butadiene rubber vulcanizate by in situ silica prepared by the sol–gel reaction of tetraethoxysilane. Journal of Materials Chemistry 1997; 7:1497-1503.

DOI:10.1039/A700648I

52. L.E. Nielsen, R.F. Landel. Mechanical Properties of Polymers and Composites. Marcel Dekker, Inc.: New York (1994).
ISBN: 0 8247 8964 4

53. L.E. Nielsen. Morphology and elastic modulus of block polymers and polyblends. Rheological Acta 1974; 13:86-92.

54. Y.-P. Wu, Q.-X. Jia, D.-S. Yu, L.-Q. Zhang. Modeling Young's modulus of rubber-clay nanocomposites using composite theories. Polymer Testing 2004; 23:903-909.
DOI: 10.1016/j.polymertesting.2004.05.004

55. T.K. Jayasree, P. Predeep. Effect of filler on mechanical properties of dynamically crosslinked styrene butadiene rubber/high density polyethylene blends. Journal of Elastomers and Plastics 2008; 40:127-146.
DOI: 10.1177/0095244307083865

56. S. Ahmed, F.R. Jones. A review of particulate reinforcement theories for polymer composites. Journal of Materials Science 1990; 25:4933-4942.

57. S. Mazzullo. Methods of mathematical physics applied to polymer composites. "Giulio Natta" Research Centre, LyondellBasell 2008; 1:1-22.
DOI: 10.1685/SELN08003

Chapter 2

Preparation and characterization of EPDM rubber modified with *in situ* generated silica

This chapter has been published as:
D. Morselli, F. Bondioli, A.S. Luyt, T.H. Mokhothu, M. Messori. Preparation and characterization of EPDM rubber modified with in situ generated silica. Journal of Applied Polymer Science 2013; 128:2525-2532.
DOI: 10.1002/app.38566

Abstract

The present paper is concerned with the preparation of a filled elastomer by means the non-conventional bottom-up approach to polymer composites, alternatively with the conventional mechanical compounding of preformed filler particles with rubber. EPDM rubber was modified with in situ generated silica particles prepared by means of a sol-gel process adopting a solution process. The used synthetic procedure permitted the preparation of highly filled rubbers (up to 40 wt% of silica) with silica particle dimensions ranging from 0.2 to 2 μm. Equilibrium swelling and extraction tests indicated a hindering effect of the presence of in situ generated silica on the vulcanization process which reduced the cross-linking degree of the rubber matrix. Both tensile tests and dynamic-mechanical analysis showed a significant improvement in the mechanical properties due to the presence of the reinforcing filler, with an enhancement more significant than that expected from a simple hydrodynamic reinforcing mechanism.

Keywords: EPDM, silica, sol-gel, filled rubber

2.1 Introduction

Rubbers usually require the addition of inorganic fillers to enhance their basic properties and make them useful for practical applications. In addition to carbon black, which is one of the most used reinforcing fillers for rubber materials (especially in the tire industry), silica represents another important filler used for reinforced elastomers. Silica compounding offers several advantages with compared to carbon black, such as better combination of tear

strength, abrasion resistance and ageing resistance. Furthermore, in the tire industry, silica imparts to tire treads a lower rolling resistance than carbon black and at the same time an equal wear resistance and wet grip [1].

One of the main disadvantages of the use of silica prepared by the conventional ex-situ synthesis methods is the high tendency for the particles to agglomerate within the rubber matrix due to the strong particle-particle interactions, which can result in high compound viscosity and reduced processability. Furthermore, the incompatibility between silica and non-polar elastomers, such as styrene-butadiene rubber or natural rubber, often requires the use of silane coupling agents to improve the reinforcing efficiency of silica [2].

An alternative and interesting approach to the incorporation of preformed particles into the elastomer matrix by mechanical mixing (compounding) before its vulcanization (ex situ process), is the in situ generation of inorganic oxides (silica or other) through a sol-gel process, which is the so-called bottom-up approach to obtain organic-inorganic hybrid materials. The sol-gel process involves the generation of ceramic-type materials by the hydrolysis and condensation reactions of organometallic compounds such as metal alkoxides [3]. One of the mostly used reactions is the hydrolysis and condensation of tetraethoxysilane (TEOS) to form silica according to the following reaction:

$$Si(OCH_2CH_3)_4 + 2\ H_2O \rightarrow SiO_2 + 4\ CH_3CH_2OH$$

Organic-inorganic hybrid materials can be prepared with these reactions in the presence of organic molecules or macromolecules, which should preferably contain functional groups to improve their bonding to the inorganic phase. The possibility of preparing rubbers, modified with metal oxides generated in situ by a sol-gel process, has already been reviewed by several authors in recent publications [4-9].

It is generally accepted that the extent of mechanical reinforcement of elastomers is controlled by three main factors, namely: the dispersion state of the filler, the filler-matrix interactions and the filler-filler interactions [10-12]. A major potential of the sol-gel technique stems from the possibility to control the amount of silica generated *in situ* and its morphological characteristics by a proper selection of the reaction conditions (e.g. amount of TEOS, type and amount of catalyst, temperature and reaction time). Furthermore, it is possible to tailor

filler-filler and filler-rubber interactions through the incorporation of silane coupling agents in the reaction mixture. These compounds have functional groups suitable for improving filler-matrix interactions, thus allowing better silica dispersion and a higher mechanical reinforcement [4].

Messori *et al.* recently published several papers on the *in situ* generation of silica from TEOS into isoprene rubber [13-15], in particular reporting detailed studies of the interrelation between preparation conditions, structure and mechanical reinforcement. A similar approach was used in the present study on the preparation and characterization of ethylene-propylene-diene-monomer (EPDM) rubbers. Concerning EPDM-based materials modified by *in situ* generation of silica, Das *et al.* [16] swelled triethoxysilyl-grafted EPDM in TEOS and activated the sol-gel process by adding *n*-butyl amine as a basic catalyst. After rubber vulcanization, mechanical characterization showed that *in situ* sol-gel derived fillers had superior reinforcing efficiency, compared to the externally added silica at the same concentration of these fillers in an EPDM matrix.

The main limitation of the proposed synthetic method was the relative low value of the maximum concentration of *in situ* generated silica, which appeared limited by diffusion phenomena of TEOS within the unvulcanized rubber matrix during the swelling step. In order to overcome this drawback, a solution process [15] was proposed in this work as described in the following:

(i) dissolution of both the metal alkoxide (metal oxide precursor) and unvulcanized rubber in a common solvent;

(ii) addition of water, sol-gel catalysts and vulcanization ingredients and activation of the sol-gel process at a given temperature and for a given reaction time;

(iii) removal of solvent and by-products by evaporation;

(iv) Vulcanization of the filled rubber.

In principle, this solution procedure ensures a highly homogeneous dispersion of the in situ generated filler in the rubbery matrix, also for high reinforcing metal oxide contents.

2.2 Experimental section

2.2.1 Materials

EPDM rubber (Polimeri Europa Dutral® TER 4038, density ρ_{EPDM} = 0.91 g·cm^{-3}) was kindly provided by ATG Italy (Castel d'Argile, BO, Italy). Tetraethoxysilane (TEOS), toluene, ethanol (EtOH) and dicumyl peroxide (DCP) were purchased from Sigma Aldrich (Milan, Italy). All materials were high purity reactants and were used as received without any further purification.

2.2.2 Preparation and characterization of EPDM-silica composites

For kinetic analysis, EPDM rubber was dissolved in toluene (about 3 g in 100 ml) at room temperature. After complete dissolution, a given amount of TEOS, H_2O, EtOH (TEOS: H_2O: EtOH = 1:4:4 mol) and dibutyltin dilaurate (2 wt % relative to TEOS, as a catalyst for the sol process) were added. TEOS was added in different quantities in order to obtain silica contents ranging from 0 to 45 wt%. The mixture usually assumed the emulsion state due to the presence of a significant amount of water in an organic medium. The mixture was magnetically stirred and heated at 80 °C to activate the hydrolytic condensation of TEOS to silica. After a given reaction time (from 1 to 9 h), a portion of the suspension was collected and toluene and other volatile products, such as H_2O and EtOH, were eliminated with a rotary evaporator operating at a reduced pressure and room temperature to prevent any significant further progress of the sol-gel reaction.

The actual silica content in the filled rubber was determined by thermogravimetric analysis (TGA). For the preparation of the samples for the other characterizations, the above described procedure was adopted for a fixed reaction time of 6 h. Solvents and other volatile products were partially eliminated (approximately 50% of the total amount) and DCP was added to the suspension at a concentration of 2 phr (parts per hundred resin). The suspensions were cast into Petri dishes and the volatiles were completely eliminated by leaving the systems under an aspiration hood overnight.

The films (about 0.5 mm thick) were vulcanized by hot-pressing at 160 °C for 20 min. The filled materials were coded as EPDM_*x* in which *x* represents the nominal final weight per cent of silica (by assuming the complete conversion of TEOS to silica during the sol-gel reaction).

Nominal and actual silica concentrations are reported in Table 2.1. Volume fraction values were calculated under the assumption of volume additivity after experimental determination of the density of silica obtained from TEOS (under experimental conditions similar to those used for the EPDM_*x* composites, $\rho_{SiO2} = 1.66\ g \cdot cm^{-3}$) [15].

Table 2.1 Composition of the prepared materials ([1]nominal value calculated by assuming complete conversion of TEOS to silica; [2]experimental value obtained by thermogravimetry)

Material code	SiO_2 content[1] / wt.%	SiO_2 content[2] / wt.%	SiO_2 volume fraction /-
EPDM_0	0	0.0	0.00
EPDM_05	5	5.0	0.03
EPDM_15	15	15.0	0.09
EPDM_30	30	27.8	0.17
EPDM_45	45	40.7	0.27

The morphological investigation was carried out with scanning electron microscopy (SEM, TESCAN VEGA3 scanning electron microscope) by the application of an accelerating voltage of 15 kV. The samples (cross section) were coated with gold (thickness 10 nm) by an electro-deposition method to impart electrical conduction before the SEM micrographs were recorded.

Swelling experiments were carried out by the immersion of punch-cut specimens (size $7 \times 3 \times 0.5\ mm^3$) in 50 ml of toluene at room temperature for several hours. Toluene was replaced hourly with fresh solvent to eliminate all uncross-linked fractions, such as unvulcanized EPDM chains, which would lead to wrong values of the swelling ratio. When the swollen mass (m_s) reached a constant value, the sample was dried to a constant mass (i.e., the dried mass m_d), and the absolute swelling ratio (q) was evaluated according to the following equation:

$$q = \frac{m_s}{m_d} \quad (2.1)$$

The absolute extractable fraction (*f*) was determined as follows:

$$f = \frac{m_o - m_d}{m_o} \times 100 \quad (2.2)$$

where m_0 is the mass of the sample before its immersion in toluene. The values of q and f were also normalized to the actual EPDM weight (i.e., the swellable phase and, in the case of incomplete vulcanization, the extractable phase), and these values were called q_{EPDM} and f_{EPDM}, respectively. Their values were calculated as follows:

$$q_{EPDM} = \frac{q}{w_{EPDM}} \quad (2.3)$$

$$f_{EPDM} = \frac{f}{w_{EPDM}} \quad (2.4)$$

where w_{EPDM} is the weight fraction of EPDM present in the composite.

Uniaxial tensile tests were performed by a Hounsfield dynamometer (model H5KS). The experiments were run at room temperature, on strips of 65×12×0.5 mm^3 in size, using a gauge length of 20 mm and a crosshead speed of 100 mm min^{-1}. Tensile test data were presented as nominal stress $\sigma_n = F/A_0$ versus elongation $\varepsilon = \Delta l/l_0$ curves, where F is the applied force and A_0 is the initial cross-sectional area of the specimen, while Δl and l_0 are the change in length and the gauge length, respectively. The initial modulus E_{in} was calculated as the slope of the initial portion of the σ_n- ε curves. The secant modulus at a given elongation $E_{sec,\varepsilon}$ was calculated as $E_{sec,\varepsilon} = \sigma_{n(\varepsilon)}/\varepsilon$ where $\sigma_{n(\varepsilon)}$ is the nominal stress at the elongation ε considered. All mechanical properties were determined on an average of at least five specimens.

The glass transition temperature (T_g), storage modulus (*E'*) and loss factor (tan δ) were determined through dynamic-mechanical analysis (DMA) using a Diamond DMA (Perkin Elmer); punch-cut specimens (40×10×0.5 mm^3) were tested in tensile mode at a constant frequency of 1 Hz, while heated from -100 to 100 °C at a rate of 3 °C·min^{-1} under nitrogen gas.

T_g values were also determined by using differential scanning calorimetry (DSC). The DSC curves were recorded at a heating/cooling rate of 5 °C·min^{-1} over the range -70/0 °C by using a TA Instruments DSC 2010 purged with nitrogen.
Thermogravimetric analysis (TGA) was carried out on a Perkin–Elmer TGA7 thermogravimetric analyzer under nitrogen flow (20 ml·min^{-1}), from 30 up to 600 °C at a heating rate of 10 °C·min^{-1}.

Film transparency was characterized by UV–V spectrophotometry (Perkin–Elmer, Lambda 19) in the 400-800 nm range. The reported spectra were normalized against air and with respect to the thickness of unfilled vulcanized rubber.

2.3 Results and discussion

2.3.1 Kinetic analysis

The progress of the sol-gel reaction was followed by determining the actual silica content through TGA at different reaction times. The real silica content values are reported as a function of the reaction time, as shown in Figure 2.1, for the EPDM_*x* samples.

As expected, the actual silica content, correlated with the degree of conversion of TEOS to silica, increased with the sol-gel reaction time, i.e. with the time allowed for the mixture to react before it underwent the solvent elimination step. Under the used experimental conditions (time and temperature) for the *in situ* generation of silica within the rubber matrix, the maximum silica weight percentages for EPDM_15, EPDM_30 and EPDM_45 were 15.0, 27.7 and 40.7 wt %, respectively.

The data indicate a quantitative conversion of TEOS to silica for relatively low TEOS initial content (EPDM_15 sample) and a progressive reduction of TEOS conversion by increasing the amount of TEOS present at the beginning of the reaction. However, it is important to observe that generally a very high conversion value (higher than 90%) was obtained.

The data reported in Figure 2.1 indicate that silica content values very close to the maximum (i.e. by assuming the complete conversion of TEOS to silica) were obtained for all of the

samples after a reaction time in the range 4-6 h. On the basis of these results, the subsequent characterizations were carried out on samples prepared with a reaction time fixed at 6 h.

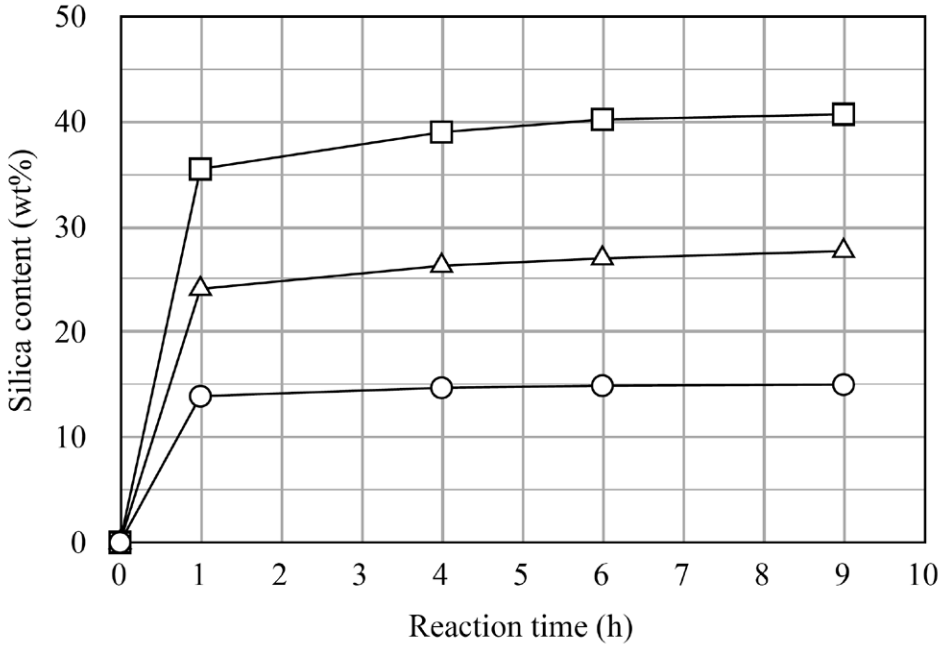

Figure 2.1 Silica content (determined by TGA) as a function of the reaction time for (○) EPDM_15, (∆) EPDM_30 and (□) EPDM_45

2.3.2 Morphology

The specimens were broken in liquid nitrogen and the cross-sections were analyzed by scanning electron microscopy (SEM). The typical SEM micrographs of vulcanized rubber with a nominal silica content of 5 and 30 wt% are reported in Figure 2.2. The cross-section of the EPDM_5 sample shows the presence of a dispersed phase with a homogeneous distribution of silica particles in the rubber matrix and good particle-matrix adhesion, supporting the effectiveness of the *in situ* filler generation process adopted for the preparation of the filled rubbers. The dispersion degree was also good as indicated by the almost negligible presence of particles agglomerates. The average dimension of the spherical silica particles was below 0.2 μm.

By increasing the initial TEOS content (EPDM_30 sample), the particles distribution remained good enough, though a significant increase in particle size and size distribution

clearly occurred. In particular, large particles having diameters larger than 10-15 μm were present together with smaller particles (about 1 μm in size). Particles aggregation was also present indicating a general reduction in the degree of dispersion. This behaviour has already been observed and reported by other authors for similar systems [15,17], and can be tentatively explained by considering that an increase in the amount of *in situ* formed dispersed phase (silica from TEOS) gives rise to an increase in the coalescence of the growing silica particles, and thus an increase in both the average dimension of the dispersed particles and aggregation phenomena are expected.

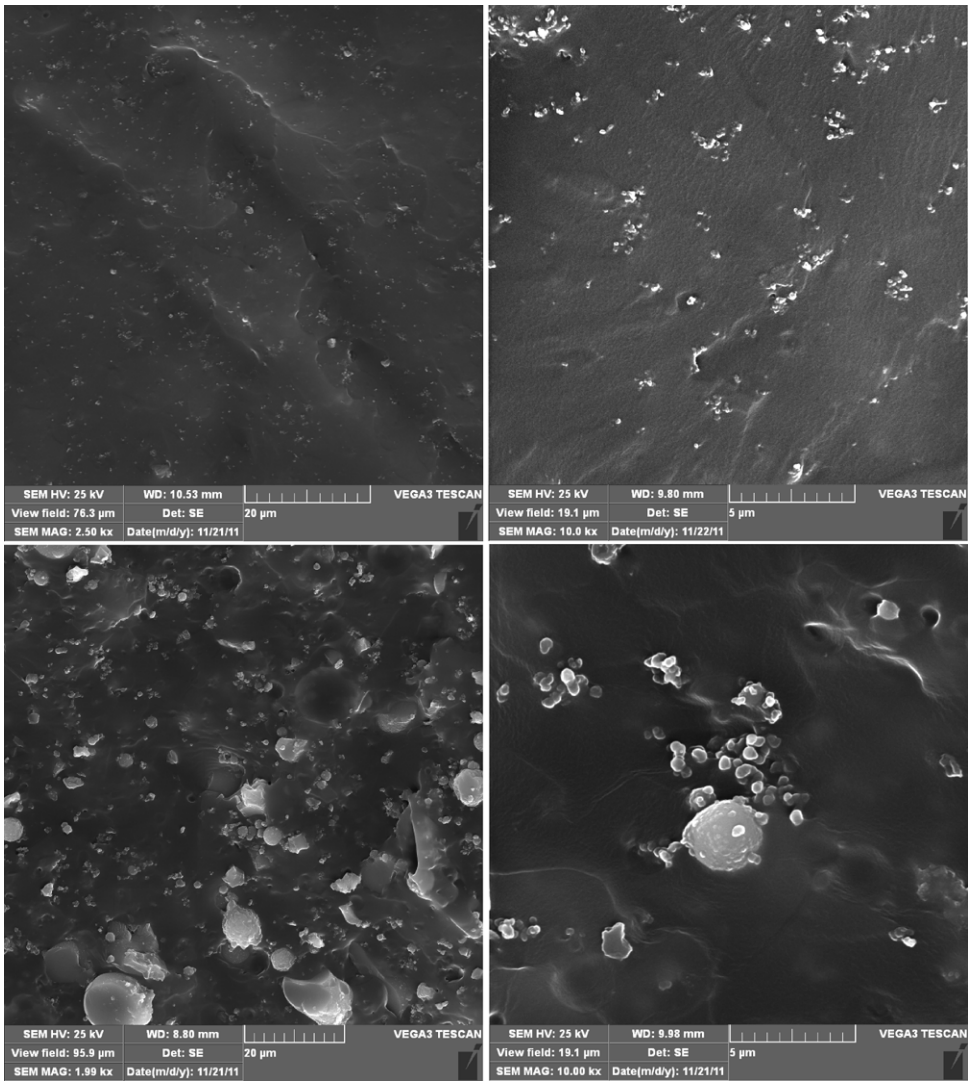

Figure 2.2 SEM micrographs of cross-section of EPDM_5 (top) and EPDM_30 (bottom)

2.3.3 Equilibrium swelling analysis and extractable fraction

The values of q, q_{EPDM}, f and f_{EPDM} in toluene are reported in Table 2.2. For the unfilled rubber, equilibrium swelling analysis is a well-known method to evaluate the number of effective network chains per volume unit (i.e. the crosslinking density) of an elastomer after vulcanization.
In the case of the filled vulcanized rubber, the swelling behaviour depends on complex and different phenomena, such as the crosslinking degree of the rubber matrix, the solvent absorption contribution of the silica phase, the ability of the silica particles to act as crosslinking points (i.e. density of polymer-filler attachments), and so on.

Taking into account that conversion of TEOS to silica was almost quantitative for the samples of Table 2.2, as indicated by the above discussed kinetics analysis, the extractable fraction in toluene was mainly derived from the uncrosslinked fraction of EPDM. In other words, it could be considered an indicator of the progress of the vulcanization process of EPDM.

In principle, the presence of inorganic filler should lead to a reduction of the swelling ratio with respect to the unfilled vulcanized rubber, because of the fact that the filler does not absorb toluene during the experiment. In the present case an opposite trend was observed with both the absolute and normalized swelling ratio values q and q_{EPDM} progressively increasing with the content of silica in the vulcanized rubber. In particular, the increment of q_{EPDM} (i.e., the swelling ratios referring only to the organic rubber phase) was attributable to the decreasing crosslinking density of the rubber phase after vulcanization. This hypothesis is also supported by the observation that f_{EPDM} in toluene increased with increasing silica content (and thus the initial TEOS concentration); this clearly indicates an interfering effect of the sol-gel reaction of TEOS to silica on the vulcanization process of the rubber.

From the swelling and extraction tests, it is possible to conclude that the *in situ* generation of silica particles by means of the sol-gel process led to a hindering effect on the vulcanization process, which limited the extent of the crosslinking of the EPDM phase, as already observed for similar materials based on isoprene rubber. [14]

Table 2.2 Swelling/extraction tests: absolute swelling ratio (*q*) and extractable fraction (*f*) and values normalized with respect to the EPDM content (q_{EPDM} and f_{EPDM})

Material code	q	q_{EPDM}	f / %	f_{EPDM} / %
EPDM_0	3.0	3.0	5.3	5.3
EPDM_05	3.1	3.3	6.8	7.2
EPDM_15	3.7	4.3	7.2	8.5
EPDM_30	5.1	7.0	15.1	20.9

2.3.4 Tensile properties

The results obtained by mechanical characterization (tensile tests) are summarized in Table 2.3. Extraction tests clearly show that the materials under investigation were characterized by different cross-linking densities inversely depending on the silica content. The mechanical properties of the EPDM rubber matrix would then presumably be different for the EPDM_*x* series (in particular the modulus and strength were expected to decrease as a result of the decreasing cross-linking density). Notwithstanding this important consideration, data shown in Table 2.3 indicate that the presence of silica as rigid filler in the elastomeric EPDM matrix led to a significant increase in stiffness (both initial and secant moduli) and of the ultimate properties such as stress at break (σ_b). Concerning the low deformation range, the initial modulus increased monotonically by increasing the silica content with an average value for EPDM_30 (4.48 MPa) 2.5 times higher than that of the unfilled vulcanized EPDM_0 (1.76 MPa). Stiffening and reinforcing effects due to the presence of silica were also observed in a large deformation range with values of secant modulus $E_{sec,\varepsilon=1}$, $E_{sec,\varepsilon=2}$ and $E_{sec,\varepsilon=3}$ and of stress at break σ_b being systematically higher than those of the unfilled rubber. In this case, the maximum values of $E_{sec,\varepsilon}$ and σ_b were observed for the intermediate silica contents (EPDM_15), suggesting that the ultimate properties in the large deformation range were the result of a complex balance between the increasing content of rigid filler and the decreasing crosslinking density of the rubber matrix.

Das and co-workers [16] proposed a 'reinforcing efficiency' (*RE*) parameter to evaluate the reinforcing effect due to the presence of silica with respect to the unfilled rubber. *RE* is defined as the quotient of the difference of the secant moduli at 100% elongation of filled and

unfilled vulcanized rubber ($(E_{sec,\varepsilon=1})_{filled}$ and $(E_{sec,\varepsilon=1})_{unfilled}$, respectively), with reference to the amount of filler ($wt\%SiO_2$). The reinforcing efficiency is thus defined by:

$$RE = \frac{(E_{100\%})_{filled} - (E_{100\%})_{unfilled}}{wt\%\ SiO_2} \qquad (2.5)$$

RE values varied from 0.008 to 0.018, showing a maximum value for the intermediate silica content (EPDM_15, see Table 2.3) as already discussed for secant moduli. Even if a direct comparison can be debatable, taking into account the different vulcanizing agents used and thus the different cross-linking degrees, it is interesting to observe that the present *RE* values are about one order of magnitude lower than those observed by Das *et al*. [16] (in the range 0.03-0.12). These results can be tentatively explained taking into account the absence of any coupling agent for the improvement of filler-matrix interfacial bonding for the materials reported here. The use of triethoxysilyl-grafted EPDM in the above mentioned paper presumably resulted in a better interfacial interaction between the silica particles and the rubber matrix, and thus to a higher reinforcement effect. In this respect, the present solution process could be reasonably enhanced by using a suitable coupling agent for the improvement of filler-matrix adhesion.

Table 2.3 Mechanical characterization: initial modulus (E_{in}), second modulus at an elongation ε= 1,2,3 ($E_{sec,\ \varepsilon=1}$, $E_{sec,\ \varepsilon=2}$, $E_{sec,\ \varepsilon=3}$), stress at break (σ_b), deformation at break (ε_b) and reinforcing efficiency (RE)

Material code	E_{in} / MPa	$E_{sec,\ \varepsilon=1}$ / MPa	$E_{sec,\ \varepsilon=2}$ / MPa	$E_{sec,\ \varepsilon=3}$ / MPa	σ_b	ε_b	RE / MPa.wt%$^{-1}$
EPDM_0	1.76	1.01	0.63	0.53	1.57	3.35	-
EPDM_05	2.06	1.08	0.67	0.53	2.07	4.57	0.013
EPDM_15	2.93	1.28	0.78	0.59	2.32	6.10	0.018
EPDM_30	4.48	1.24	0.69	0.49	2.09	10.14	0.008

Concerning the initial modulus, the effect due of the inclusion of rigid filler particles is known as hydrodynamic reinforcement and can be quantitatively predicted by using the Smallwood-Guth-Einstein equation: [18]

$$E = E_0(1 + 2.5\phi + 14.1\phi^2) \qquad (2.6)$$

in which ϕ represents the filler volume fraction. Notwithstanding the strict assumptions of this equation (the filler particles are spherical, completely wetted by the rubber and interact only pair-wise), it could be a useful preliminary evaluation of the expected hydrodynamic reinforcement due to addition of a rigid filler. The initial elastic modulus E_{in} of filled EPDM predicted by the Smallwood-Guth-Einstein equation is reported in Figure 2.3, together with the experimental data obtained with tensile tests. The figure clearly shows significantly higher modulus values with respect to the theoretical calculation based only on a hydrodynamic effect. Remembering once again that the investigated materials were formed by a rubber matrix having a crosslinking density which decreases by increasing the silica content, it is very interesting to observe the presence of an additional reinforcement with respect to the theoretical prediction, which is attributed to structure effects (the filler aggregates into chair-like structures producing a greater stiffening) and to the introduction of additional crosslinks into the network by the filler.

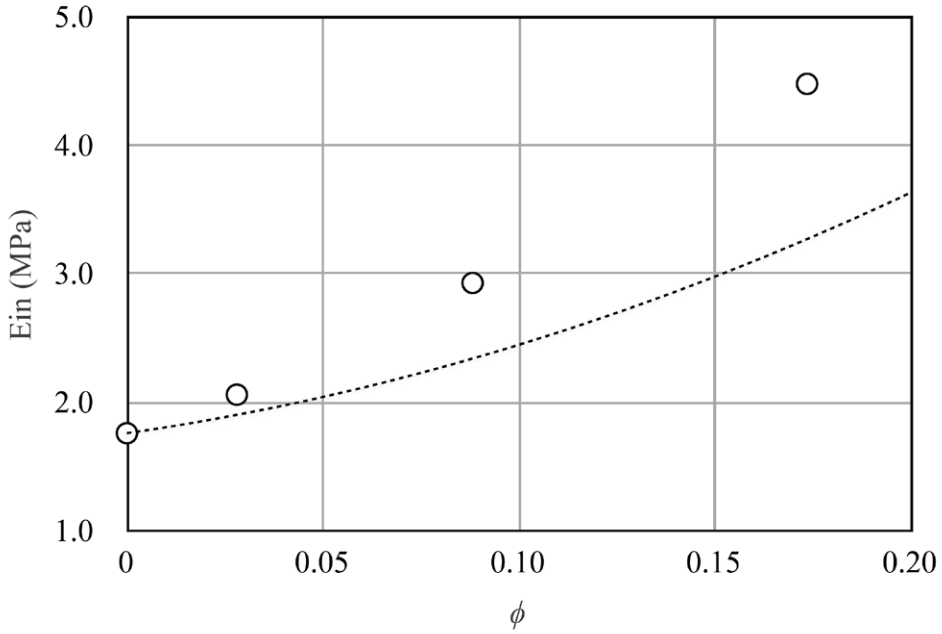

Figure 2.3 Initial elastic modulus as a function of filler volume fraction for EPDM_x: (dashed line) predicted values from the Smallwood-Guth-Einstein equation and (○) experimental data

Kinetic theory predicts that the equilibrium stress in an unfilled vulcanized rubber is proportional to the number of elastically effective network chains supporting the load [19]. This number depends on the primary molecular weight of the rubber, the number of crosslinks forming the network and the number of chain entanglements isolated between these crosslinks. In this respect, additional fixed points in the network generated by filler-rubber attachments could be regarded simply as additional crosslinks. In other words, the mechanical properties of the rubber are modified more than it would have been by means of a mere addition of rigid particles to a soft elastomeric matrix. An additional contribution arises from molecular interaction between the rubber and the filler which can be evaluated by equilibrium swelling tests.

2.3.5 Dynamic-mechanical analysis (DMA)

Storage modulus (*E'*) and loss factor (tan δ) as a function of temperature are reported in Figure 2.4 for the EPDM_*x* samples. The values of storage modulus measured in the rubbery region (at a temperature of 60 °C, that is at about T_g + 100 °C), damping (expressed as maximum value of loss factor, tan δ_{max}) and of the glass transition temperature (determined as the peak temperature value of the loss factor tan δ) are reported in Table 2.4. The DMA results show that some dynamic-mechanical properties of the vulcanized rubber were significantly affected by the silica content. It is usually expected that in particulate filled polymers, the addition of rigid fillers to the polymer matrix restricts the movement of the polymer chains leading to a reduction in damping and a shift of T_g values to higher temperatures [20].

In the present study, a significant reduction of damping (here evaluated as tan δ_{max}) was observed by increasing the silica content in the vulcanized rubber. On the contrary, the glass transition temperature was not affected by the presence of *in situ* generated silica with values ranging from -43 to - 41 °C independent on the silica content. The same results were also obtained by measuring the T_g values by means of differential scanning calorimetry (data reported in Table 2.4). The absence of a significant shift in T_g values to higher temperatures by increasing the filler content could be tentatively attributed to a weak filler-matrix interface or, more probably, to the decrease in the crosslinking density of the rubber matrix (as discussed above) which counterbalanced the presence of the rigid filler.

Concerning the mechanical properties in the rubbery region, a significant increase in storage modulus $E'_{T=60°C}$ was observed by increasing the silica content in the vulcanizates. The $E'_{T=60°C}$ values determined at T_g + 100 °C of unfilled EPDM_0 (1.89 MPa) increased to 2.44, 2.94 and 6.27 MPa for EPDM_05, EPDM_15 and EPDM_30, respectively. The observed trend was in perfect agreement with the tensile properties measured at low deformation (initial modulus, E_{in}) and previously discussed.

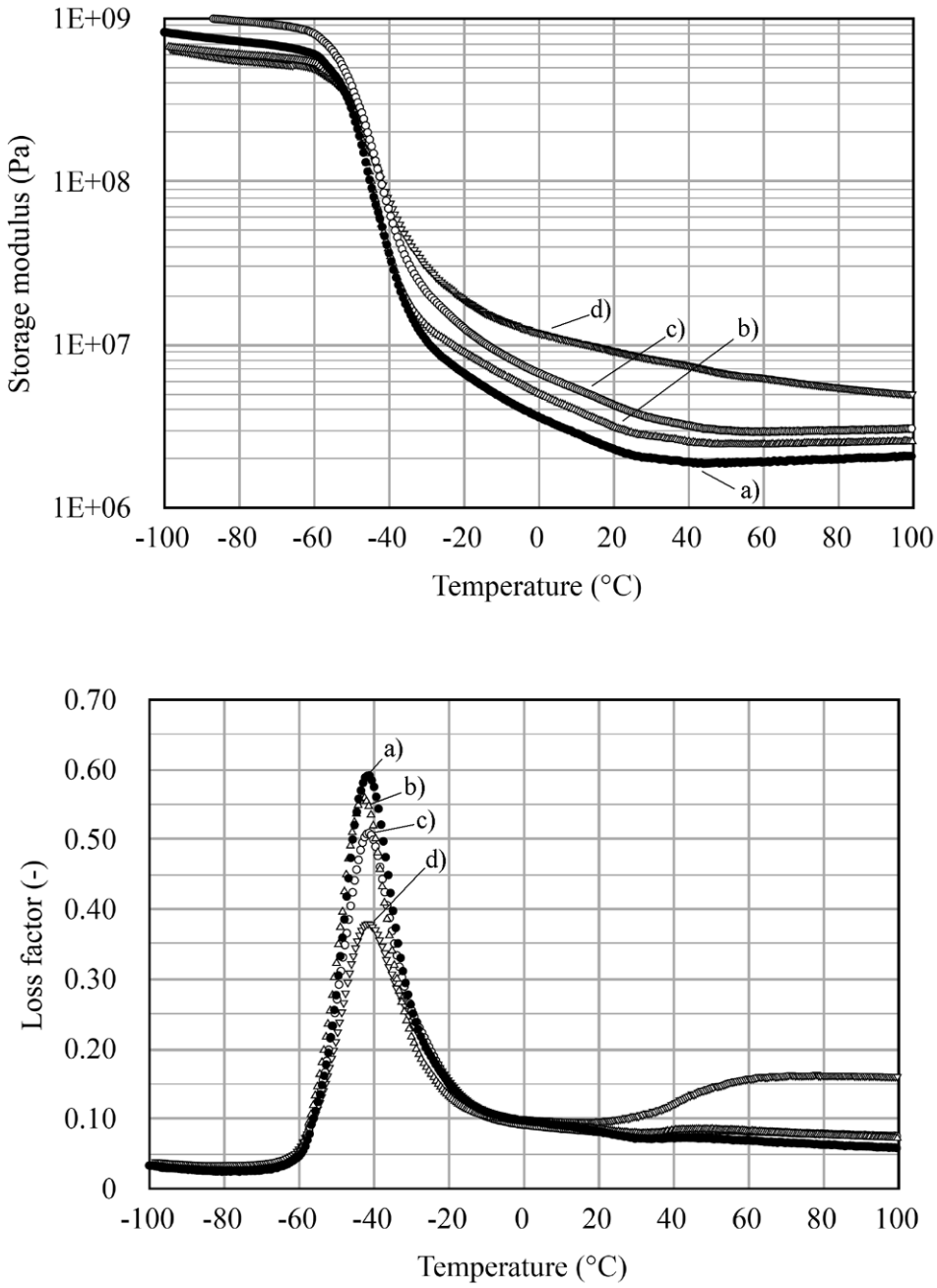

Figure 2.4 Dynamic-mechanical analysis: storage modulus (*E')* and loss factor (tan δ) as a function of temperature a) EPDM_0, b) EPDM_5, c) EPDM_15 and d) EPDM_30

Table 2.4 Storage modulus measured in the rubbery region (at temperature of 60°C, $E'_{T=60°C}$), damping (maximum value of tan δ tan δ_{max}) and glass transition temperature ($T_{g,\,DMTA}$ from tan δpeak value, $T_{g,\,DSC}$ from DSC analysis)

Material code	$E'_{T=60°C}$ / MPa	tan δ_{max}	$T_{g,\,DMTA}$ / °C	$T_{g,\,DSC}$ / °C
EPDM_0	1.89	0.591	-41.6	-50.3
EPDM_05	2.44	5.60	-42.9	-51.2
EPDM_15	2.94	0.509	-41.1	-50.9
EPDM_30	6.26	0.379	-41.4	-51.8

2.3.6 Thermal stability

Representative TGA curves of EPDM_*x* are reported in Figure 2.5. The weight losses of the filled vulcanized rubber (curves b, c and d) occurred in two distinct steps. In the first step, the weight loss at around 100-350 °C was probably due to the evaporation of strongly absorbed water and/or condensation by-products of the reaction of TEOS to silica. The second step, corresponding to the maximum weight loss in the range of 400-470 °C, was ascribed to the thermal decomposition of the polymer chains.

The behaviour of the unfilled EPDM_0 was slightly different due to the absence of silica and eventual by-products of the sol-gel reaction. The first decomposition started at about 270°C up to the main weight loss in the range of 400-470 °C. It is interesting to observe the presence of a third step with a small weight loss at around 470-550 °C, presumably due to the combustion of char residues previously formed.

In general terms, the presence of *in situ* generated silica produced a very limited curve shift towards higher temperatures indicating an almost negligible enhancement of the thermal stability of the filled rubber compared to the unfilled one.

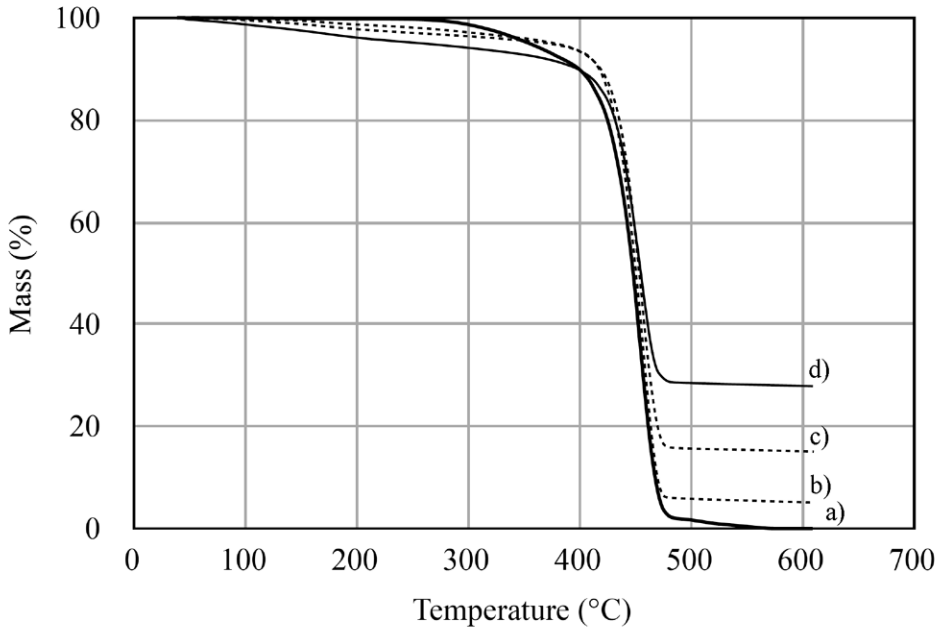

Figure 2.5 Thermograms of a) EPDM_0, b) EPDM_5, c) EPDM_15 and d) EPDM_30

2.3.7 Optical properties

The optical properties of the EPDM_x films can be deduced from the optical photographs and visible spectra reported in Figures 2.6 and 2.7, respectively.

As expected, the transparency evaluated by visual inspection (Figure 2.6) progressively decreased by increasing the filler content, presumably due to scattering phenomena present in the biphasic filled vulcanized rubber, and to the increasing average size of the silica particles. The spectrophotometric analysis carried out in the visible wavelength range (400-800 nm), reported in Figure 2.7, shows that the unfilled EPDM_0 appeared relatively highly transparent with transmittance values ranging from 61 to 76% according to its amorphous and homogeneous character. The presence of a limited amount of silica particles influenced the transparency of the films as shown by the EPDM_5 sample with the transmittance values approximately reduced by half. The transparency was significantly inhibited by further increasing the filler content and particle sizes (EPDM_15 and EPDM_30).

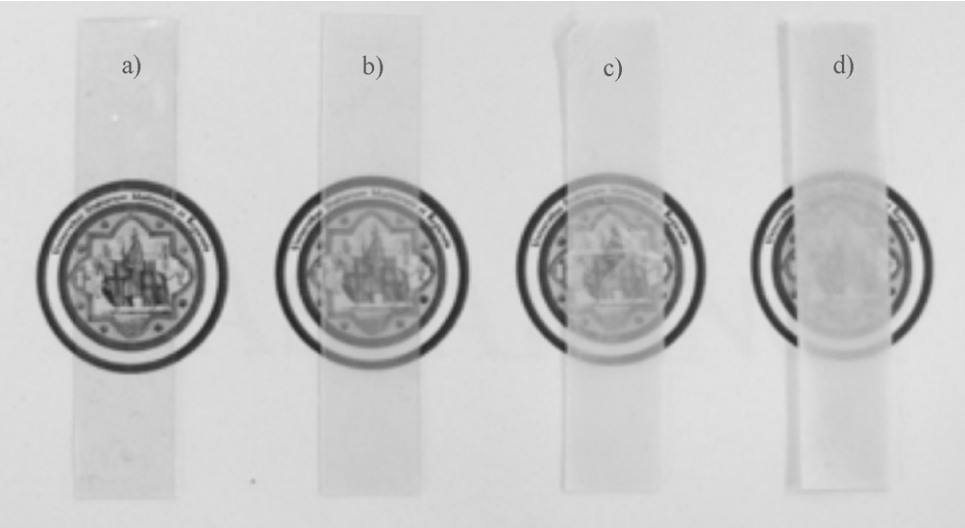

Figure 2.6 Photographs of a) EPDM_0, b) EPDM_5, c) EPDM_15 and d) EPDM_30 films

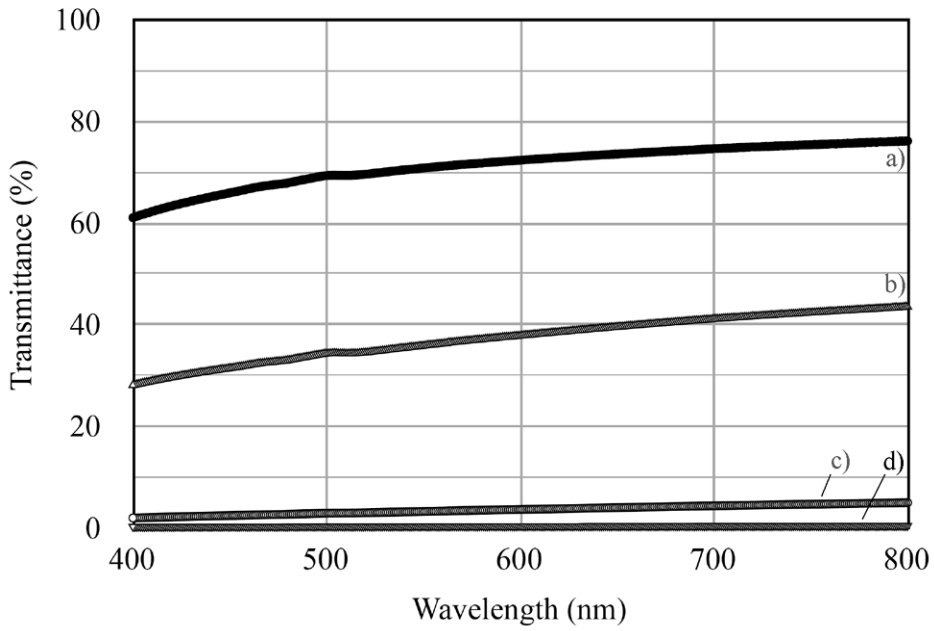

Figure 2.7 Visible spectra of a) EPDM_0, b) EPDM_5, c) EPDM_15 and d) EPDM_30 films

2.4 Conclusions

Silica particles were *in situ* generated in an EPDM matrix by using a sol-gel process. The solution process adopted permitted the preparation of rubbers with very high filler content (greater than 40 wt%) with particle dimensions ranging from 0.2 μm to 2 μm. Particle

diameter, size distribution and agglomeration phenomena were found to increase by increasing the silica content due to coalescence phenomena during the growing of the particles. Optical properties (transparency) were accordingly reduced. Equilibrium swelling and extraction tests indicated a hindering effect of the presence of *in situ* generated silica on the vulcanization process which reduced the cross-linking degree of the vulcanized EPDM rubber. Notwithstanding the decrease in the cross-linking degree of the matrix, both quasi-static tensile tests and dynamic-mechanical analysis showed a significant enhancement in the mechanical properties due to the presence of the reinforcing filler with improvements higher than those expected for a simple hydrodynamic reinforcing mechanism. The thermal stability of the filled rubbers was almost unchanged with respect the unfilled vulcanized rubber.

In conclusion, the use of the solution procedure, possibly coupled with the presence of suitable coupling agent for the enhancement of filler-matrix adhesion, seems to be a very promising way to produce silica reinforced vulcanized EPDM.

2.5 References

1. H. Mouri, K. Akutagawa. Improved tire wet traction through the use of mineral fillers. Rubber Chemistry and Technology 1999; 72:960-968.
   DOI: 10.5254/1.3538845
2. J.W. ten Brinke, S.C. Debnath, L.A.E.M. Reuvekamp, J.W.M. Noordermeer. Mechanistic aspects of the role of coupling agents in silica-rubber composites. Composites Science and Technology 2003; 63:1165-1174.
   DOI: 10.1016/S0266-3538(03)00077-0
3. C.J. Brinker, G.W. Scherer. Sol-gel Science: The Physics and Chemistry of Sol-gel Processing; Academic Press, Inc.: Boston (1990)
   ISBN: 13: 978-0-12-134970-7
4. M. Messori, In Recent Advances in Elastomeric Nanocomposites; V. Mittal; J. K. Kim; K. Pal, Eds.; Springer Berlin Heidelberg, 2011.
5. A. Bandyopadhyay, A.K. Bhowmick. Rubber-silica hybrid nanocomposites. 2008, pp 57.
   DOI: 10.1201/9781420007183.ch3

6. A. Bandyopadhyay, A.K. Bhowmick. Factors influencing the structure and properties of nanocomposites derived by sol-gel technique. Journal of Polymer Engineering. 2006; 26:821-852.
DOI: 10.1515/POLYENG.2006.26.8-9.821
7. J.E. Mark. Ceramic-modified elastomers. Current Opinion in Solid State and Materials Science 1999; 4:565-570.
DOI: S1359-0286(00)00007-3
8. J.E. Mark. Some novel polymeric nanocomposites. Accounts of Chemical Research 2006; 39:881-888.
9. A. Bandyopadhyay, M. Maiti, A.K. Bhowmick. Synthesis, characterisation and properties of clay and silica based rubber nanocomposites. Materials Science and Technology 2006; 22:818-828.
DOI: 10.1179/174328406X101265
10. F. Yatsuyanagi, N. Suzuki, M. Ito, H. Kaidou. Effects of secondary structure of fillers on the mechanical properties of silica filled rubber systems. Polymer 2001; 42:9523-9529.
DOI: 10.1016/S0032-3861(01)00472-4
11. J. Berriot, F. Martin, H. Montes, L. Monnerie, P. Sotta. Reinforcing of model filled elastomers: characterization of the cross-linking density at the filler-elastomer interface by ^{1}H NMR measurements. Polymer 2003; 44:1437-1447.
DOI: S0032-3861(02)00882-0
12. J. Frohlich; W. Niedermeier; H.D. Luginsland. Composites Part a-Applied Science and Manufacturing 36, 449 2005.
13. F. Bignotti, S. Borsacchi, R.de Santis, M.Geppi, M. Messori, U. P. Sudhakaran. Interrelation between preparation conditions, structure, and mechanical reinforcement in isoprene rubber filled with *in situ* generated silica. Journal of Applied Polymer Science2012; 125:E398-E412.
DOI: 10.1002/app.36337
14. M. Messori, M. Fiorini. Isoprene rubber filled with silica generated *in situ*. Journal of Applied Polymer Science 2011; 119:3422-3428.
DOI: 10.1002/app.32992
15. M. Messori, F. Bignotti, R. De Santis, R. Taurino. Modification of isoprene rubber by *in situ* silica generation. Polymer International 2009; 58:880-887.
DOI: 10.1002/pi.2606

16. A. Das, R. Jurk, K.W. Stöckelhuber, G. Heinrich. Silica-ethylene propylene diene monomer rubber networking by *in situ* sol-gel method. Journal of Macromolecular Science, Part A: Pure and Applied Chemistry 2008; 45:101-106.
DOI: 10.1080/10601320701683447
17. Y. Ikeda, Y. Kemeda. Preparation of "green" composites by the sol-gel process: *In situ* filled natural rubber. Journal of Sol-Gel Science and Technology 2004; 31:137-142.
DOI: 10.1023/B:JSST.0000047975.48812.1b
18. G. Kraus. Reinforcement of elastomers; Kraus, G., Ed.; Wiley: New York, 1965, Chap. 4.
19. P.J. Flory, Principles of Polymer Chemistry; Cornell University Press: Ithaca, 1953.
20. L.E. Nielsen, R.F. Landel. Mechanical Properties of Polymers and Composites. Marcel Dekker, Inc.: New York (1994)
ISBN: 0 8247 8964 4

Chapter 3

Influence of *in situ* generated silica nanoparticles on EPDM morphology, thermal, thermomechanical and mechanical properties

This chapter has been accepted as a publication:
T.H. Mokhothu, A.S. Luyt, D. Morselli, F. Bondioli, M. Messori. Influence of in situ generated silica nanoparticles on EPDM morphology, thermal, thermomechanical and mechanical properties. Polymer Composites.

Abstract

Silica nanoparticles were synthesized by means of a sol-gel method and generated in ethylene propylene diene monomer rubber (EPDM) by *in situ* synthesis. The properties were determined using scanning electron microscopy, attenuated total reflectance Fourier-transform infrared spectroscopy, thermogravimetric analysis, tensile testing, dynamic mechanical analysis, swelling tests and gel content determination. The silica particles were homogenously dispersed in the EPDM matrix, with the presence of agglomerates, especially for high silica contents. The swelling experiments showed a decrease in the crosslinking density of the vulcanized rubber due to the presence of the silica nanoparticles. The mechanical properties, however, were significantly improved by the presence of the stiff silica nanoparticles. The effect of the amount of silica on the thermomechanical properties and thermal degradation of EPDM was also investigated. The presence of silica showed an increase in the storage and loss moduli at high temperatures, probably due to the increasing filler content. The thermal degradation analysis showed that the presence of silica particles incorporated in the EPDM matrix had no significant influence on the thermal stability of the composites.

Keywords: EPDM; silica; nanocomposites; morphology; properties

3.1 Introduction

Reinforcing of rubber materials with fillers is the most important aspect in rubber science and technology and has drawn considerable attention in recent years [1-4]. Carbon black has been the most widely used reinforcing filler in the rubber industry for rubbers prepared by conventional methods [5,6]. Silica has also been receiving more attention because of better reduction in heat build-up, tear strength and ageing resistance. Furthermore, silica imparts to the tyre treads a low rolling, wear and abrasion resistance than carbon black [3,6]. However, the main disadvantage of the use of silica, compounded by conventional methods such as melt mixing, is its tendency to form agglomerates inside the rubber matrix, often resulting in poor particle dispersion and high viscosities during mixing. In addition, the incompatibility of the inorganic silica with non-polar matrices such as styrene-butadiene rubber or natural rubber is another major setback.

To solve this problem, the use of different silane coupling agents to improve rubber-filler interaction has been reported [3-5,7,8]. An alternative and interesting method for overcoming the abovementioned difficulties is the application of *in situ* generation of an inorganic oxide (silica, alumina, titania and others) in the rubber matrix by means of a sol-gel process. In principle, *in situ* synthesis allows fine control of particle size and distribution owing to the low the temperature conditions typical of the sol-gel processes. One of the most widely used precursors in sol-gel is the hydrolysis and condensation of tetraethoxysilane (TEOS) to form silica (SiO_2).

The extent of mechanical reinforcement of elastomers is controlled by three main factors, namely filler-matrix interactions, filler-filler interactions and the dispersion state of the filler in the matrix. It is also possible to modify the filler-matrix and filler-filler interactions through the introduction of silane coupling agents in the reaction mixture [7,8]. Studies conducted on the morphology of *in situ* prepared silica composites indicated well dispersed particles in the rubber matrix [8]. Silica/natural rubber composites were investigated, and the silica nanoparticles were functionalized with alkylthiol or alkylpolysulfide. It was observed that the presence of functionalized particles resulted in well-dispersed particles and good interaction with the rubber matrix.

The incorporation of silica nanoparticles for reinforcement is usually associated with improvement in the mechanical, thermal, and thermomechanical properties, as well as the morphology. Das *et al.* [5] investigated the influence of silica particles *in situ* generated in a silane grafted EPDM matrix. The mechanical characterization results indicated an improvement in the reinforcing efficiency. In the present study we investigated the preparation and characterization of EPDM filled with *in* situ generated silica nanoparticles. Our approach is similar to the investigations of Messori *et al.* on the *in situ* generation of silica from TEOS into isoprene [1,6] and EPDM [9] rubbers with *in situ* generated silica. In this investigation, the reaction time of preparation was increased in order to improve the mechanical, thermomechanical and thermal properties of the EPDM matrix.

3.2 Experimental

3.2.1 Materials

Tetraethoxysilane (TEOS), tin(II)2-ethylhexanoate, dicumyl peroxide, toluene and ethanol were all supplied by Sigma-Aldrich. The materials were used as received without further purification. Ethylene propylene diene monomer rubber (EPDM), Polimeri Europa Dutral® TER 4038, density 0.91 g cm^{-3}, was provided by ATG Italy (Castel d'Argile, BO, Italy).

3.2.2 Preparation of EPDM/SiO_2 nanocomposites

The EPDM/SiO_2 composites were prepared by dissolving EPDM rubber in toluene (3g/100ml) at room temperature. This was followed by the addition of TEOS, H_2O, ethanol and tin(II)2-ethylhexanoate (1.0:4.0:4.0:0.04 mol ratio). The reaction mixtures were magnetically stirred and heated at 80 °C for 20 hours to activate the hydrolytic condensation of TEOS to silica (SiO_2). The solutions were cooled to room temperature, followed by the addition of dicumyl peroxide (DCP) (1 wt% with respect to EPDM) under stirring. The reactions were taken to a rotating evaporator for elimination of about 80% of solvent and other by-products. The samples were obtained by casting the solution in Petri dishes and dried overnight. The cast samples of EPDM/SiO_2 (90/10, 80/20, 70/30 w/w) were vulcanized by compression at 160 °C for 20 min.

3.2.3 Characterization methods

The morphologies of the EPDM/SiO_2 nanocomposites were examined by a TESCAN VEGA3 scanning electron microscope (SEM) at a voltage of 25 kV. Cross-sections of the samples were coated with gold by an electro deposition method to impart electrical conduction before the SEM micrographs were recorded.

ATR-FTIR spectra of the pure EPDM and its silica filled composites were obtained using a Perkin Elmer Spectrum 100 FTIR spectrometer. The samples were analyzed over a range of 600-4000 cm^{-1} with a resolution of 4 cm^{-1}. All the spectra were averaged over 16 scans.

The crosslinking degree was determined through equilibrium swelling tests by immersing at least three rectangular specimens for each composition in 15 ml of toluene at room temperature for several hours, and the mean values are reported. The solvent was replaced hourly after each measurement to eliminate all uncross-linked fractions, such as unvulcanized EPDM chains, which could lead to incorrect values of the swelling ratio. Equilibrium swelling was determined until the swollen mass (m_s) reached a constant value, after which the samples were dried to constant mass (dried mass (m_d)) and the absolute swelling ratio (q) was evaluated according to Equation 3.1.

$$q = \frac{m_s}{m_d} \tag{3.1}$$

The absolute extractable fraction (f), where m_0 is the mass of the sample before immersion in toluene, was determined using Equation 3.2.

$$f = \frac{m_o - m_d}{m_o} \times 100 \tag{3.2}$$

The values of q and f were also normalized to the actual EPDM weight. Their values were determined using Equations 3.3 and 3.4.

$$q_{EPDM} = \frac{q}{c_{EPDM}} \tag{3.3}$$

$$f_{EPDM} = \frac{f}{c_{EPDM}} \quad (3.4)$$

where c_{EPDM} is the weight fraction of EPDM present in the composites. The gel content was determined using Equations 3.5 to 3.7, where m_{EPDM} is the mass of EPDM without silica and $\%wt_{EPDM}$ is the weight % EPDM in the composite.

$$m_{EPDM} = m_0 \times \%wt_{EPDM} \quad (3.5)$$

$$\%\, Extraction = \frac{m_o - m_d}{m_{EPDM}} \times 100 \quad (3.6)$$

$$\%\, Gel = 100 - \%\, Extraction \quad (3.7)$$

Thermogravimetric analysis (TGA) was performed with a Perkin Elmer STA6000 simultaneous thermal analyzer. The analysis was done under flowing nitrogen at a constant flow rate of 20 ml min^{-1} and the samples (20-25 mg) were heated from 25 to 600 °C at a heating rate of 10 °C min^{-1}.

The tensile properties of the samples were determined using a Hounsfield H5KS tensile tester at a crosshead speed of 100 mm min^{-1} and 20 mm gauge length at ambient temperature. The samples were rectangular shaped with a width of 12 mm and a thickness varying between 0.47 and0.67 mm. At least five specimens were tested for each composition, and the mean values are reported. For comparison, Young's modulus was predicted according to Nielsen's theoretical model [10-14].

The dynamic mechanical analysis (DMA) of the samples was done in a Perkin Elmer Diamond DMA dynamic mechanical analyzer. Rectangular shaped samples with dimensions of 40 mm length, 10 mm width and thickness varying between 0.47 and 0.67 mm thick were tested in the tensile mode, while heated under nitrogen flow from -100 ºC to 100 ºC at a heating rate of 3 ºC min^{-1}, and at a frequency of 1 Hz.

3.3 Results and discussion

3.3.1 Scanning electron microscopy (SEM)

The SEM micrographs of cross-sections of the EPDM/SiO_2 composites are shown in Figures 3.1 to 3.3, while the particle size distributions are shown in Figure 3.4. The particle size distribution was determined from an average of 40 particles per sample. The light areas in the micrographs correspond to the silica particles and are spherically shaped. The EPDM/SiO_2 samples show that the silica particles are homogeneously dispersed in the rubber matrix and have good particle-matrix adhesion, which confirms the effectiveness of the *in situ* filler generation process used for the preparation of the filled rubbers. In this investigation, the silica filled composites showed both large and small particles in the composites (Figures 3.1 to 3.3) and the particle size distribution (Figure 3.4) was determined from the fairly visible particles. Figure 3.4 shows an obvious increase in particle size with increasing amount of filler in EPDM, but Figure 3.2 shows a fairly good dispersion of filler agglomerates in the EPDM matrix. By increasing the TEOS content in order to obtain higher silica content in EPDM, an increase in the particle sizes occurred. The presence of an increase in agglomeration have been observed and reported by other authors for similar systems [1,2]. This behaviour can be explained by an increase in coalescence of the growing silica particles when increasing the amount of *in situ* formed dispersed phase. Furthermore, the silica particles may also have agglomerated in the suspension, because the hydrophilic silica particles have a tendency to associate via hydrogen bonding [3].

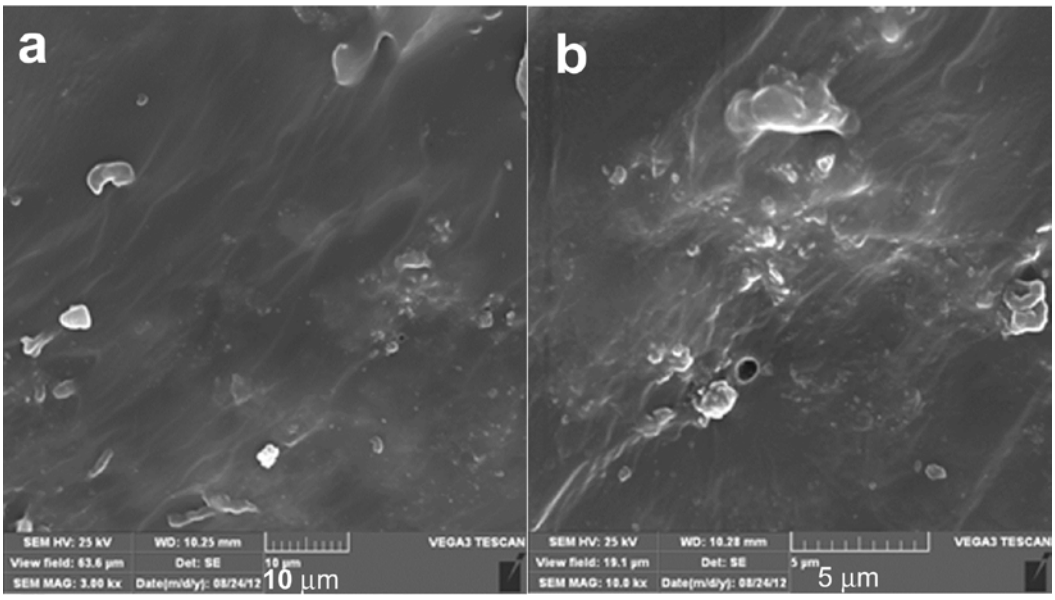

Figure 3.1 SEM micrographs of the 90/10 w/w EPDM/SiO_2 composite

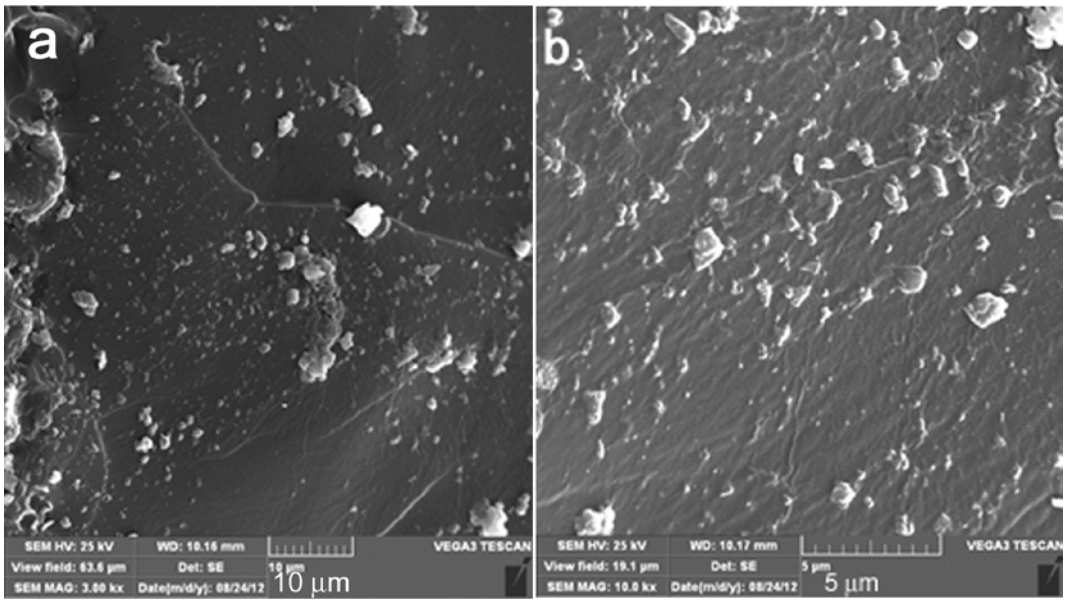

Figure 3.2 SEM micrographs of the 80/20 w/w EPDM/SiO_2 composite

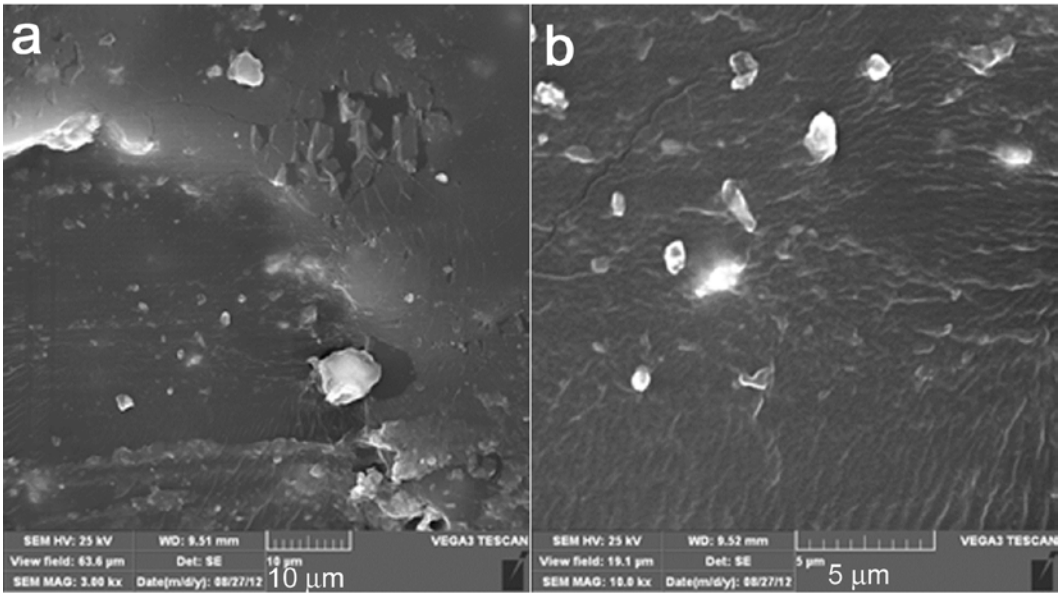

Figure 3.3 SEM micrographs of 70/30 EPDM/SiO_2 composite

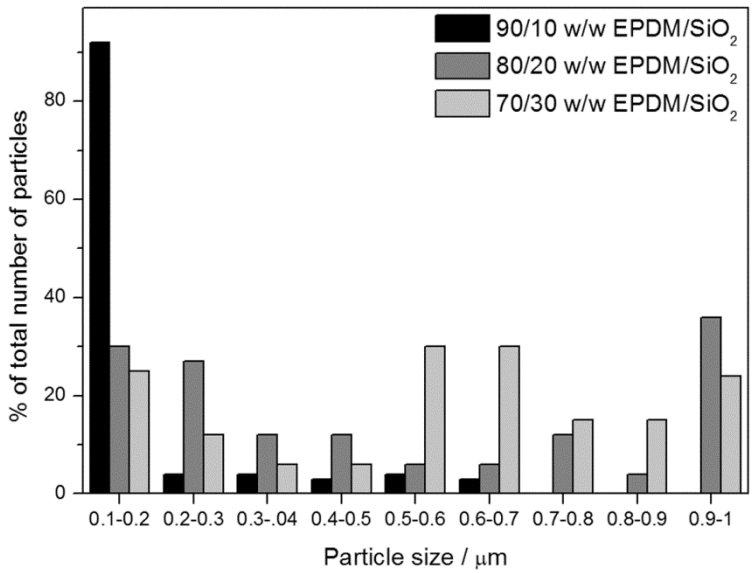

Figure 3.4 Particle size distribution graphs of the EPDM/SiO_2 composites

3.3.2 Fourier-transform infrared (FTIR) spectroscopy

The FTIR spectra of EPDM and the EPDM/SiO_2 composites are shown in Figure 3.5, where both the neat rubber and its composites have two strong absorption peaks around 2920 and 2850 cm^{-1} assigned to the C-H stretching vibration. A small broad absorption band in the region of 3400-3500 cm^{-1} indicates the stretching vibration of the –OH groups, due to surface silanol groups and/or water absorption taking place during synthesis. The peaks at 721, 1376 and 1464 cm^{-1} are assigned to the CH_2 stretching, and the CH_3 and CH_2 bending respectively [15,16]. During the sol-gel process, the inorganic silica is generated from hydrolysis and condensation of TEOS through the following chemical reactions:

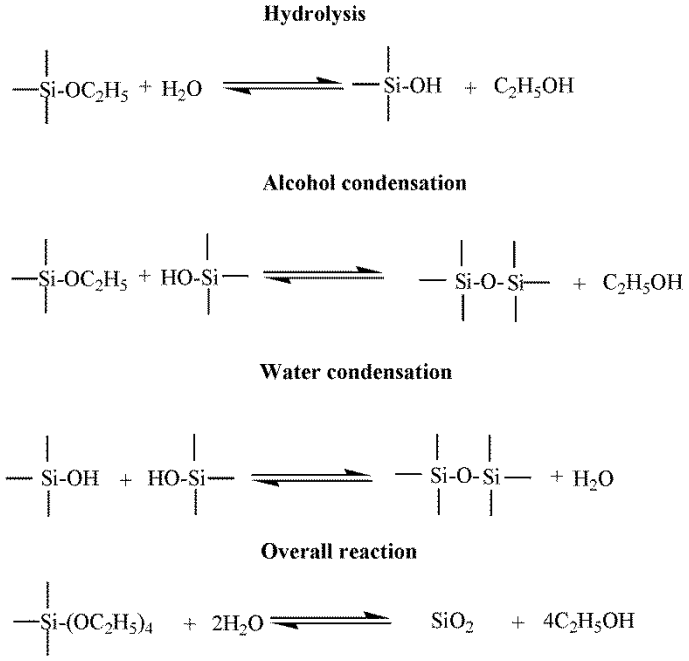

The ethoxysilane group (-Si-OC_2H_5) from TEOS can undergo hydrolysis by water to form silanol (Si-OH). The resulting silanol groups can then react further with the ethoxysilane or with each other to form siloxane (Si-O-Si). The presence of siloxane is observed from the FTIR spectra of the EPDM/SiO_2 composites (Figure 3.5) showing the stretching vibrations of the siloxane (Si-O-Si) bonds in the region of 1060 cm^{-1}. The siloxane networks form silica that can be observed as white particles embedded in the rubber matrix. However, it seems as if not all of the ethoxysilane groups have hydrolyzed to form silanol groups, or some may have hydrolyzed to form silanol groups and did not react to form siloxane networks. This can be seen from the presence of an asymmetric stretch in the region of 802 cm^{-1} assigned to the Si-O-C linkage in unhydrolyzed TEOS, or in siloxane grafted to the matrix during vulcanization. Such a grafting reaction would have consumed DCP so that less DCP would be available to initiate rubber crosslinking. The presence of a small C-O bending vibration around 1644 cm^{-1} may come from ethoxysilane groups grafted onto the matrix [7]. The small peak at 951 cm^{-1} is due to Si-O stretching, indicating the presence of some silanol (Si-O-H) groups in the samples that did not react to form siloxane groups [17-19].

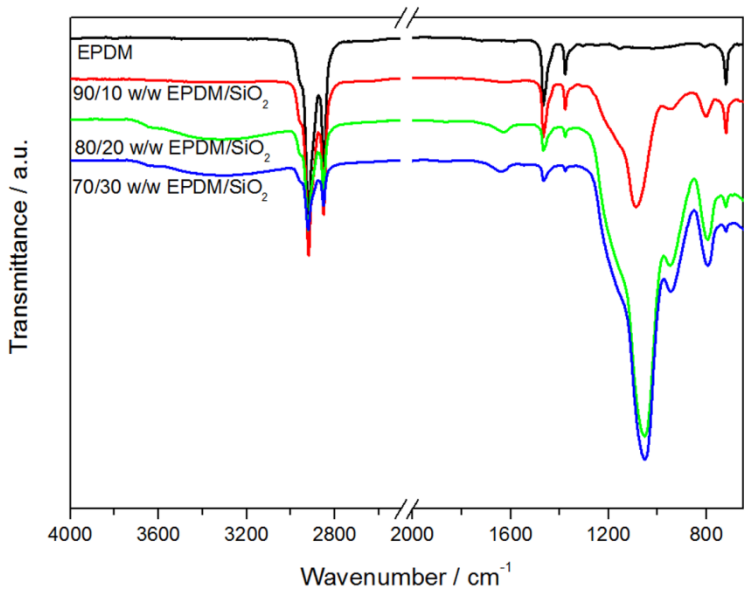

Figure 3.5 FTIR spectra of EPDM and the EPDM/SiO_2 composites

3.3.3 Nominal and actual silica content

The nominal and actual silica concentrations are reported in Table 3.1. The volume fraction values were calculated using the experimentally determined density of silica obtained from TEOS in similar experimental conditions (ρ_{SiO2} = 1.66 g cm^{-3}), and assuming complete conversion of TEOS to silica during the sol-gel reaction. The actual silica content after conversion was determined through TGA analysis as the percentage residue after heating to 600 ^{o}C. The data in Table 3.1 indicate incomplete conversion of TEOS to silica and the silica yield was in the range of 68-89%. Higher conversion of TEOS to silica was observed for the composites with high silica content. The small standard deviation values in Table 3.1 indicates that the silica particles were fairly well dispersed in the rubber matrix, because samples were taken from different positions in the pressed sheets for the repeat TGA analyses.

Table 3.1 Composition of the prepared materials ([1]nominal value calculated by assuming complete conversion of TEOS to silica; [2]experimental value obtained by TGA)

Samples	SiO_2 content[1] / wt%	SiO_2 content[2] / wt%	SiO_2 volume fraction
90/10 w/w EPDM/SiO_2	10	6.8 ± 0.4	0.06
80/20 w/w EPDM/SiO_2	20	16.8 ± 1.5	0.12
70/30 w/w EPDM/SiO_2	30	26.70 ± 0.01	0.18

3.3.4 Equilibrium swelling and gel content

The equilibrium swelling and gel content analysis of vulcanized EPDM and EPDM/SiO_2 composites are reported in Table 3.2. The absolute swelling ratio (q) and absolute extractable fraction (f) were determined from equations 3.1 and 3.2, while the normalized values with respect to the EPDM content (q_{EPDM} and f_{EPDM}) from equations 3.3 and 3.4. Equilibrium swelling analysis is well known to evaluate the crosslinking density obtained after vulcanization of unfilled rubber. In the case of silica filled rubber composites, the swelling behaviour could be influenced by (1) the ability of the silica particles to act as crosslinking points and/or absorb solvent; (2) the crosslinking degree of the unfilled rubber matrix. In the present study the silica particles did not act as crosslinking points in the vulcanized rubber matrix. This can be seen in the linear increase in the absolute and normalized swelling ratio (q and q_{EPDM}) and extractable phase (f_{EPDM}) values, and in the decreasing gel content values, with increasing SiO_2 content (Table 3.2). The reason for the lower crosslink densities of the rubber with increasing silica content, and therefore with increasing amounts of TEOS during the sol-gel reaction in the presence of the rubber, is that increasing amounts of DCP were utilised for the grafting of silanol or ethoxysilane groups onto the rubber chains so that less DCP was available to initiate crosslinking of the rubber chains. Similar observations were made by Messori *et al*. [6] who filled isoprene rubber (IR) with silica particles generated by means of *in situ* synthesis through a sol-gel process. It was clear that the presence of *in situ* generated silica particles inhibited the vulcanization process and, therefore, limited the extent of crosslinking of the IR rubber, similar to our observations on EPDM rubber. This was also observed in another study where EPDM rubber was reinforced with *in situ* generated silica [9], but where much shorter reaction times were used. Here the absolute swelling ratio (3.3-5.1) and extractable fraction (6.8-15.1) values also increased with increasing silica content, but they were in the same range as the ones listed in Table 3.2. However, as explained later

on, the samples in our study show significantly higher modulus values. The reason for this is probably that gelation occurs after relatively short reaction times, but that the crosslinked network formed immediately after gelation still allows a fair amount of chain mobility. With longer reaction times a more extensive crosslinked network is formed when grafted and/or unreacted fractions of TEOS react further to form more crosslinks between the rubber chains.

Table 3.2 Swelling ratio and gel content of EPDM and EPDM/SiO_2 composites

Samples (w/w)	q	q_{EPDM}	f / %	f_{EPDM} / %	*Gel* / %
EPDM	3.7 ± 0.2	3.7 ± 0.2	6.4 ± 2.5	6.4 ± 2.5	93.6 ± 2.5
90/10 EPDM/SiO_2	4.7 ± 0.5	5.1 ± 0.5	8.5 ± 1.2	9.4 ± 1.3	90.6 ± 1.4
80/20 EPDM/SiO_2	5.9 ± 0.4	7.0 ± 0.4	14.5 ± 5.0	18.1 ± 6.2	81.9 ± 6.2
70/30 EPDM/SiO_2	4.7 ± 0.3	6.6 ± 0.4	18.1 ± 4.8	22.3 ± 4.6	77.7 ± 4.6

Absolute swelling ratio (q) and extractable fraction (f) and values normalized with respect to the EPDM content (q_{EPDM} and f_{EPDM})

3.3.5 Thermogravimetric analysis (TGA)

The TGA curves of the EPDM rubber and the silica filled composites are shown in Figure 3.6. The thermal stabilities were characterized in terms of temperatures taken at the onset and at 50% mass loss (Table 3.3). The TGA curves of the EPDM/SiO_2 nanocomposites show two distinct mass loss steps, and the amount of char increases with silica content (Table 3.3). The first volatilization observed from 100 °C is due to the loss of water and alcohol, and at higher temperatures around 350 °C to organic by-products such as unhydrolyzed TEOS. The second volatilization step around 400-470 °C is related to the main degradation of the EPDM rubber. Figure 3.6 also shows that, except for the increase in the amount of residue at 600 °C with increasing silica content, the presence of silica nanoparticles in the vulcanized rubber had little influence on the thermal stability of EPDM, which was also observed and likewise explained by Morselli *et al*. [9]. Therefore, the longer reaction times did not have a significant influence on the thermal stability. This is probable because the longer reaction times did not have a significant influence on the silica content or dispersion in the EPDM [9].

Table 3.3 Summary of the TGA results for the EPDM rubber and its composites

Samples	T_{onset} / °C	$T_{50\ \%}$ / °C	% SiO_2
EPDM	445 ± 0	468 ± 0	0
90/10 w/w EPDM/SiO_2	448 ± 5	471 ± 2	6.8 ± 0.4
80/20 w/w EPDM/SiO_2	443 ± 3	471 ± 1	16.8 ± 1.5
70/30 w/w EPDM/SiO_2	443 ± 4	472 ± 2	26.7 ± 0.01

T_{onset} and $T_{50\%}$ means temperatures at the onset and 50% weight loss

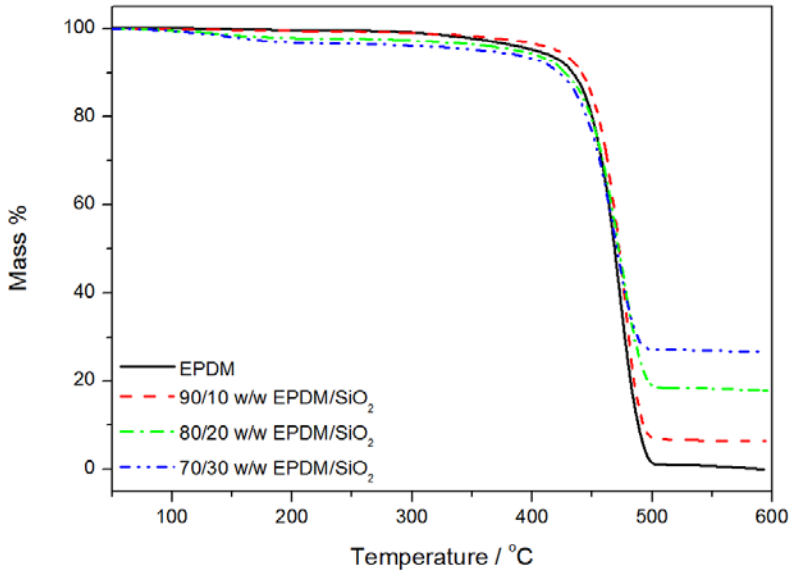

Figure 3.6 TGA curves of EPDM and the EPDM/SiO_2 composites

3.3.6 Tensile testing

The Young's modulus as function of volume fraction of neat EPDM and its silica filled composites are shown in Figures 3.7. The values for Young's modulus, reinforcing efficiency (RE), as well as stress and elongation at break, are summarized in Table 3.4. In Figure 3.7, the Young's modulus was predicted according to Nielsen's theoretical model [10-14]. For composite materials consisting of spherical particles in the matrix, the Nielsen equation has the form given in Equations 3.8 and 3.9.

$$E = E_1 \left[\frac{1+AB\phi_2}{1-B\psi\phi_2}\right] \qquad (3.8)$$

$$B = \frac{{}^{E_2}/_{E_1} - 1}{{}^{E_2}/_{E_1} + A} \qquad (3.9)$$

where E, E_2 and E_1 are the modulus values of the composite, filler and matrix respectively, while ϕ_2 is the volume fraction of the filler assuming spherical particles. The theoretical modulus of silica particles used was E_2 = 70 GPa [20]. The factor ψ takes into account the values of ϕ_m of the dispersed phase and it is given by Equation 3.10.

$$\psi = 1 + \left[\left(\frac{1 - \phi_m}{\phi_m^2}\right)\phi_2\right] \qquad (3.10)$$

where ϕ_m is the maximum packing fraction which is equal to 0.37 [13,14]. The constant B takes into account the relative moduli of the filler and matrix phases; its value is 1.0 for very large E_2/E_1 ratios (the values for E_2 and E_1 are 70 GPa and 2.4 MPa, respectively, and therefore we could confidently use a value of 1.0). The constant A is related to the Einstein coefficient and is determined by the morphology of the system; for strong aggregates, the value of A can become quite large and ϕ_m of the dispersed phase decreases. In our case the values of A were varied (16, 25 and 30) and they are higher than the average values used for spherical particles. It is clear from Figure 3.7 that A = 25 gives the best fit of the experimental modulus values. It is difficult to explain the exceptionally high value of A since the constant A does not uniquely define the morphology of the system and it can be the same for more than one kind of morphology. For example, aggregates of spheres can have the same coefficient as short fibres or rods [13,14]. One explanation for this large value of A is the increased and considerable agglomeration of the silica particles with increasing silica content in the EPDM, as can be seen from the particle size distributions in Figure 3.4. The effect can be so strong that the particles form chains and networks which decreases ϕ_m and therefore increase the modulus.

It is further interesting to observe that both the stress and elongation at break increase for 10 and 20 wt.% silica (Table 3.4). This is probably the result of improved adhesion between the filler and the matrix because of good interfacial interaction between the matrix and the filler resulting from the sol-gel process, giving rise to effective stress transfer. The decrease of both the stress and elongation at break for the composite containing 30 wt.% silica is probably the result of less effective stress transfer between the filler and the matrix as a result of more

extensive aggregation. Aggregation of fillers in the composite can cause a dewetting or crazing effect in which the adhesion between the filler and matrix phase is destroyed and can result in a significant decline in mechanical properties. Morselli *et al*. [9], who investigated the same system at much shorter reaction times, also observed an increase in tensile modulus (1.76-4.48 MPa), stress at break (1.57-2.09 MPa) and elongation at break (335-1014%) values with increasing silica content, but their modulus values were significantly lower than the ones listed in Table 3.4, while the stress at break values were slightly lower and the elongation at break values compared well with the ones in Table 3.4. These observations may be explained through the formation of a more extensive crosslinked network when grafted and/or unreacted fractions of TEOS react further to form more crosslinks between the rubber chains.

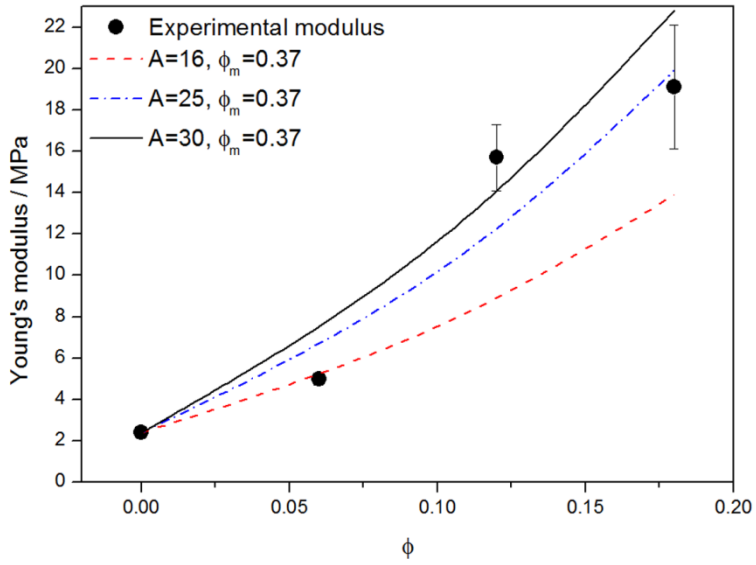

Figure 3.7 Young's modulus as a function of volume fraction of silica in the EPDM/SiO_2 composites, and comparison of the experimental data with predictions by Nielsen model

Table 3.4 Summary of tensile results of unfilled and filled EPDM composites

Samples	σ_b / MPa	ε_b / %	E / MPa	RE / MPa.wt%$^{-1}$
EPDM	1.7 ± 0.5	482 ± 84	2.4 ± 0.3	-
90/10 w/w EPDM/SiO_2	3.4 ± 0.8	949 ± 371	5.0 ± 0.3	0.08 ± 0.01
80/20 w/w EPDM/SiO_2	2.9 ± 0.5	956 ± 242	15.7 ± 1.6	0.03 ± 0.00
70/30 w/w EPDM/SiO_2	1.9 ± 0.2	540 ± 280	19.1 ± 3.0	0.02 ± 0.01

The reinforcing efficiency (RE) was calculated using Equation 3.11, where $E_{100\%}$ is the modulus at 100% elongation and wt% SiO_2 is the amount of filler in the investigated sample, and the values are listed in Table 3.4.

$$RE = \frac{(E_{100\%})_{filled} - (E_{100\%})_{unfilled}}{wt\%\ SiO_2} \qquad (3.11)$$

The 90/10 w/w EPDM/SiO_2 sample shows the highest reinforcing efficiency because the silica particles were less agglomerated which would have improved the interaction between EPDM and the filler particles. Das *et al*. [5] investigated the influence of silica particles *in situ* generated in silane grafted EPDM. They observed that the well dispersed particles, that probably had a good interaction with the matrix due to the silane grafting, showed a reasonably good RE (ranging from 0.06-0.03, dependent on the modification times). In our case no coupling agent was used and the dispersion was not that good, but we still achieved similar reinforcing efficiencies. We did observe well dispersed particles, and the relatively high RE values indicate that in addition there may also be good interaction between the EPDM matrix and the silica filler.

3.3.7 Dynamic mechanical analysis (DMA)

The dynamic mechanical analysis results are shown in Figure 3.8. The maximum damping factor (tan δ) values, the glass transition temperature (T_g), and the storage modulus at 50 °C are summarized in Table 3.5. Above the glass transition temperature these composites show an increase in the storage and loss moduli with increasing silica content (see $E'_{T=50°C}$ values in Table 3.5). These modulus values depend on both the crosslinking degree of the rubber matrix and the content of the rigid dispersed phase. Both these factors will contribute to an increase in modulus. However, as discussed above, in our case the crosslinking density decreased with increasing filler content, which would cause a decrease in modulus. It is, however, clear that the effect of increasing amounts of silica dominated the effect of decreasing crosslinking degree on the rubber modulus. Similar observations and explanations were reported in the investigation of IR/SiO_2 composites generated *via in situ* synthesis by Messori *et al.* [6]. This group also investigated EPDM rubber reinforced with *in situ* generated silica [9], but in their case much shorter reaction times were used. Their storage modulus values also increased with increasing silica content, but they were significantly lower than the ones listed in Table 3.5.

The reason for this is the same than the one mentioned during the discussion of the tensile modulus results. When shorter reaction times were used, the number of crosslinks were probably enough to form sufficient networks to give relatively high gel content values, but the crosslink density was low enough to allow sufficient chain movement so that the modulus values were not too high. The higher crosslink density that resulted from secondary reactions during longer reaction times then led to higher modulus values.

Table 3.5 Values extracted from the DMA curves of unfilled and silica filled EPDM

Samples	$E'_{T=50°C}$ / MPa	$(\tan \delta)_{max}$	T_g / °C
EPDM	3.2	0.622	-41.5
90/10 w/w EPDM/SiO_2	7.9	0.459	-42.6
80/20 w/w EPDM/SiO_2	10.2	0.320	-45.0
70/30 w/w EPDM/SiO_2	26.2	0.270	-43.1

The tan δ curves (Figure 3.8) show a decrease in peak intensity at the glass transition of the rubber with increasing silica content. This is due to the decreasing amount of rubber with increasing silica content. The glass transition temperature (T_g) decreased by 1–4 °C for the silica-containing samples (Table 3.5), which is in agreement with the equilibrium swelling and gel content results, that indicated a decrease in the crosslinking density of the vulcanized rubber. Further explanations of this behaviour was suggested by Messori *et al.* [6], who investigated IR/SiO_2 composites generated via *in situ* synthesis, and by Ikeda *et al.* [22], who investigated styrene-butadiene rubber (SBR) filled composites generated via *in situ* synthesis. Messori suggested that the decrease is due to the higher mobility of the polymer chains due to larger free volume caused by the presence of non-adhering nano-objects inside the polymer bulk, while Ikeda suggested that the rubber may have been plasticized by residual oligomers from the sol-gel reaction. Another explanation may be that the swelling in TEOS caused disentanglement of the EPDM chains in the vulcanizates. In general the presences of silica particles have significantly improved the thermomechanical properties of the EPDM, which is in agreement with the observed improvement in mechanical properties.

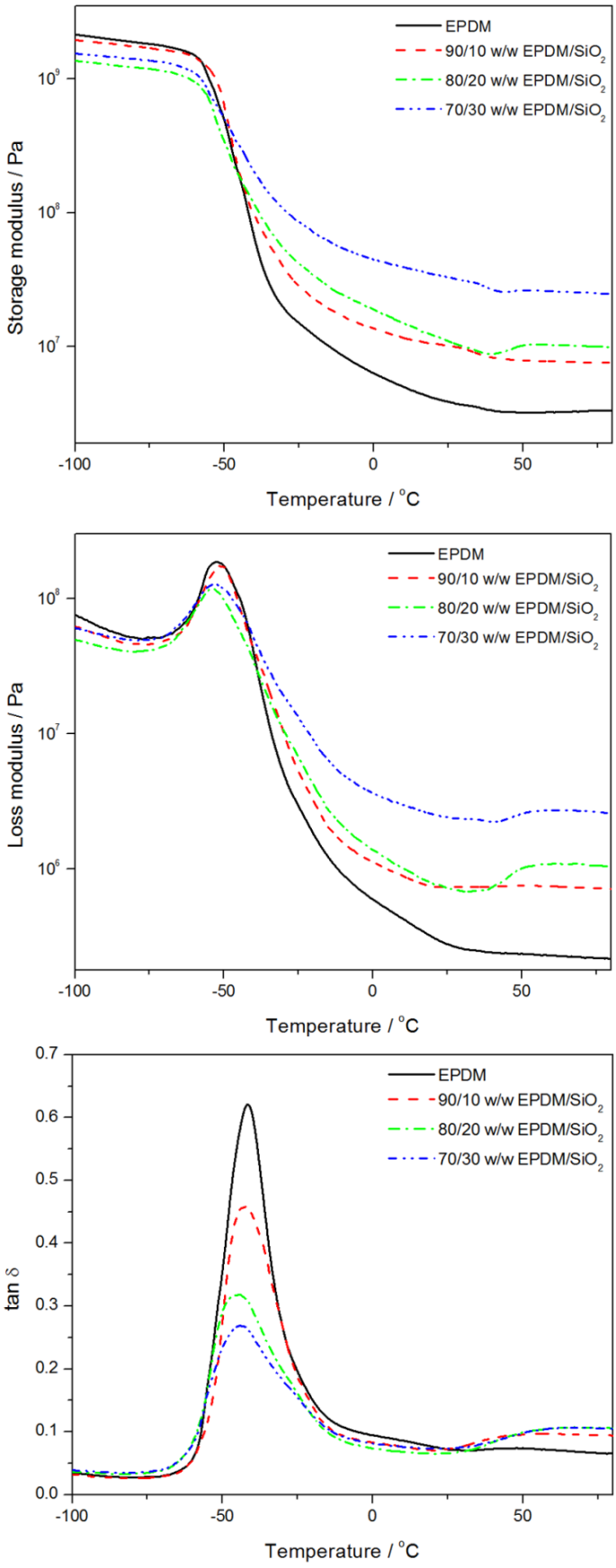

Figure 3.8 DMA storage modulus, loss modulus and damping factor as a function temperature of EPDM and the silica filled composites

3.4 Conclusions

The influence of *in* situ generated silica particles on the morphology and properties of vulcanized EPDM rubber was investigated. The particle size and agglomeration of the silica particles increased with increasing the silica content, due to the stronger particle-particle interactions. The swelling and gel content studies indicated a decrease in the crosslinking density of the vulcanized EPDM rubber, which was caused by a reduced amount of DCP available to initiate crosslinking, because the DCP was partially utilised in the grafting of ethoxysilane groups onto the rubber chains. Although the gel content decreased, there was a significant increase in modulus with increasing silica content. This seems to be primarily due to the high modulus of the silica particles, especially when they agglomerate and form particle-particle networks at higher silica contents. The silica particles had no significant influence on thermal stability of the vulcanised EPDM. When the results of this study are compared with those of another similar study, where much shorter reaction times were used, it is clear that only the properties that are determined by the extent of crosslinking (which is higher for the longer reaction times) show significant differences when compared with the results where shorter reaction times were used.

3.5 References

1. M. Messori, F. Bignotti, R. De Santis, R. Taurino. Modification of isoprene rubber by *in situ* silica generation. Polymer International 2009; 58:880-887.
   DOI: 10.1002/pi.2606
2. Y. Ikeda, Y. Kemeda. Preparation of “green” composites by the sol-gel process: *In situ* filled natural rubber. Journal of Sol-Gel Science and Technology 2004; 31:137-142.
3. S. Prasertsri, N. Tattanasom. Mechanical and damping properties of silica/natural rubber composites prepared from latex system. Polymer Testing 2011; 30:515-526.
   DOI: 10.1016/j.polymertesting.2011.04.001
4. J. Siramanont, V. Tangpasuthadol, A. Intasiri, N. Na-Ranong, S. Kiatkamjornwon. Sol-gel process of alkyltriethoxysilane in latex for alkylated silica formation in natural rubber. Polymer Engineering and Science 2009; 49:1099-1106.
   DOI 10.1002/pen.21363

5. A. Das, R. Jurk, K.W. Stöckelhuber, G. Heinrich. Silica-ethylene propylene diene monomer rubber networking by *in situ* sol-gel method. Journal of Macromolecular Science, Part A: Pure and Applied Chemistry 2008; 45:101-106.
DOI: 10.1080/10601320701683447
6. M. Messori, M. Fiorini. Isoprene rubber filled with silica generated *in situ*. Journal of Applied Polymer Science 2011; 119:3422-3428.
DOI: 10.1002/app.32992
7. L. Bokobza. The reinforcement of elastomeric networks by fillers. Macromolecular Materials and Engineering 2004; 289:607-621.
DOI: 10.1002/mame.200400034
8. R. Scotti, L. Wahba, M. Crippa, M. D'Arienzo, R. Donetti, N. Santod, F. Morazzoni. Rubber–silica nanocomposites obtained by in situ sol–gel method: Particle shape influence on the filler-filler and filler-rubber interactions. Soft Matter 2012; 8:2131-2143.
DOI: 10.1039/c1sm06716h
9. D. Morselli, F. Bondioli, A.S. Luyt, T.H. Mokhothu, M. Messori. Preparation and characterization of EPDM rubber modified with *in situ* generated silica. Journal of Applied Polymer Science 2012; 128:2525-2532
DOI: 10.1002/app.38566
10. Y.-P. Wu, Q.-X. Jia, D.-S. Yu, L.-Q. Zhang. Modeling Young's modulus of rubber-clay nanocomposites using composite theories. Polymer Testing 2004; 23:903-909.
DOI: 10.1016/j.polymertesting.2004.05.004
11. T.K. Jayasree, P. Predeep. Effect of filler on mechanical properties of dynamically crosslinked styrene butadiene rubber/high density polyethylene blends. Journal of Elastomers and Plastics 2008; 40:127-146.
DOI: 10.1177/0095244307083865
12. S. Ahmed, F.R. Jones. A review of particulate reinforcement theories for polymer composites. Journal of Materials Science 1990; 25:4933-4942.
13. L.E. Nielsen. Morphology and elastic modulus of block polymers and polyblends. Rheological Acta 1974; 13:86-92.
14. L.E. Nielsen, R.F. Landel. Mechanical Properties of Polymers and Composites. Marcel Dekker, Inc.: New York (1994)
ISBN: 0 8247 8964 4

15. G.M.O. Barra, J.S. Crespo, J.R. Bertolino, V. Soldi, A.T.N. Pires. Maleic anhydride grafting on EPDM: Qualitative and quantitative determination. Journal of Brazilian Chemical Society 1999; 10:31-34
16. A.I. Hussain, M.L. Tawfic, A.A. Khalil, T.E. Awad. High performance emulsified EPDM grafted with vinyl acetate as compatibilizer for EPDM with polar rubber. Nature and Science 2010; 8:348-357.
17. A. Bandyopadhyay, A.K. Bhowmick, M. De Sarkar. Synthesis and characterization of acrylic rubber/silica hybrid composites prepared by sol-gel technique. Journal of Applied Polymer Science 2004; 93:2579-2589.
DOI: 10.1002/app.20681
18. M.A. De Luca, M.M. Jacobi, L.F. Orlandini. Synthesis and characterisation of elastomeric composites prepared from epoxidised styrene butadiene rubber, 3-aminopropyltriethoxysilane and tetraethoxysilane. Journal of Sol-Gel Science and Technology 2009; 49:150-158.
DOI: 10.1007/s10971-008-1851-8
19. N.D. Meeks, S. Rankin, D. Bhattacharyya. Sulfur-functionalization of porous silica particles and application to mercury vapor sorption. Industrial and Engineering Chemistry Research 2010; 49:4687-4693.
20. T.H. Hsieh, A.J. Kinloch, K. Masania, J.S. Lee, A.C. Taylor, S. Sprenger. The toughness of epoxy polymers and fibre composites modified with rubber microparticles and silica nanoparticles. Journal of Materials Science 2010; 45:1193-1210.
DOI: 10.1007/s10853-009-4064-9
21. Y. Ikeda, A. Tanaka, S. Kohjiya. Reinforcement of styrene-butadiene rubber vulcanizate by in situ silica prepared by the sol-gel reaction of tetraethoxysilane. Journal of Materials Chemistry 1997; 7:1497-1503

Chapter 4

Reinforcement of EPDM rubber with *in situ* generated silica particles in the presence of a coupling agent *via* a sol-gel route

---

This chapter has been published as:
T.H. Mokhothu, A.S. Luyt, M. Messori. Reinforcement of EPDM rubber with in situ generated silica particles in the presence of a coupling agent via a sol-gel route. Polymer Testing 2014; 33:97-106.
http://dx.doi.org/10.1016/j.polymertesting.2013.11.009

Abstract

Ethylene propylene diene monomer rubber (EPDM)-silica (SiO_2) composites were prepared by means of an *in situ* sol-gel process with tetraethoxysilane (TEOS) as precursor and bis-[-3-(triethoxysilyl)-propyl]-tetrasulfide (TESPT) as coupling agent. Homogenous dispersion of the silica particles was observed in all cases, as well as good adhesion between the filler and the matrix. The swelling and gel content results indicated that the number of crosslinks decreased, while the network was still extensive enough to maintain the high gel content. These results indicate that the coupling agent acted as a bridge between the hydrophilic silica and the hydrophobic rubber and enhanced the rubber-silica interactions. This enhanced interaction gave rise to increased thermal stability of the EPDM. The values of the Nielsen model parameters, that gave rise to a good agreement with the experimentally determined Young's modulus values, indicate improved dispersion and reduced size of silica aggregates in the EPDM matrix. Good agreement was found between the storage modulus and Young's modulus values. The filler effectiveness (Factor C) indicated a mechanical stiffening effect and a thermal stability contribution by the filler, while the damping reduction (DR^{Norm}) values confirmed that the EPDM interacted strongly with the well dispersed silica particles and the polymer chain mobility was restricted.

Keywords: EPDM; silica; nanocomposites; coupling agent; reinforcement

4.1 Introduction

Growing of *in situ* sol-gel derived inorganic metal oxides (silica, titania, zirconia) is one of the promising routes for producing rubber matrices filled with uniformly dispersed particles [1-8]. However, an important disadvantage of reinforcement with inorganic fillers is their incompatibility with the rubber matrix, which ultimately gives rise to the formation of large aggregates in the matrix. An example is the very strong interaction between the silica particles caused by the hydrogen bonding of the silanol groups to the silica surface [1,2]. This interaction prevents the filler from uniformly dispersing in the matrix and therefore results in the formation of silica aggregates. This problem can be solved by the introduction of different types of silane coupling agents in the sol-gel process during the *in situ* generation, which should make it possible to modify the filler-matrix and filler-filler interactions [1,6,9,10]. The sol-gel reaction of tetraethoxysilane (TEOS) occurs in two steps, hydrolysis and condensation, and results in the formation of SiO_2, as shown in Scheme 1. This application of the sol–gel process in rubber chemistry is related to the use of silane coupling agents and of moisture or silane curing, and it has already been carried out on natural rubber (NR), styrene-butadiene, ethylene propylene diene monomer rubber (EPDM) and butadiene rubber [2-5,9,11-14].

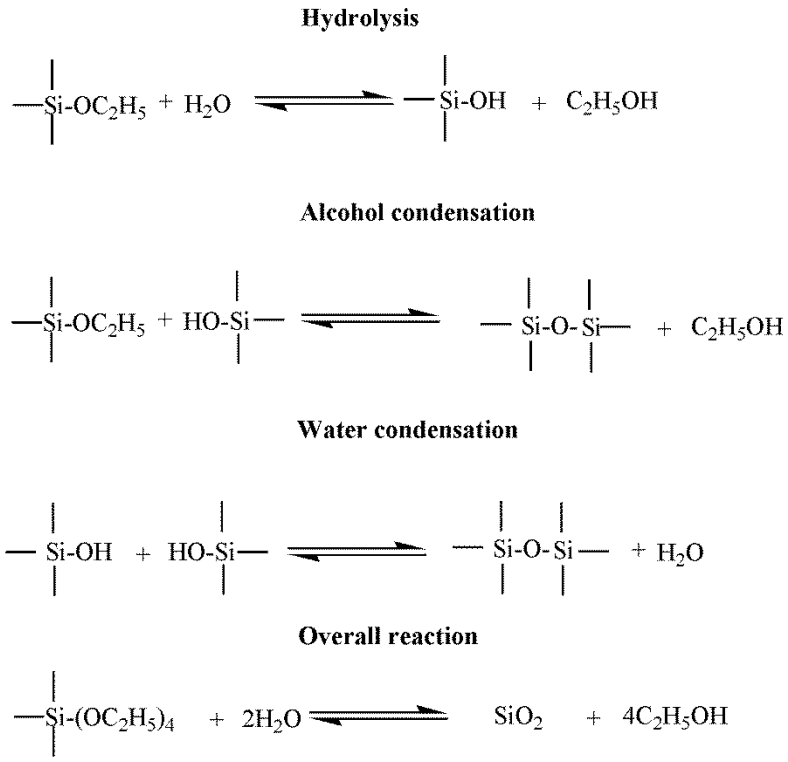

Scheme 1 Sol-gel reaction of tetraethoxysilane (TEOS)

The *in situ* generation of silica reinforced rubber composites using the sol-gel reaction of TEOS in the presence of bis-[-3-(triethoxysilyl)-propyl]-tetrasulfide (TESPT) as coupling agent has been reported in several papers [1,6,9,11]. The function of TESPT as a coupling agent is to enhance the rubber-silica interaction by acting as a bridge between the hydrophilic silica and the hydrophobic rubber. The interaction is promoted by two chemically active chemical groups in TESPT, the ethoxy (CH_3CH_2O-) and the sulphide (-S-) groups, as shown in the structure below. The ethoxy group is capable of reacting with the silanol on the silica surface, whereas the sulphide can participate in sulphur vulcanization leading to a strong chemical linkage between the silane coupling agent and the rubber molecule [11].

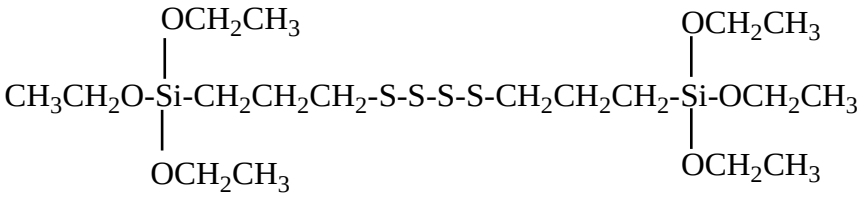

Murakami *et al.* [3] investigated the effect of a silane-coupling agent on natural rubber (NR) filled with *in situ* generated silica. They reported that the simultaneous use of *in situ* silica and the silane coupling agent γ-mercaptopropyltrimethoxysilane (γ -MPS) significantly prevented the delay of sulphur curing and increased the wettability of NR onto *in situ* silica, which resulted in an increase in the reinforcement of the NR vulcanizate. The reinforcing efficiency offered by the *in situ* sol-gel reaction of TEOS in the presence of coupling agents is much higher than those obtained either by conventional mechanical mixing or by the *in situ* reaction without any coupling agent. Studies on the reinforcement of NR, where *in situ* generated silicas and nanofibres of sepiolite were used, indicated that the silica particles generated before vulcanization seem to inhibit the crosslinking reaction of NR by sulphur and form a silica–silica network *via* the silanol groups present on the silica surface. The use of TESPT as silane coupling agent, however, led to a substantial extent of reinforcement [12]. Furthermore, the mixing with the silane coupling agent gave rise to an important decrease in the swelling ratio, which indicated a better crosslinking effect between the organic and inorganic components.

Reinforcement of rubber matrices with *in situ* generated inorganic metal oxide by using a sol-gel route is associated with the improvement of properties such as thermal, thermomechanical and mechanical properties, as well as the morphology and the crosslinking efficiency. Studies

on EPDM rubber reinforced with *in situ* generated silica [13,14] showed an increased agglomeration with increasing filler content as well as a decrease in the crosslinking density of the matrix as a result of the presence of silica particles. In this work, we focused on the preparation of *in situ* silica-EPDM rubber composites by introducing a silane coupling agent bis-[-3-(triethoxysilyl)-propyl]-tetrasulfide in the sol-gel process. The coupling agent was first pre-mixed with the EPDM matrix, followed by the addition of the precursor TEOS, after which the sol-gel reaction was initiated. This approach is expected to reduce the filler-filler interaction and give rise to improved thermal, mechanical and thermomechanical properties, as well as a better morphology and improved crosslinking.

4.2 Experimental

4.2.1 Materials

Tetraethoxysilane (TEOS), tin(II)2-ethylhexanoate, dicumyl peroxide, toluene, bis-[-3-(triethoxysilyl)-propyl]-tetrasulfide (TESPT, commonly known as Si-69) and ethanol were all supplied by Sigma-Aldrich. The materials were used as received without further purification. Ethylene propylene diene monomer rubber (EPDM), Polimeri Europa Dutral® TER 4038, density 0.91 g cm^{-3}, was provided by ATG Italy (Castel d'Argile, BO, Italy).

4.2.2 Preparation of EPDM/SiO_2 nanocomposites

EPDM rubber was dissolved in toluene (3g/100ml) at room temperature, followed by addition of TESPT (4 wt% with respect to EPDM) under stirring. The EPDM/SiO_2 composites were prepared by the addition of TEOS, H_2O, ethanol and tin(II)2-ethylhexanoate (1:4:4:0.04 mol ratio) respectively in the EPDM-TESPT solution. The reaction mixtures were magnetically stirred and heated at 80°C for 20 hours to activate the hydrolytic condensation of TEOS to silica (SiO_2). The solutions were cooled to room temperature, followed by the addition of dicumyl peroxide (DCP) (1 wt% with respect to EPDM) under stirring. The reactions were taken to a rotating evaporator for elimination of about 80% of solvent and other by-products. The samples were obtained by casting the solution in Petri dishes and dried overnight. The cast samples of EPDM/SiO_2 (90/10, 80/20, 70/30 w/w) were vulcanized by compression at 160°C for 20 min.

4.2.3 Characterization methods

The morphologies of the EPDM/SiO_2nanocomposites were examined by a TESCAN VEGA3 scanning electron microscope (SEM) at a voltage of 25 kV. Cross-sections of the samples were coated with gold by an electro deposition method to impart electrical conductivity before the SEM micrographs were recorded.

ATR-FTIR spectra of the pure EPDM and its silica filled composites were obtained using a Perkin Elmer Spectrum 100 FTIR spectrometer. The samples were analyzed over a range of 600-4000 cm^{-1} with a resolution of 4 cm^{-1}. All the spectra were averaged over 16 scans.

The crosslinking degree was determined through equilibrium swelling tests by immersing of at least three rectangular specimens for each composition in 15 ml of toluene at room temperature for several hours, and the mean values are reported. The solvent was replaced hourly after each measurement to eliminate all uncrosslinked fractions, such as unvulcanized EPDM chains, which could lead to incorrect values of the swelling ratio. Equilibrium swelling was determined until the swollen mass (m_s) reached a constant value, after which the samples were dried to constant mass (dried mass (m_d)) and the absolute swelling ratio (q) was evaluated using Equation 4.1.

$$q = \frac{m_s}{m_d} \tag{4.1}$$

The absolute extractable fraction (f), where m_0 is the mass of the sample before immersion in toluene, was determined using Equation 4.2.

$$f = \frac{m_o - m_d}{m_o} \times 100 \tag{4.2}$$

The values of q and f were also normalized to the actual EPDM weight. Their values were determined using Equations 4.3 and 4.4.

$$q_{EPDM} = \frac{q}{C_{EPDM}} \tag{4.3}$$

$$f_{EPDM} = \frac{f}{c_{EPDM}} \quad (4.4)$$

where c_{EPDM} is the weight fraction of EPDM present in the composites. The gel content was determined using Equations 4.5 to 4.7, where m_{EPDM} is the mass of EPDM without silica and $\%wt_{EPDM}$ is the weight % EPDM in the composite.

$$m_{EPDM} = m_0 \times \%wt_{EPDM} \quad (4.5)$$

$$\% \, Extraction = \frac{m_o - m_d}{m_{EPDM}} \times 100 \quad (4.6)$$

$$\% \, Gel = 100 - \% \, Extraction \quad (4.7)$$

Thermogravimetric analysis (TGA) was performed with a Perkin Elmer STA6000 simultaneous thermal analyzer. The analysis was done under flowing nitrogen at a constant flow rate of 20 ml min^{-1} and the samples (20-25 mg) were heated from 25 to 600 °C at a heating rate of 10 °C min^{-1}.

The tensile properties of the samples were determined using a Hounsfield H5KS tensile tester at a crosshead speed of 100 mm $min^{-1}$and 20 mm gauge length at ambient temperature. The samples were rectangular shaped with a width of 12 mm, and thicknesses varying between 0.47 and 0.69 mm. At least five samples were tested for each composition, and the mean values are reported. Young's modulus was predicted according to Nielsen's theoretical model [15-19].

The dynamic mechanical analysis (DMA) of the samples was done on a Perkin Elmer Diamond DMA dynamic mechanical analyzer. Rectangular shaped samples with dimensions of 40 mm length and 10 mm width and thicknesses varying between 0.47 and 0.69 mm were tested in the tensile mode, while heated under nitrogen flow from -100 to 100 ºC at a heating rate of 3 ºC min^{-1}, and at a frequency of 1 Hz.

4.3 Results and discussion

4.3.1 Scanning electron microscopy (SEM)

The SEM micrographs of cross-sections of the EPDM/SiO_2 composites are shown in Figures 4.1 to 4.3, while the particle size distributions are shown in Figure 4.4. The particle size distribution was determined from an average of 40 particles per sample. The light areas in the micrographs correspond to the silica particles and are spherically shaped. The silica particles in the EPDM/SiO_2 samples are homogeneously dispersed in the rubber matrix and have a good particle-matrix adhesion, which confirms the effectiveness of the *in situ* filler generation process used for the preparation of the filled rubbers.

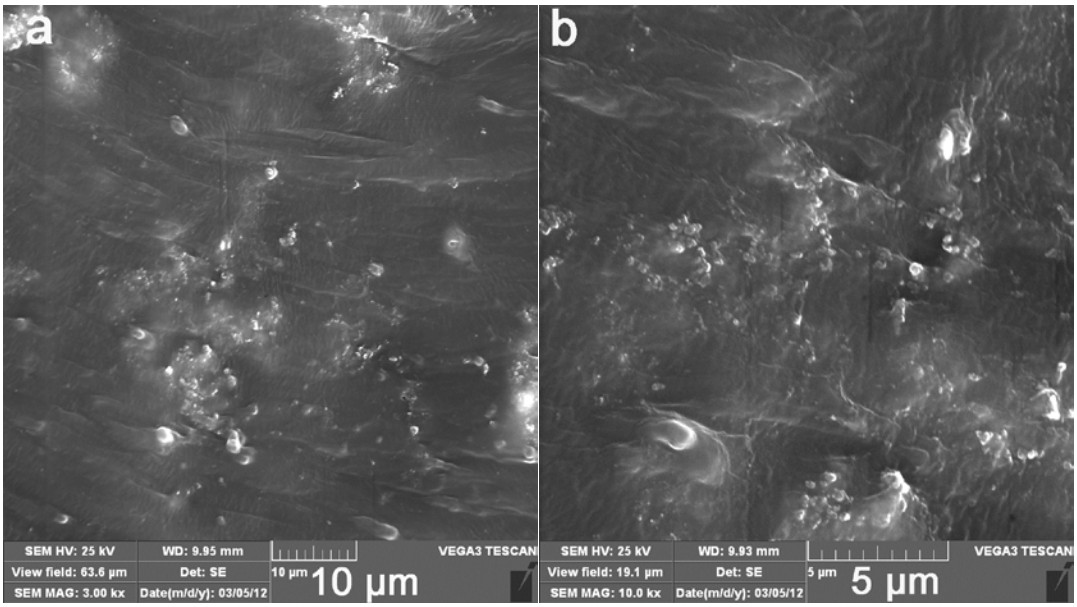

Figure 4.1 SEM micrographs of the 90/10 w/w EPDM/SiO_2 composite

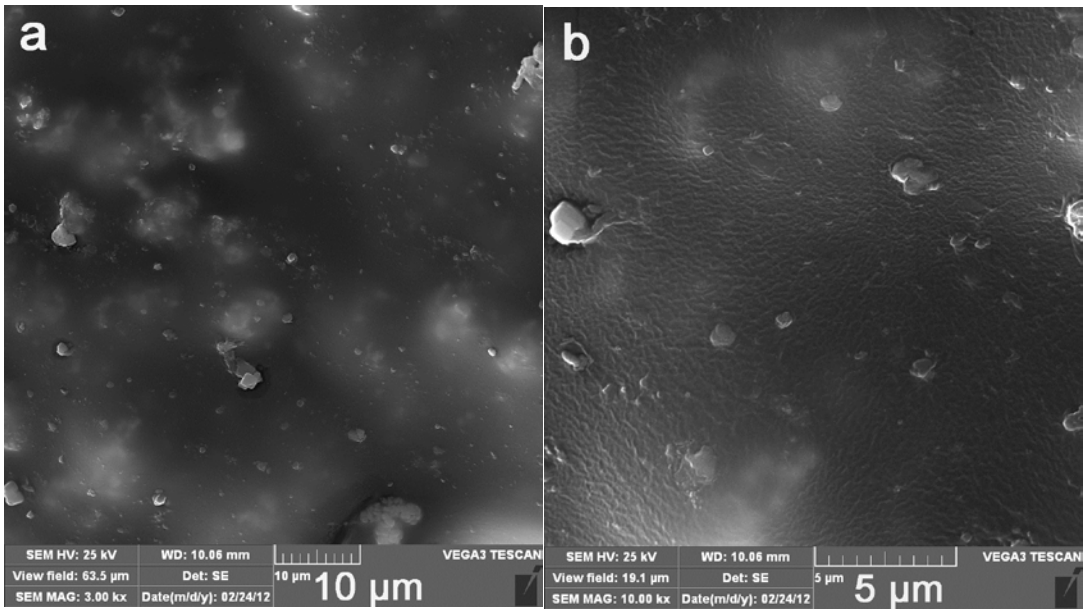

Figure 4.2 SEM micrographs of the 80/20 w/w EPDM/SiO_2 composite

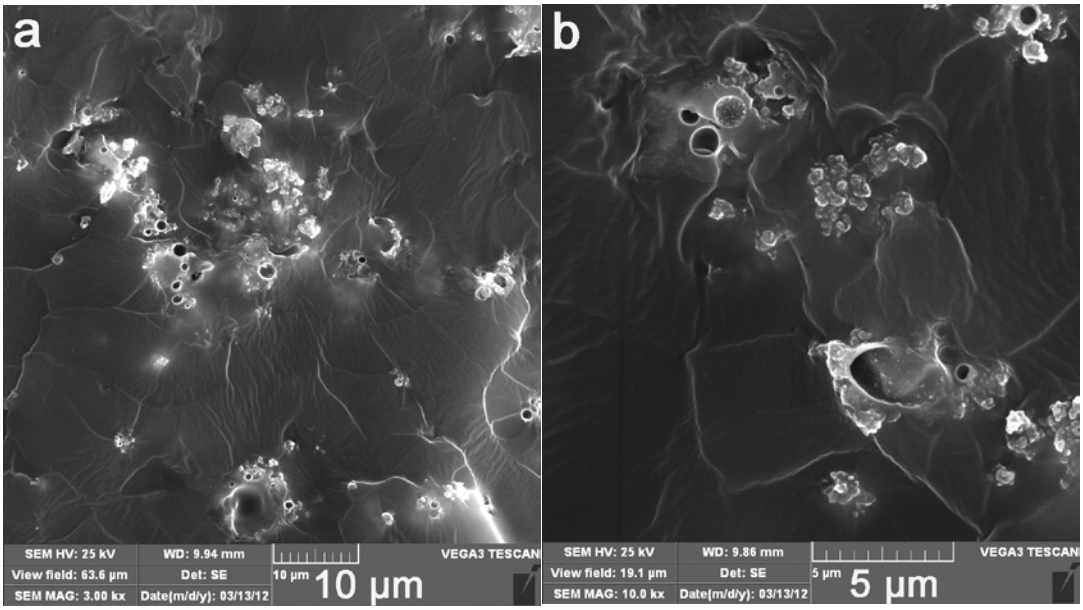

Figure 4.3 SEM micrographs of the 70/30 w/w EPDM/SiO_2 composite

The silica filled composites show both large and small particles at higher silica contents in the composites (Figure 4.3), and the particle size distribution determined from the visible particles confirms the increase in particle size (Figure 4.4). Figure 2 shows that some particles are fully imbedded in the EPDM matrix, which indicates good particle-matrix interactions. The increased agglomeration with increasing filler content has been observed and reported by other authors for similar systems [20-22], and is the result of increased coalescence of the growing silica particles when increasing the amount of *in situ* formed dispersed phase. The silica particles may also have agglomerated in the suspension, because the hydrophilic silica

particles have a tendency to associate *via* hydrogen bonding [22]. When comparing these results with those obtained during our study on the same system, but with the samples prepared in the absence of a coupling agent [14], similar particle size distributions were observed. It is, however, difficult to draw any conclusions from this observation, since SEM analysis only shows the surface morphology of the investigated samples, and not enough particles could be measured to ensure statistically sound conclusions.

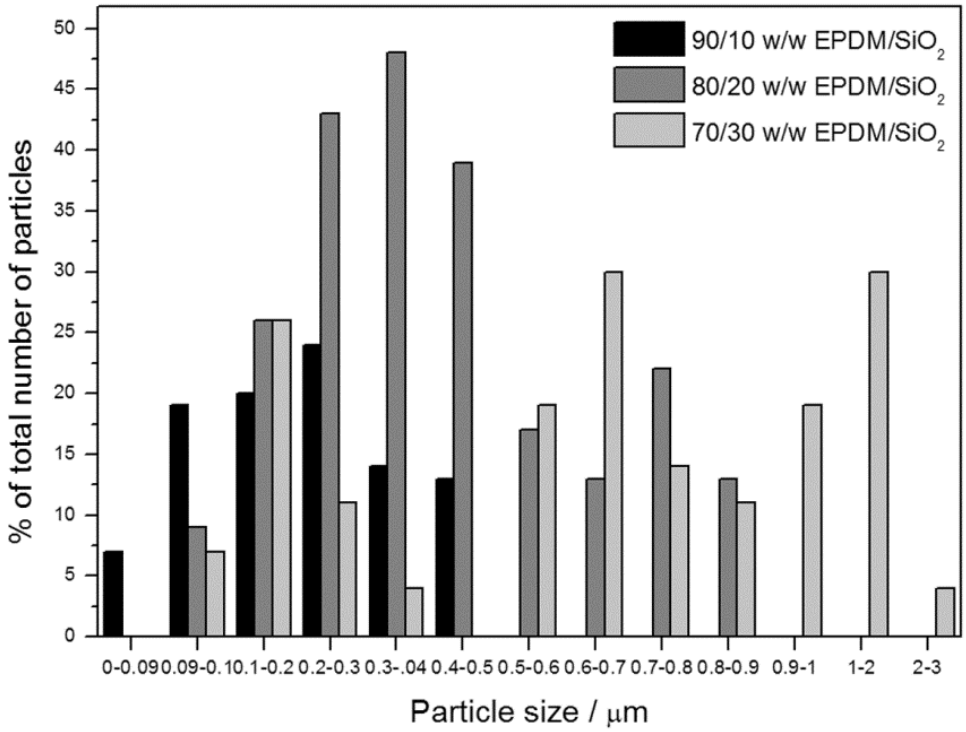

Figure4.4 Particle size distribution graphs of the EPDM/SiO_2 composites

4.3.2 Fourier-transform infrared (FTIR) spectroscopy

The FTIR spectra of EPDM, TESPT, EPDM-TESPT and the EPDM/SiO_2 composite containing 30 wt.% SiO_2 are shown in Figure 4.5. The neat rubber can be identified by two strong absorption peaks at 2920 cm^{-1} and 2850 cm^{-1} assigned to the C-H stretching vibration. The peaks at 721, 1376 and 1464 cm^{-1} are assigned to the CH_2 stretching, and CH_3 and CH_2 bending, respectively [23,24]. The modification of the neat EPDM matrix with TESPT resulted in additional bands observed at 1073 and 952 cm^{-1}, both assigned to Si-O-CH_2CH_3 as a result of the asymmetric stretching of the Si-O group [25]. The FTIR spectrum for TESPT shows the following additional bands: asymmetric stretching of CH_3 (Si-O-CH_2CH_3) in the

region 1390 cm^{-1}, CH_2CH_3 rocking of Si-O-CH_2CH_3 around 1167 cm^{-1}, band stretching of Si-C at 780 cm^{-1}, CH_2 wagging in CH_2-S- at 1246 cm^{-1}, and C-H stretching at 2973 cm^{-1}[25].

TEOS undergoes hydrolysis by water to produce silanol groups (Si-OH) in the presence of the EPDM matrix during the sol-gel process. The silanol groups react with the ethoxysilane (Si-OCH_3CH_2) and produce siloxane groups. The ethoxy group (CH_3CH_2O) from TESPT can also react with silanol to form a siloxane linkage. Networks of siloxane linkages will therefore form silica particles embedded in the rubber matrix. The siloxane linkage can be identified from the FTIR spectra of the vulcanized EPDM/SiO_2 composite, as an asymmetric stretch (Si-O-Si) in the region 1055 cm^{-1} (Figure 4.5). The vulcanized composite shows additional FTIR peaks at 803 and 944 cm^{-1}. They are assigned to Si-OH, which shows the presence of silanol groups, and to the asymmetric stretching of Si-O-C from unreacted TEOS [26-28]. The appearance of these functional groups implies that some of the silanol and ethoxysilane/ethoxy groups from both the TEOS and the coupling agent might have grafted on the rubber chains through reacting with the dicumyl peroxide initiator during vulcanization. The sulphide from the coupling agent has probably participated in sulphur vulcanization, as observed from the absence of a sulphide peak (CH_2-S-) for the EPDM/SiO_2 composite. The coupling agent probably formed bridges between the silica particles and the EPDM rubber, thereby leading to stronger chemical linkage between the silane coupling agent and the rubber molecule. The –OH bending vibration around 3300 cm^{-1} is much weaker than that observed in the spectra of the samples prepared in the absence of coupling agent [14]. In the presence of coupling agent the interaction between the EPDM rubber and the silica particles follows the reaction scheme proposed by Das *et al.* [1]. According to this scheme the silanol groups are incorporated in the coupling agent generated crosslinks between the rubber chains. However, in the present case the silanol groups that formed part of the crosslinks obviously reacted further to form silica links, with the accompanying reduction in the number of free –OH groups.

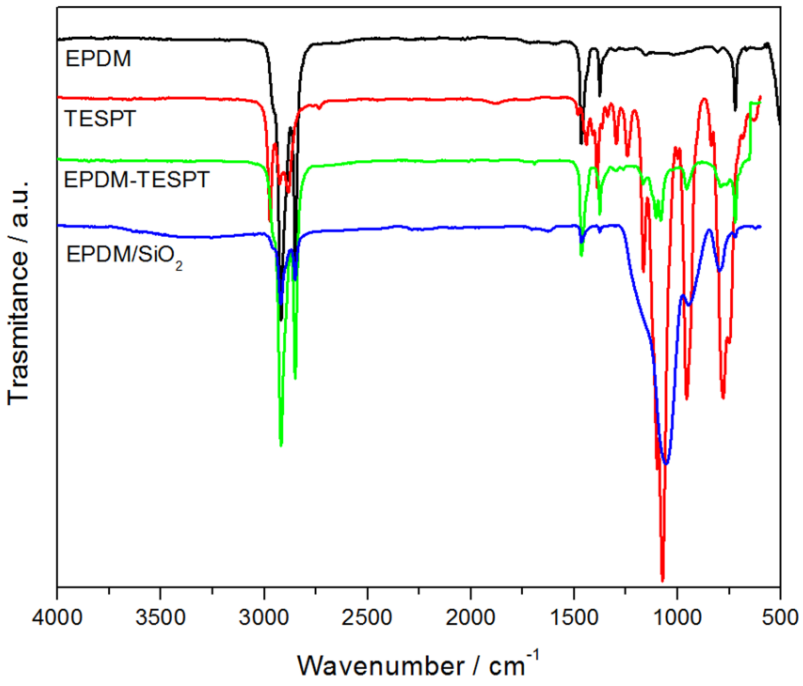

Figure 4.5 FTIR spectra of EPDM, TESPT, EPDM-TESPT and the EPDM/SiO_2 composite containing 30 wt.% silica

4.3.3 Equilibrium swelling and gel content

The equilibrium swelling and gel content results of the vulcanized EPDM and the EPDM/SiO_2 composites are reported in Table 4.1. Equilibrium swelling analysis is well-known to evaluate the crosslinking density obtained after vulcanization of an unfilled rubber. In the case of silica filled rubber composites, the swelling behaviour could be influenced by (1) the ability of the silica particles to act as crosslinking points and/or absorb solvent and (2) the crosslinking degree of the unfilled rubber matrix.

Table 4.1 Swelling ratio and gel content of EPDM and EPDM/SiO_2 composites

Samples (w/w)	q	q_{EPDM}	f / %	f_{EPDM}/ %	*Gel* / %
EPDM	3.7 ± 0.2	3.7 ± 0.2	6.4 ± 2.5	6.4 ± 2.5	93.6 ± 2.5
90/10 EPDM/SiO_2	5.9 ± 0.6	6.6 ± 0.6	1.8 ± 0.4	2.0 ± 0.4	98.2 ± 0.3
80/20 EPDM/SiO_2	4.3 ± 0.6	5.0 ± 0.7	3.0 ± 1.6	3.6 ± 1.9	96.2 ± 2.0
70/30 EPDM/SiO_2	4.3 ± 0.0	6.0 ± 0.0	2.5 ± 1.5	3.6 ± 2.2	96.4 ± 2.2

Swelling ratios (q and q_{EPDM}), extractable fraction (f and f_{EPDM}) and gel content for EPDM and EPDM/SiO_2 nanocomposites

The normalised swelling ratio in Table 4.1 shows an increase for the silica containing samples, while the gel content values remained effectively constant. This indicates that the number of crosslinks decreased, while the network is still extensive enough to maintain the high gel content. Another possibility is that longer chain crosslinks have been formed between the rubber chains (as proposed by Das *et* al. [1]). In this case an extensive network will still exist, but there will be enough free volume between the chains to accommodate the toluene molecules during the swelling test, which explains the increase in swelling ratios. In our previous paper [14] where the nanocomposites were prepared in the absence of a coupling agent we also observed an increase in swelling ratio, but in that case the extractable fraction increased and the gel content decreased significantly, which clearly showed an inhibition of the rubber crosslinking in the presence of the silica nanoparticles. In this case the silica particles became part of the crosslinks through the action of the coupling agent [1]. The introduction of TESPT therefore has an influence on the effectiveness of crosslinking and on the length of the crosslinks in the vulcanized EPDM/SiO_2 composites

4.3.4 Thermogravimetric analysis (TGA)

The TGA curves of EPDM rubber and silica filled composites are shown in Figure 6. The thermal stability was characterized through temperatures taken at the onset and at 50% mass loss (Table 4.2). The TGA curves of the EPDM/SiO_2 nanocomposites clearly show two distinct mass loss steps, and an increasing amount of char with increasing silica content (Figure 4.6 and Table 4.2). The first mass loss is observed from 100 °C and is due to a loss of water and alcohol, and progresses to higher temperatures due to the presence of organic by-products such as unhydrolyzed TEOS that decompose and evaporate around 350 °C. The second mass loss around 400-470 °C is related to the main degradation of EPDM rubber chains or segments. The degradation temperatures of EPDM initially decrease for the 10% silica containing sample, but increase to temperatures higher than that of EPDM for the samples containing 20 and 30% silica (Table 4.2). The introduction of the coupling agent obviously improved the interaction with and dispersion of silica particles in the EPDM matrix, which gave rise to the increased thermal stability of the EPDM. The strongly bound and well dispersed silica particles reduced polymer chain mobility and retarded the diffusion of volatile products from the sample. It probably also changed the decomposition mechanism of EPDM, similar to what has been reported in other thermal degradation studies [7,29-32].

Our previous results, obtained in the absence of a coupling agent, showed very little influence of the silica filler on the thermal stability of the matrix.

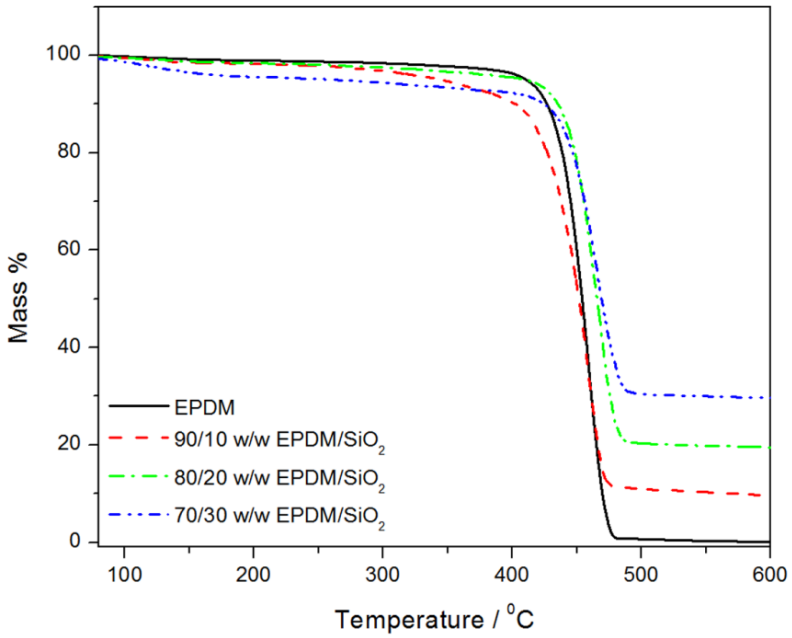

Figure4.6 TGA curves of EPDM and silica filled EPDM composites

The actual silica content after conversion was determined through TGA analysis as the percentage residue after heating to 600 °C. The data in Table 4.2 show a very good correlation between the % residue and the amount of silica introduced through the sol-gel reaction. The small standard deviation values in Table 4.2 indicate that the silica particles were well dispersed in the rubber matrix, because samples were taken from different positions in the pressed sheets for the repeat TGA analyses.

Table 4.2 Summary of TGA results for the EPDM rubber and its composites

Samples (w/w)	T_{onset} / °C	$T_{50\ \%}$ / °C	% SiO_2
EPDM	426 ± 0.1	454 ± 0.1	0
90/10 EPDM/SiO_2	420 ± 2.7	452 ± 1.3	9.0 ± 0.4
80/20 EPDM/SiO_2	435 ± 1.6	463 ± 3.4	19.1 ± 2.3
70/30 EPDM/SiO_2	436 ± 2.8	469 ± 0.1	29.0 ± 0.7

T_{onset} and $T_{50\%}$ are the temperatures at the onset and at 50% mass loss

4.3.5 Tensile testing

The Young's modulus as function of volume fraction of neat EPDM and its silica filled composites are shown in Figure 4.7, together with its prediction according to the Nielsen theoretical model [15-19]. The values for Young's modulus, stress and elongation at break, are summarized in Table 3. For composite materials consisting of spherical particles in the matrix, the Nielsen equation has the form given in Equations 4.8 and 4.9.

$$E = E_1 \left[\frac{1+AB\phi_2}{1-B\psi\phi_2}\right] \quad (4.8)$$

$$B = \frac{E_2/E_1 - 1}{E_2/E_1 + A} \quad (4.9)$$

where E, $E_2$and E_1 are the modulus values of the composite, filler and matrix respectively, and ϕ_2 is the volume fraction of the filler assuming spherical particles. The theoretical modulus used for the silica particles was E_2 = 70 GPa [33]. The factor ψ takes into account the values of ϕ_m of the dispersed phase and it is given by Equation 4.10.

$$\psi = 1 + \left[\left(\frac{1-\phi_m}{\phi_m^2}\right)\phi_2\right] \quad (4.10)$$

where ϕ_m is the maximum packing fraction. The constant B takes into account the relative moduli of the filler and matrix phases, and its value is 1.0 for very large E_2/E_1 ratios (the values for E_2 and E_1 are 70 GPa and 2.4 MPa, respectively, and therefore we could confidently use a value of 1.0). The constant A is related to the Einstein coefficient given by Equation 4.11 and is determined by the morphology of the system; for strong aggregates, the value of A can become quite large while ϕ_m of the dispersed phase will decrease.

$$A = k_E - 1 \quad (4.11)$$

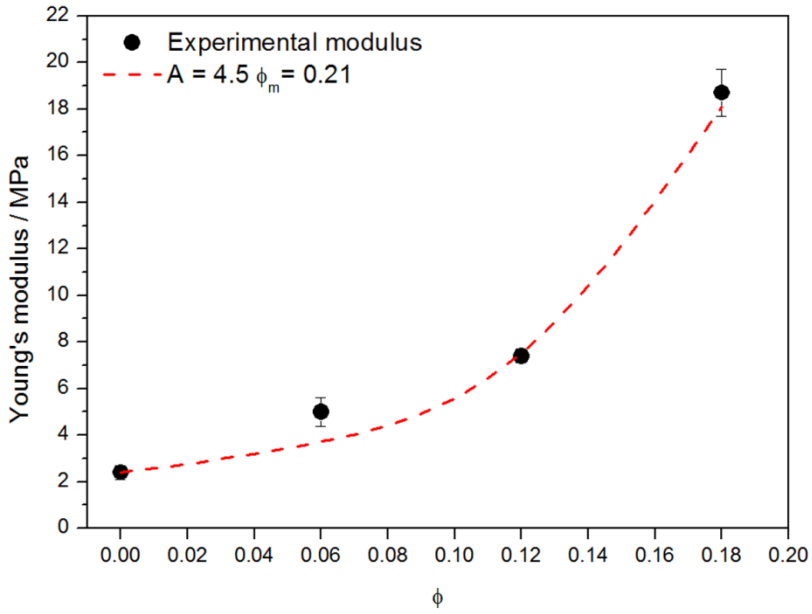

Figure 4.7 Young's modulus as a function of volume fraction of SiO_2 in EPDM/SiO_2 composites: experimental modulus and Nielsen predicted modulus

An A value of 4.5 gave the best fit of the experimental modulus values (Figure 4.7). It is interesting to observe that the addition of TESPT reduced the value of A and ϕ_m significantly when compared to our previous study, where the same system in the absence of a coupling agent was investigated [14]. The values of A and ϕ_m were then 25 and 0.37 respectively, which indicated a large extent of silica aggregation in the EPDM matrix with increasing silica content. Furthermore, the silica aggregates were large enough to increase the value of A and reduce the value of ϕ_m. In the current study the introduction of a coupling agent improved the dispersion of the filler and reduced the size of the aggregates, as was also observed from the SEM images in Figures 4.1 to 4.3. The low value of ϕ_m indicates the presence of agglomerated silica particles, but the aggregates are small enough for the value of A to be significantly reduced.

Table 4.3 Summary of tensile results of EPDM and the EPDM/SiO_2 composites

Samples	σ_b / MPa	ε_b / %	E / MPa
EPDM	1.7 ± 0.5	482 ± 84	2.4 ± 0.3
90/10 w/w EPDM/SiO_2	3.1 ± 0.4	763 ± 62.9	5.0 ± 0.6
80/20 w/w EPDM/SiO_2	3.7 ± 0.7	1060 ± 20.0	7.4 ± 0.3
70/30 w/w EPDM/SiO_2	3.2 ± 0.4	730 ± 28.9	18.7 ± 1.0

ε_b, σ_b, and E are elongation at break, stress at break, and Young's modulus of elasticity

It is further interesting to observe that both the stress and elongation at break increase with increasing filler content for 10 and 20 wt.% silica (Table 4.3). This is the result of improved adhesion between the filler and the matrix because of good interfacial interaction brought about by the coupling agent, giving rise to effective stress transfer. Das *et al*. [1] also reported high stress and elongation at break values in their investigation of silica-EPDM rubber networks by an *in situ* sol-gel method. They explained this as the polysulfidic linkage from the TESPT causing a strong reinforcement between the rubber and the filler, which explains the larger stress at break values. The longer crosslink chains formed in the presence of the coupling agent explain the larger elongation at break values. A larger amount of filler led to agglomeration of the filler particles, which resulted in a decrease in the stress and elongation at break for the sample containing 30 wt.% silica. In this case there were probably silica particles that were not incorporated in the crosslinks through the action of the coupling agent, and that formed agglomerates acting as stress concentration points. Aggregation of the filler in the composite probably caused a dewetting or crazing effect in which the adhesion between the filler and matrix phase was destroyed, and this resulted in a decline in the mechanical properties. When comparing these results with those obtained during our study on the same system, but with the samples prepared in the absence of a coupling agent [14], it is observed that the tensile modulus values for the different nanocomposites, prepared in the absence and presence of TESPT, are similar, but that the stress and elongation at break values for the samples prepared in the presence of TESPT are significantly higher. This can also be explained by the better interaction between the rubber chains and the silica particles incorporated in the crosslinks [1], which improved the interfacial interaction and reduced the number of stress concentration points, and by the longer crosslink chains, which increased the strain-ability of the nanocomposites.

4.3.6 Dynamic mechanical analysis (DMA)

The DMA results of EPDM and its nanocomposites are shown in Figure 4.8. The glass transition temperature, the tan δ value at the glass transition peak maximum, the storage modulus at 50 °C, Factor C and the damping reduction values are summarized in Table 4.4. From the values of the storage modulus obtained in the glassy and rubbery regions, the filler effectiveness (Factor C) in the rubber matrix can be evaluated from Equation 4.12 [35].

$$Factor\ C = \frac{(E'_g/E'_r)composites}{(E'_g/E'_r)matrix} \quad (4.12)$$

where, E'_g and E'_r are the storage moduli determined in the glassy and rubbery regions, respectively. The state of filler dispersion in the rubber matrix was determined by calculation of the damping reduction (DR) from the normalised damping values obtained from the maxima of the tan δ peaks (tan δ_{rubber} and tan $\delta_{composite}$) and is given by Equation 4.13 [35].

$$DR = \frac{\tan \delta_{EPDM} - \tan \delta_{composite}}{\tan \delta_{EPDM}} \times 100\% \quad (4.13)$$

In the rubbery region there is a significant increase in the storage modulus with increasing silica content in the vulcanizates (see $E'_{T=50^oC}$ values in Table 4.4). These modulus values depend on both the degree of crosslinking the rubber matrix and the content of the rigid dispersed phase. Both these factors will contribute to an increase in modulus. As can be seen from Table 4.1, the degree of crosslinking remained fairly constant with increasing silica content (see q_{EPDM} values for filled samples). However, the content of the rigid dispersed phase increased significantly and the interaction between the rubber and filler was very good because of the presence of coupling agent during the preparation of the composites. These factors gave rise to much higher storage modulus values that correlate well with the tensile modulus values in Table 4.3. The modulus values, reported in Table 4.4, are very similar to those reported for the same samples prepared in the absence of a coupling agent [14]. This indicates that the rigidity of the fillers makes the biggest contribution to the elastic modulus of the EPDM nanocomposites.

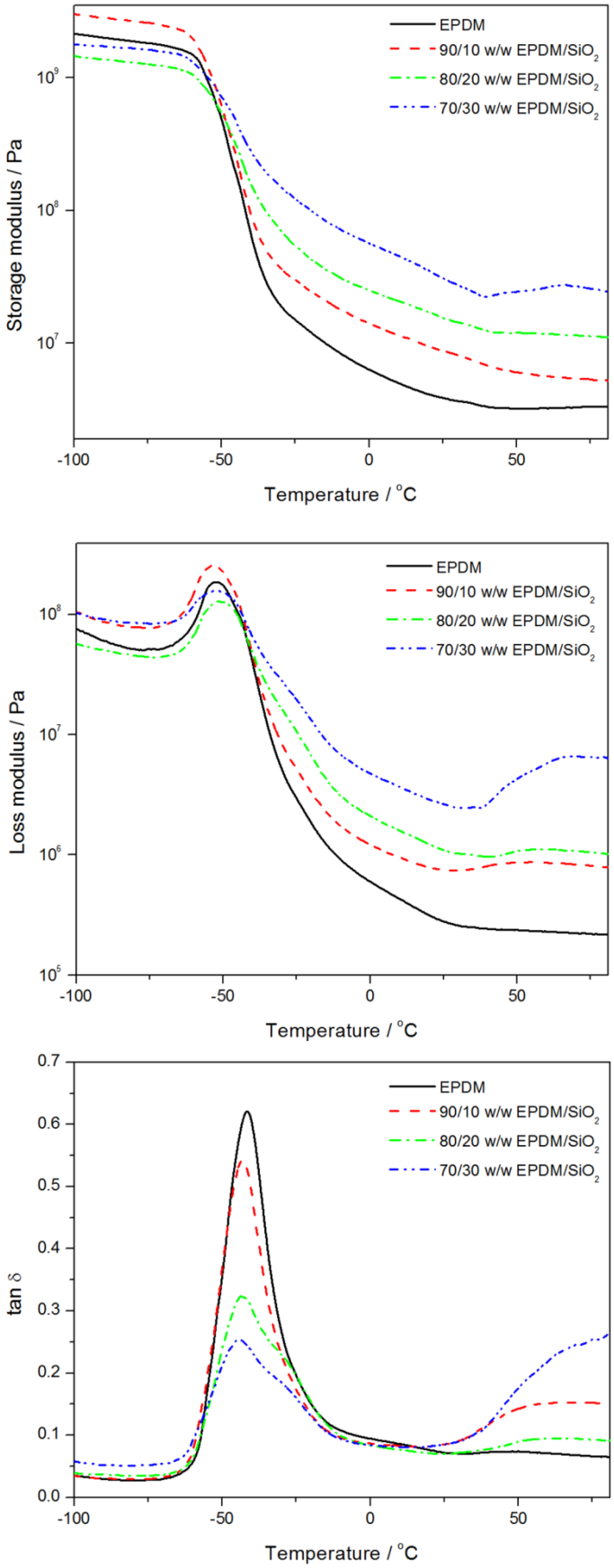

Figure 4.8 DMA storage modulus, loss modulus and damping factor curves of EPDM and its composites

Table 4.4 Summary of DMA results of EPDM and EPDM/SiO_2 composites

Samples (w/w)	$E'_{T=50°C}$ / MPa	$\tan\delta_{max}^{Norm}$	T_g / °C	Factor C	DR / %
EPDM	3.2	0.622	-41.5	1	-
90/10 EPDM	6.0	0.603	-41.9	0.77	3.1
80/20 EPDM	12.0	0.390	-42.5	0.18	37.3
70/30 EPDM	24.5	0.363	-42.3	0.11	41.6

$E'_{T=50°C,}$ $\tan\delta_{max}^{Norm}$, T_g, Factor C and DR^{Norm} are the modulus at 50 °C, maximum tan δ (normalised to the amount of rubber in the nanocomposites), glass transition temperature, filler effectiveness and the damping reduction (calculated from $\tan\delta_{max}^{Norm}$)

The filler effectiveness (Factor C) (Table 4.4) can be used to indicate the composite reinforcing capacity. By definition an unfilled rubber matrix has a Factor C equal to 1, and a Factor C lower than 1 indicates a mechanical stiffening effect as well as a thermal stability contribution of the used filler [35]. The values in Table 4 clearly show that the silica particles contributed to the EPDM matrix stiffness as the silica content increases.

The addition of rigid fillers to a polymer matrix is expected to restrict the mobility of the polymer chains leading to a decrease in the damping and a shift in the glass transition temperature to higher values. The normalized tan δ values in Table 4.4 clearly decrease with increasing silica content. The decrease in the damping factor is attributed to good adhesion between the filler and the matrix, which resulted in a restriction in the mobility of rubber chains in the composite. The increasing damping reduction (DR^{Norm}) values with increasing silica content confirm that the EPDM interacts strongly with the well dispersed silica particles which lead to a reduction in polymer chain mobility. The glass transition temperature slightly increased for the silica containing samples, which is expected because of the reduced chain mobility of EPDM in the nanocomposites.

4.4 Conclusions

Reinforcing of EPDM rubber with *in situ* generated silica particles in the presence of a coupling agent (TESPT) *via* a sol-gel route was investigated. The silica filled composites showed both large and small particles at higher silica contents in the composites and some particles were fully imbedded in the EPDM matrix, which indicated good particle-matrix

interactions. The particle size distribution increased with increasing silica content as a result of increased coalescence of the growing silica particles when increasing the amount of *in situ* formed dispersed phase. The FTIR results indicate that the TEOS and TESPT reacted to form silica containing crosslinks between the rubber chains. In the presence of the silica particles there was a decrease in crosslink density, but the networks were still extensive enough to maintain a high gel content. The introduction of the coupling agent improved the interaction of the silica particles with and dispersion in the EPDM matrix, which gave rise to an increased thermal stability of the EPDM. The tensile results showed that longer crosslink chains formed in the presence of the coupling agent gave rise to larger elongation at break values, and the polysulfidic linkage from the TESPT caused a strong reinforcement between the rubber and the filler, which gave rise to the larger stress at break values. However, larger amounts of filler led to agglomeration of the filler particles, which resulted in a decrease in the stress and elongation at break. A Nielsen's model fit to the Young's modulus values shows improved dispersion and reduced size of the silica aggregates in the EPDM matrix. There is a good correlation between the storage modulus and Young's modulus values, and these values increased significantly with increasing filler content. The increased stiffness and thermal stability are confirmed by the filler effectiveness factor values. The damping reduction values confirm that the EPDM interacted strongly with the well dispersed silica particles, which led to a reduction in the polymer chain mobility. When the results of this study are compared with those of our previous study on the same system in the absence of a coupling agent, it is clear that the introduction of the coupling agent improved the interaction and dispersion of silica particles in the EPDM matrix, and had an influence on the effectiveness of crosslinking and on the length of the crosslinks in the vulcanized EPDM/SiO_2 composites. Because of this influence, the EPDM/silica nanocomposites showed much better thermal and mechanical properties.

4.5 References

1. A. Das, R. Jurk, K.W. Stöckelhuber, G. Heinrich. Silica-ethylene propylene diene monomer rubber networking by in situ sol-gel method. Journal of Macromolecular Science, Part A: Pure and Applied Chemistry 2008; 45:101-106.
   DOI: 10.1080/10601320701683447

2. Y. Ikeda, A. Tanakaa, S. Kohjiyab. Effect of catalyst on in situ silica reinforcement of styrene–butadiene rubber vulcanizate by the sol–gel reaction of tetraethoxysilane. Journal of Materials Chemistry 1997; 7:455–458.
3. K. Murakami, S. Iio, Y. Ikeda, H. Ito, M. Tosaka, S. Kohjiya. Effect of silane-coupling agent on natural rubber filled with silica generated in situ. Journal of Materials Science 2003;38:1447-1455.
4. S. Kohjiya, Y. Ikeda. In situ formation of particulate silica in natural rubber matrix by the sol-gel reaction. Journal of Sol-Gel Science and Technology 2003; 26:495-498. DOI: 10.1023/A:1020743214628
5. Y. Ikeda, S. Kohjiya. In situ formed silica particles in rubber vulcanizate by the sol-gel method. Polymer 1997; 38:4417-4423.
6. M. Messori. In situ synthesis of rubber nanocomposites. Advanced Structured Materials 2011; 9:57-85. DOI: 10.1007/978-3-642-15787-5_2
7. T.E. Motaung, A.S. Luyt, S. Thomas. Morphology and properties of NR/EPDM rubber blends filled with small amounts of titania nanoparticles. Polymer Composites 2011; 32:1289-1296. DOI:10.1002/pc.21150
8. D. Fragiadakis, L. Bokobza, P. Pissis. Dynamics near the filler surface in natural rubber-silica nanocomposites. Polymer 2011; 52:3175-3182. DOI:10.1016/j.polymer.2011.04.045
9. R. Scotti, L. Wahba, M. Crippa, M. D'Arienzo, R. Donetti, N. Santod, F. Morazzoni. Rubber–silica nanocomposites obtained by in situ sol–gel method: Particle shape influence on the filler-filler and filler-rubber interactions. Soft Matter 2012; 8:2131-2143. DOI: 10.1039/c1sm06716h
10. L. Bokobza. The reinforcement of elastomeric networks by fillers. Macromolecular Materials and Engineering 2004; 289:607-621. DOI: 10.1002/mame.200400034
11. V. Tangpasuthadol, A. Intasiri, D. Nuntivanich, N. Niyompanich, S. Kiatkamjornwong. Silica-reinforced natural rubber prepared by the sol–gel process of ethoxysilanes in rubber latex. Journal of Applied Polymer Science 2008; 109:424–433. DOI: 10.1002/app.28120

12. L. Bokobza, J.-P.Chauvin. Reinforcement of natural rubber: Use of *in situ* generated silicas and nanofibres of sepiolite. Polymer 2005; 46:4144-4151.
DOI: 10.1016/j.polymer.2005.02.048
13. D. Morselli, F. Bondioli, A.S. Luyt, T.H. Mokhothu, M. Messori. Preparation and characterization of EPDM rubber modified with *in situ* generated silica. Journal of Applied Polymer Science 2012; 128: 2525–2532.
DOI: 10.1002/app.38566
14. T.H. Mokhothu, A.S. Luyt, D. Morselli, F. Bondioli, M. Messori. Influence of *in situ* generated silica nanoparticles on EPDM morphology, thermal, thermomechanical and mechanical properties. Submitted for publication in Polymer Composites.
15. L.E. Nielsen. Morphology and elastic modulus of block polymers and polyblends. Rheological Acta 1974; 13:86-92.
16. L.E. Nielsen, R.F. Landel. Mechanical Properties of Polymers and Composites. Marcel Dekker, Inc.: New York (1994).
ISBN: 0 8247 8964 4
17. Y.-P. Wu, Q.-X. Jia, D.-S. Yu, L.-Q. Zhang. Modeling Young's modulus of rubber-clay nanocomposites using composite theories. Polymer Testing 2004; 23:903-909.
DOI: 10.1016/j.polymertesting.2004.05.004
18. T.K. Jayasree, P. Predeep. Effect of filler on mechanical properties of dynamically crosslinked styrene butadiene rubber/high density polyethylene blends. Journal of Elastomers and Plastics 2008; 40:127-146.
DOI: 10.1177/0095244307083865
19. S. Ahmed, F.R. Jones. A review of particulate reinforcement theories for polymer composites. Journal of Materials Science 1990; 25:4933-4942.
20. M. Messori, F. Bignotti, R. De Santis, R. Taurino. Modification of isoprene rubber by *in situ* silica generation. Polymer International 2009; 58:880-887.
DOI: 10.1002/pi.2606
21. Y. Ikeda, Y. Kemeda. Preparation of "green" composites by the sol-gel process: *In situ* filled natural rubber. Journal of Sol-Gel Science and Technology 2004; 31:137-142.
DOI: 10.1023/B:JSST.0000047975.48812.1b
22. S. Prasertsri, N. Tattanasom. Mechanical and damping properties of silica/natural rubber composites prepared from latex system. Polymer Testing 2011; 30:515-526.
DOI: 10.1016/j.polymertesting.2011.04.001

23. G.M.O. Barra, J.S. Crespo, J.R. Bertolino, V. Soldi, A.T.N. Pires. Maleic anhydride grafting on EPDM: Qualitative and quantitative determination. Journal of Brazilian Chemical Society, 1999; 10:31-34.
24. A.I. Hussain, M.L. Tawfic, A.A. Khalil, T.E. Awad. High performance emulsified EPDM grafted with vinyl acetate as compatibilizer for EPDM with polar rubber. Nature and Science 2010; 8:348-357.
25. D. Zhu, W.J. van Ooij. Structural characterization of bis-[triethoxysilylpropyl] tetrasulfide and bis-[trimethoxysilylpropyl]amine silanes by Fourier-transform infrared spectroscopy and electrochemical impedance spectroscopy. Journal of Adhesion Science and Technology 2002; 16:1235–1260.
DOI: 10.1163/156856102320256873
26. A. Bandyopadhyay, A.K. Bhowmick, M. De Sarkar. Synthesis and characterization of acrylic rubber/silica hybrid composites prepared by sol-gel technique. Journal of Applied Polymer Science 2004; 93:2579-2589.
DOI: 10.1002/app.20681
27. M.A. De Luca, M.M. Jacobi, L.F. Orlandini. Synthesis and characterisation of elastomeric composites prepared from epoxidised styrene butadiene rubber, 3-aminopropyltriethoxysilane and tetraethoxysilane. Journal of Sol-Gel Science and Technology 2009; 49:150-158.
DOI: 10.1007/s10971-008-1851-8
28. N.D. Meeks, S. Rankin, D. Bhattacharyya. Sulfur-functionalization of porous silica particles and application to mercury vapor sorption. Industrial and Engineering Chemistry Research 2010; 49:4687-4693.
DOI:10.1021/ie901580k
29. Q. Ji, X. Wang, Y. Zhang, Q. Kong, Y. Xia. Characterization of poly(ethylene terephthalate)/SiO_2 nanocomposites prepared by sol-gel method. Composites: Part A 2009; 40:878-882.
DOI: 10.1016/j.compositesa.2009.04.010
30. K. Chrissafis, D. Bikiaris. Can nanoparticles really enhance thermal stability of polymers? Part I: An overview on the thermal decomposition of addition polymers. Thermochimica Acta 2011; 523:1-24.
DOI: 10.1016/j.tca.2011.06.010

31. D. Bikiaris. Can nanoparticles really enhance thermal stability of polymers? Part II: An overview on the thermal decomposition of polycondensation polymers. Thermochimica Acta 2011; 523:25-45.
DOI: 10.1016/j.tca.2011.06.012
32. T.K. Dey, M. Tripathi. Thermal properties of silicon powder filled high-density polyethylene composites. Thermochimica Acta 2010; 502:35-42.
DOI: 10.1016/j.tca.2010.02.002.
33. T.H. Hsieh, A.J. Kinloch, K. Masania, J.S. Lee, A.C. Taylor, S. Sprenger. The toughness of epoxy polymers and fibre composites modified with rubber microparticles and silica nanoparticles. Journal of Materials Science 2010; 45:1193-1210.
DOI: 10.1007/s10853-009-4064-9
34. R. Tlili, V. Cecen, I. Krupa, A. Boudenne, L. Ibos, Y. Candau, I. Novák. Mechanical and thermophysical properties of EVA copolymer filled with nickel particles. Polymer Composites 2011; 32:727–736.
DOI: 10.1002/pc.21091
35. A. Gregorova, M. Machovsky, R. Wimmer. Viscoelastic properties of mineral-filled poly(lactic acid) composites. International Journal of Polymer Science 2012; 2012:1-6.
DOI: 10.1155/2012/252981

Chapter 5

Preparation and characterization of EPDM/silica composites prepared through non-hydrolytic sol-gel in the absence and presence of a coupling agent

This chapter has been submitted as a publication:
T. H. Mokhothu, A.S. Luyt, M. Messori. Preparation and characterization of EPDM/silica nanocomposites prepared through non-hydrolytic sol-gel in the absence and presence of a coupling agent. Polymer Degradation and Stability.

Abstract

Ethylene propylene diene monomer (EPDM) rubber containing *in situ* generated silica particles was prepared through a non-hydrolytic sol-gel (NHSG) method with silicon tetrachloride as precursor. The silica particles were homogenously dispersed in the EPDM matrix, but there were agglomerates at high silica contents. The swelling experiments showed a decrease in the crosslinking density of the vulcanized rubber due to the presence of the silica particles for both the composites prepared in the presence and absence of a coupling agent, bis-[-3-(triethoxysilyl)-propyl]-tetrasulfide (TESPT). Unlike the composites prepared through a hydrolytic sol-gel (HSG) method with TEOS as precursor, the TESPT did not seem to take part in the sol-gel reaction. The presence of TESPT influenced the interaction and dispersion of the silica particles in the EPDM matrix, which gave rise to increased thermal stability of the EPDM when compared to the composites prepared in the absence of TESPT. However, t-butyl chloride and TESPT evaporated from the samples at temperatures below the EPDM decomposition range. The values of the Nielsen model parameters, that gave rise to a good agreement with the experimentally determined Young's modulus values, indicated improved dispersion and reduced size of the silica aggregates in the EPDM matrix. There was also good agreement between the storage modulus and Young's modulus values. The filler effectiveness (Factor C) indicated a mechanical stiffening effect and a thermal stability contribution by the filler, while the damping reduction (DR) values confirmed that the EPDM interacted strongly with the well dispersed silica particles and the polymer chain mobility was restricted. The tensile properties, however, were in some cases worse than those for the samples prepared through the HSG method in the presence of TEOS.

Keywords: EPDM; silica; non-hydrolytic; sol-gel; morphology; properties

5.1 Introduction

The incorporation of inorganic oxides such as silica and/or titania into rubber matrices prepared by the conventional sol-gel routes led to materials with enhanced properties when compared to both unfilled rubbers and rubbers filled with traditionally prepared particles. The sol-gel process is a chemical technique initially employed to prepare high purity inorganic oxides such as glasses and ceramic materials. The advantage of the sol-gel route is that it allows fine control of particle size and distribution owed to the low temperature conditions, and it is therefore suitable for organic materials to be introduced into the process. The most widely used sol-gel route is the hydrolytic process, which involves hydrolysis and condensation of the precursors (metal oxide) to form oxide networks. The hydrolytic sol-gel process is generally divided into two steps: the first step hydrolysis, which produces hydroxyl groups, and the second step condensation, which involves the polycondensation of hydroxyl groups and residual alkoxyl groups to form a three-dimensional network. The inorganic oxide can be directly grown in the organic matrix leading to the formation of organic-inorganic hybrid structures composed of metal oxide and organic phases intimately mixed with each other. The main drawback of the hydrolytic route is the low miscibility of the sol-gel aqueous system, which limits the dispersion of the filler in the polymer [1-3]. The inorganic oxide prepared in the hydrolytic sol-gel way also has low purity and crystallinity.

An alternative method to prepare organic-inorganic material is the non-hydrolytic sol-gel (NHSG) process, which can be used to produce metal oxides of high purity and crystallinity. Moreover, the NHSG route features different reactions and reaction conditions, which significantly affect the texture, homogeneity and surface chemistry of the resulting oxide [4-6]. In the past 20 years, several non-hydrolytic synthesis methods of oxides and mixed oxides have been described, involving the reaction of precursors (alkoxides, chlorides, acetylacetonates) with oxygen donors (ethers, alcohols, ketones) [4-9]. The main non-hydrolytic routes involve the reaction of a metal chloride with either a metal alkoxide or organic ether, acting as oxygen donors [7-9] as described in Scheme 1.

Step 1	$M\text{-}Cl_m + nROH \rightarrow M\text{-}(Cl)_{m-n}(OR)_n + nHCl$
Step 2	$\equiv M\text{-}OR + RO\text{-}M\equiv \rightarrow \equiv M\text{-}O\text{-}M\equiv + R\text{-}O\text{-}R$ (by ether elimination)
and/or	$\equiv M\text{-}OR + Cl\text{-}M\equiv \rightarrow \equiv M\text{-}O\text{-}M\equiv + R\text{-}Cl$ (by alkyl-halide elimination)

Scheme 1 Non-hydrolytic sol-gel reaction scheme

The NHSG process is potentially solvent-free, without problems with hydrophobic substances and it is particularly suitable for water-sensitive species [10]. On the other hand, the formation of alkyl halide and/or alkyl ethers as by-products and the potential incompatibility with oxygen containing species have to be taken into account as possible negative aspects. The possibility of preparing polymers reinforced with metal oxides generated *in situ* by a non-hydrolytic sol-gel process, has been reviewed by several authors in recent publications [2,3]. The authors focused on poly(methyl methacrylate) (PMMA)/titanium dioxide (TiO_2) and epoxy resin/titanium dioxide (TiO_2) nanocomposites. In both investigations benzyl alcohol (BzOH) was used as an oxygen donor and titanium(IV)chloride ($TiCl_4$) as a precursor. In both cases, improvements in the mechanical and functional properties were observed, independent of the chosen polymer matrix. This was due to the improved interfacial interactions between the organic and inorganic phases brought about by the non-hydrolytic sol-gel route. Morselli *et al.* [1] investigated the non-hydrolytic sol-gel synthesis of PMMA/TiO_2 nanocomposites, starting from titanium(IV)chloride as a titania (TiO_2) precursor and benzyl alcohol as an oxygen donor. The *in situ* generated titania did not have any negative effect on the PMMA molecular weight and thermal stability, and a significant increase in both the glass transition temperature and the storage modulus was observed for all the PMMA nanocomposites.

However, the use of the NHSG processes to prepare filled polymers is not widely reported in literature, and most reports are limited to rigid thermoplastics [1,2] and thermosets [3]. In the present work silica nano-particles were *in situ* generated by using an NHSG process from silicon tetrachloride ($SiCl_4$) as silica precursor and *tert*-butanol (*t*-BuOH) as oxygen donor in the presence of EPDM rubber dissolved in toluene. The low boiling point of *t*-BuOH allows the use of mild conditions during solvent elimination, in which polymer chain degradation and/or plasticizing effects can be avoided for the composites prepared by the sol-gel reaction. Moreover, the *t*-BuOH is not only used as an oxygen donor, but due to the alkyl group steric effect, it can also act as a capping agent, and therefore, as a particle size and phase controller. This approach is expected to reduce the filler-filler interaction and give rise to improved thermal, mechanical and thermomechanical properties, as well as a better morphology and improved crosslinking.

5.2 Experimental

5.2.1 Materials

Silicon tetrachloride ($SiCl_4$), *tert*-butanol (*t*-BuOH), tin(II)2-ethylhexanoate, dicumyl peroxide, bis-[-3-(triethoxysilyl)-propyl]-tetrasulfide (TESPT) and toluene were all supplied by Sigma-Aldrich. The materials were used as received without further purification. Ethylene propylene diene monomer rubber (EPDM), Polimeri Europa Dutral® TER 4038, density 0.91 g cm^{-3}, was provided by ATG Italy (Castel d'Argile, BO, Italy).

5.2.2 Preparation of EPDM/SiO_2 composites in the absence and presence of TESPT

The EPDM/SiO_2 nanocomposites were prepared by dissolving EPDM rubber in toluene (3g/100ml) at room temperature, and a coupling agent (TESPT) was added (4 wt% with respect to EPDM) to the EPDM solution for composites prepared in the presence of TESPT. The non-hydrolytic sol-gel (NHSG) system was prepared as follows: a given amount of $SiCl_4$ was added drop-wise to *t*-BuOH under vigorous stirring at room temperature for 15 minutes, followed by addition of tin(II)2-ethylhexanoate (1:25:0.04 mol ratio). The resulting sol was mixed with a previously prepared EPDM and EPDM-TESPT solutions in round-bottom flasks and heated in an oil bath at 70 °C for 24 hours in order to complete the NHSG reaction for the conversion of $SiCl_4$ to SiO_2. The solutions were cooled to room temperature, followed by the addition of dicumyl peroxide (DCP) (4 wt% with respect to EPDM) under stirring. The reaction mixtures were taken to a rotating evaporator to eliminate about 90% of the volatile substances (toluene, unreacted *t*-BuOH and by-products of the NHSG reaction). The samples with and without TESPT (90/10 w/w EPDM/SiO_2 and 80/20 w/w EPDM/SiO_2) were obtained by casting the solutions in Petri dishes, dried overnight and later vulcanized by compression at 160 °C for 20 min. The same route was used to prepare TESPT containing EPDM samples as a control for FTIR analysis. In this case no other chemicals were added.

5.2.3 Characterization methods

The transmission electron microscopy (TEM) images were obtained using a 200 kV FEI Tecnai20 transmission electron microscope fitted with Gatan Tridiem. The EPDM silica filled samples were mounted on cryo-pins and frozen in liquid nitrogen. 100-150 nm sections were

cut at -100 °C using a Reichert Ultra-Cut S ultra-microtome chuck, collected on copper grids and viewed.

Fourier-transform infrared (FTIR) spectra of the pure EPDM and its silica filled nanocomposites were obtained using a Perkin Elmer Spectrum 100 FTIR spectrophotometer. The samples were analyzed over a range of 600-4000 cm^{-1} with a resolution of 4 cm^{-1} using an attenuated total reflectance (ATR) detector. All the spectra were averaged over 16 scans.

The crosslinking degree was determined through equilibrium swelling tests by immersing at least three rectangular specimens for each composition in 15 ml of toluene at room temperature for several hours, and the mean values are reported. The solvent was replaced hourly after each measurement to eliminate all uncross-linked fractions, such as unvulcanized EPDM chains, which could lead to incorrect values of the swelling ratio. Equilibrium swelling was determined until the swollen mass (m_s) reached a constant value, after which the samples were dried to constant mass (dried mass (m_d)) and the absolute swelling ratio (q) was evaluated according to Equation 5.1.

$$q = \frac{m_s}{m_d} \tag{5.1}$$

The absolute extractable fraction (f), where m_0 is the mass of the sample before immersion in toluene, was determined using Equation 5.2.

$$f = \frac{m_o - m_d}{m_o} \times 100 \tag{5.2}$$

The values of q and f were both normalised to the actual EPDM weight. Their values were determined using Equations 5.3 and 5.4.

$$q_{EPDM} = \frac{q}{c_{EPDM}} \tag{5.3}$$

$$f_{EPDM} = \frac{f}{c_{EPDM}} \tag{5.4}$$

where c_{EPDM} is the mass fraction of EPDM present in the composites. The gel content was determined using Equations 5.5 to 5.7, where m_{EPDM} is the mass of EPDM without silica and $\%wt_{EPDM}$ is the weight % EPDM in the composite.

$$m_{EPDM} = m_0 \times \%wt_{EPDM} \quad (5.5)$$

$$\%\, Extraction = \frac{m_o - m_d}{m_{EPDM}} \times 100 \quad (5.6)$$

$$\%\, Gel = 100 - \%\, Extraction \quad (5.7)$$

Thermogravimetric analysis (TGA) was performed with a Perkin Elmer STA6000 simultaneous thermal analyzer. The analysis was done under flowing nitrogen at a constant flow rate of 20 ml min^{-1}, and the samples (20-25 mg) were heated from 25 to 600 °C at a heating rate of 10 °C min^{-1}.

The TGA-FTIR analyses were performed in a Perkin Elmer STA6000 simultaneous thermal analyser from Waltham, Massachusetts, U.S.A. The analyses were done under flowing nitrogen at a constant flow rate of 20 ml min^{-1}. Samples (20-25 mg) were heated from 30 to 600 °C at 10 °C min^{-1}. The furnace was linked to the FTIR (Perkin Elmer Spectrum 100) with a gas transfer line. The volatiles were scanned over a 400 – 4000 cm^{-1} wavenumber range at a resolution of 4 cm^{-1}. The FTIR spectra were recorded in the transmittance mode at 250 ^{o}C during the thermal degradation process.

The tensile properties of the samples were determined using a Hounsfield H5KS tensile tester at a crosshead speed of 100 mm min^{-1} and 20 mm gauge length at ambient temperature. The samples were rectangular shaped with a width of 12 mm and a thickness varying between 0.47 and 0.67 mm. At least five specimens were tested for each composition, and the mean values are reported. For comparison, Young's modulus was predicted according to Nielsen's theoretical model [11-17].

The dynamic mechanical analysis (DMA) of the samples was done in a Perkin Elmer Diamond DMA dynamic mechanical analyzer. Rectangular shaped samples with dimensions of 40 mm length, 10 mm width and thickness varying between 0.47 and 0.67 mm thick were

tested in the tensile mode, while heated under nitrogen flow from -100 to 100 ºC at a heating rate of 3 ºC min^{-1}, and at a frequency of 1 Hz.

5.3 Results and discussion

5.3.1 Transmission electron microscopy (TEM)

The TEM micrographs of the EPDM/silica composites prepared in the absence and presence of TESPT are shown in Figure 5.1. The 90/10 w/w EPDM/SiO_2 composite prepared in the absence of TESPT shows homogeneously and fairly well dispersed silica particles, but with clear evidence of particle agglomeration. Much larger agglomerates are visible for the 80/20 w/w EPDM/SiO_2 sample prepared in the absence of TESPT, indicating increased particle-particle interaction (Figure 5.1b). The introduction of TESPT during synthesis reduced the particle-particle interaction, giving rise to much more reduced agglomeration and observably better dispersion (Figures 5.1c and 5.1d). Well dispersed and non-agglomerated particles are even visible in the 80/20 w/w EPDM/SiO_2 sample (Figure 5.1d). *In situ* synthesis using the non-hydrolytic route is obviously able to overcome the typical problems of the hydrolytic route, in which the low miscibility of the sol-gel aqueous system gives rise to more agglomeration and reduced dispersion of the silica particles [1-4]. The larger agglomerates at higher silica contents is the result of an increase in coalescence of the growing silica particles when increasing the amount of *in situ* formed dispersed phase. The silica particles may also have agglomerated in the suspension, because the hydrophilic silica particles have a tendency to associate *via* hydrogen bonding [16-20].

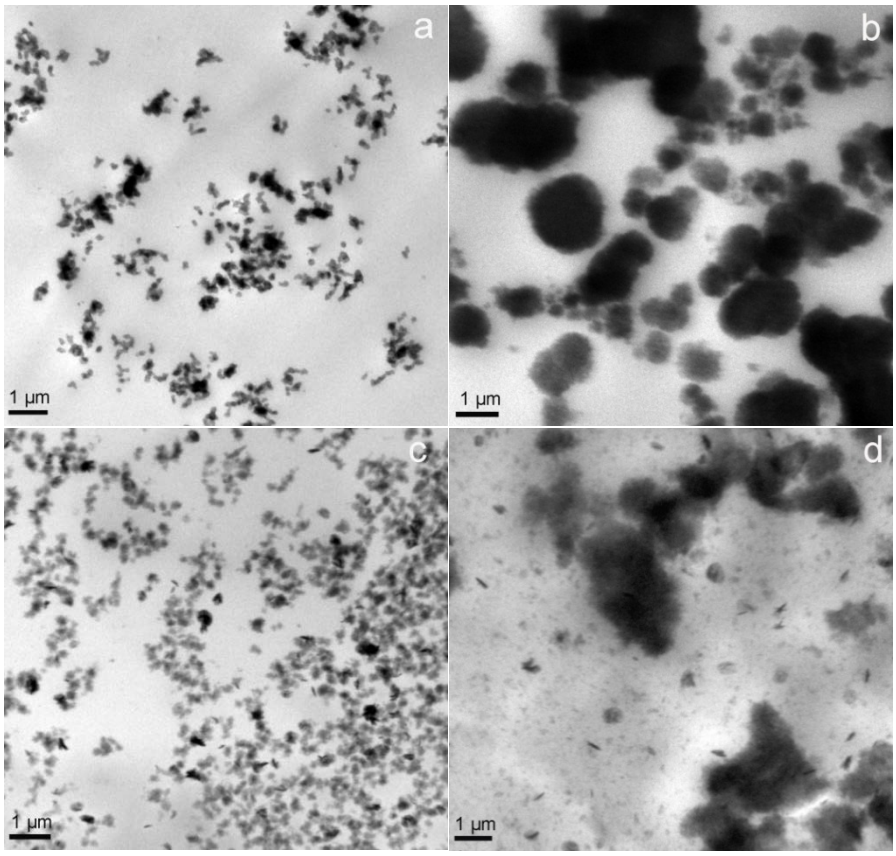

Figure 5.1 TEM micrographs of composites without TESPT (a) 90/10 w/w and (b) 80/20 w/w EPDM/SiO_2, and with TESPT (c) 90/10 w/w and (d) 80/20 w/w EPDM/SiO_2

5.3.2 Fourier-transform infrared (FTIR) spectroscopy

The FTIR spectra of all the investigated samples are shown in Figure 5.2. In the nanocomposites the EPDM can be identified by two strong peaks around 2920 and 2850 cm^{-1} assigned to the C-H stretching vibrations (Figure 5.2a). More peaks are observed at 721, 1376 and 1464 cm^{-1} and are assigned to CH_2 stretching, and CH_3 and CH_2 bending respectively [16,17]. The SiO_2 in the nanocomposites can be identified from strong stretching vibrations of the siloxane (Si-O-Si) bond at 1085 cm^{-1}, a small asymmetric stretch peak of Si-O-C at 802 cm^{-1}, and a small peak at 938 cm^{-1} assigned to Si-O stretching, indicating the presence of some silanol (Si-OH) groups, which was confirmed by comparing the FTIR spectrum of SiO_2 in Figure 2a with those of the nanocomposites. The broad peak at 3340 cm^{-1}in the SiO_2 spectrum could be assigned to the stretching vibrations of -OH groups as a result of unreacted silanols (-Si-OH). Similar peaks are observed for the EPDM/SiO_2 composites, but without the -OH peak (Figure 2a). We observed and explained the same peaks in our previous study on

the hydrolytic sol-gel (HSG) synthesis at long reaction times [16], and the peaks were the result of grafted and/or unreacted fractions of TEOS such as the ethoxysilane (-Si-OC_2H_5) and silanol groups (-Si-OH) due to unhydrolyzed silica that reacted with dicumyl peroxide (DCP) during vulcanization. The NHSG process is divided into two steps. The first step involves the reaction of a metal halide or a metal alkoxide with an organic oxygen donor (such as an alcohol or ether). The second step (condensation) can follow different pathways depending on the alkoxide used. One of the most used condensation reactions occurs through alkyl halide elimination and/or ether elimination as indicated in Scheme 1 [1,5,6,21]. However, tertiary alcohols can lead to the *in situ* formation of hydroxyl groups, which react in a second step with a chloride group according to Scheme 2. The alcohol route has been much less investigated for the preparation of oxides and mixed oxides than the alkoxide and ether routes [5].

Step 1 $\quad$ M-Cl + ROH → M-OH + R-Cl

Step 2 $\quad$ M-Cl + M-OH → M-O-M + H-Cl

Scheme 2 *In situ* formation of hydroxyl groups during the non-hydrolytic sol-gel process

In this study a tertiary alcohol (*t*-BuOH) was used and according to Scheme 2, the alcohol has reacted further to form silanol groups and this could explain the presence of the small peak at 938 cm^{-1}in the nanocomposite spectra, which is the result of silanol groups that did not react further to form siloxane groups (Si-O-Si), and that may have grafted to the rubber chains by reacting with the DCP during vulcanization (Figure 5.2a).

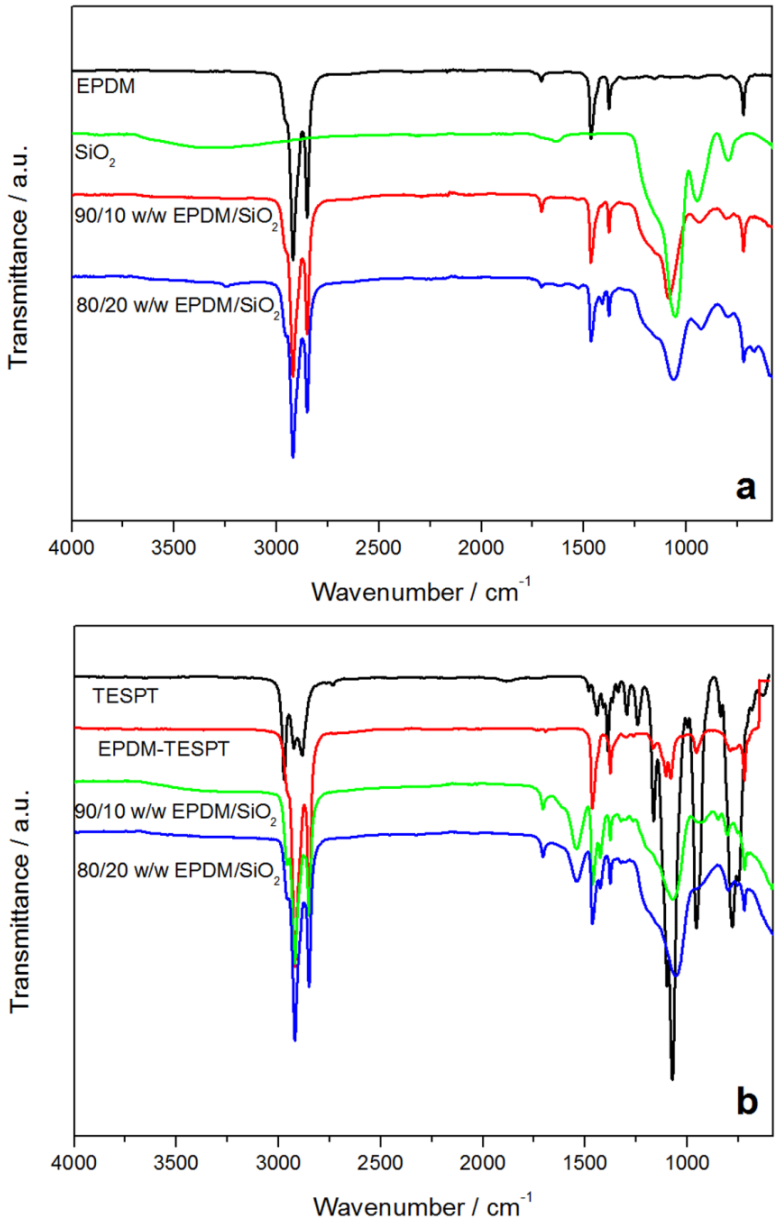

Figure 5.2 FTIR spectra of (a) EPDM, SiO_2 and the EPDM/SiO_2 composites, and (b) TESPT, EPDM-TESPT, and EPDM/SiO_2 with TESPT composites

The spectrum of EPDM-TESPT in Figure 5.2b contains a combination of the peaks observed for EPDM in Figure 5.2a and TESPT in Figure 5.2b with no new peaks or obvious peak shifts. TESPT therefore clearly did not react with EPDM under the preparation conditions used. The FTIR spectrum of the 80/20 w/w EPDM/SiO_2 prepared in the presence of TESPT shows that most of the silanols (Si-OH) reacted to form Si-O-Si bonds, with the accompanying reduction in the number of free –OH groups. This means that the silanols completely reacted to form silica links (Figure 5.2b). This spectrum also shows peaks around 1390, 1167 and 780 cm^{-1}, that were the characteristic peaks observed for TESPT in Figure

5.2b. Unlike the composites prepared through the hydrolytic sol-gel (HSG) route with TEOS as precursor [17], the TESPT did not seem to take part in the sol-gel reaction, and probably accumulated at the EPDM-silica interface.

5.3.3 Equilibrium swelling and gel content

The equilibrium swelling and gel content results for the EPDM/SiO_2 composites with and without TESPT are shown in Table 5.1. The equilibrium swelling test shows a decrease in the crosslink density with increasing filler content of the EPDM/SiO_2 composites with and without TESPT. This can be observed from the absolute swelling ratio (q and q_{EPDM}) values that increase with increasing silica content, the increasing values of the extractable fraction (f and f_{EPDM}), and the decreasing gel content values. The presence of the NHSG *in situ* generated silica particles in the EPDM inhibited the crosslinking of the rubber chains during vulcanization. The reason for this observation is that increasing amounts of DCP were used for the grafting of silanol onto the rubber chains and therefore less DCP was available to initiate the crosslinking of the rubber chains. The FTIR results also confirm this explanation, especially for composites without TESPT (10 and 20 w/w EPDM/SiO_2). From the swelling and extraction results it is clear that the *in situ* generation of silica particles through the sol-gel process led to a hindering effect on the vulcanization process, which limited the extent of crosslinking of the EPDM phase, as already observed and explained for the same material prepared through HSG synthesis with TEOS precursor at long reaction times [16].

Table 5.1 Swelling and extraction results of EPDM and the EPDM/SiO_2 composites

Samples (w/w)	q	q_{EPDM}	f / %	f_{EPDM} / %	Gel / %
EPDM	2.7 ± 0.0	2.7 ± 0.0	4.2 ± 5.5	4.2 ± 5.5	95.8 ± 5.5
Composites without TESPT					
90/10 EPDM/SiO_2	3.1 ± 0.1	3.4 ± 0.1	7.9 ± 0.5	8.7 ± 0.5	91.2 ± 0.5
80/20 EPDM/SiO_2	6.5 ± 0.0	7.7 ± 0.0	13.1 ± 1.3	15.4 ± 1.5	83.7 ± 1.6
Composites with TESPT					
90/10 EPDM/SiO_2	3.2 ± 0.0	3.5 ± 0.1	7.8 ± 0.8	8.6 ± 0.9	91.3 ± 0.9
80/20 EPDM/SiO_2	2.7 ± 0.0	3.1 ± 0.0	9.8 ± 0.4	11.5 ± 0.5	87.8 ± 0.5

The absolute swelling ratio (q) and extractable fraction (f), and their values normalized with respect to the EPDM content (q_{EPDM}, and f_{EPDM})

In the case of the composites prepared in the presence of TESPT the decrease in the crosslinking density is probably not the result of DCP reacting with the silanol groups, because the FTIR analysis of these composites does not show the presence of silanol groups indicating that most of the Si-OH reacted to form siloxane groups. A similar observation and explanation were given for HSG composites prepared from TEOS in the presence of TESPT at long reaction times [17].

5.3.4 Thermogravimetric analysis (TGA)

The TGA curves of all the investigated samples are shown in Figure 5.3, while Table 5.2 shows a summary of the TGA results. The TGA curves show two mass loss steps for all the composites. This is different from the TGA results for the same composites prepared according to the HSG route [16]. These samples did not show the first mass loss step observed here. In order to figure out the reasons for this difference, we did a TGA-FTIR analysis on the samples prepared according to the HSG and NHSG routes. The FTIR spectra obtained at 250 °C are presented in Figure 5.4. The interesting observation in Figure 4a is the peaks appearing at 2956 and 1144 cm^{-1} that indicate the CH_2 groups and the C-Cl bond in t-butyl chloride which formed in Step 1 presented in Scheme 2. There is also a strong peak at 1756 cm^{-1}, which indicates that acid chlorides may have formed part of the volatiles released at this temperature. It seems as if the t-butyl chloride is less volatile than the ethanol formed during the HSG sol-gel reaction with TEOS as precursor [16]. The ethanol probably evaporated during the course of the sol-gel reaction, while the t-butyl chloride formed during the NHSG sol-gel reaction with silicon tetrachloride remained trapped in the polymer and only evaporated at much higher temperatures during the TGA analyses of the samples. The larger mass loss observed for the TESPT containing samples prepared according to the NHSG route is clearly due to the evaporation of t-butyl chloride and other acid chlorides, as discussed above, together with unreacted TESPT (the additional peaks in Figure 5.4b correspond well with the typical peaks of TESPT, as described earlier). We can therefore confidently state that TESPT did not take part in the sol-gel reaction according to the NHSG route with $SiCl_4$ as precursor. It probably went to the interface between the polymer matrix and the silica nanoparticles, and in the process improved the interaction between EPDM and the silica nanoparticles, but not to the same extent as in the HSG process as will be shown later. At higher temperatures the TESPT then evaporated with the t-butyl chloride and other acid chlorides.

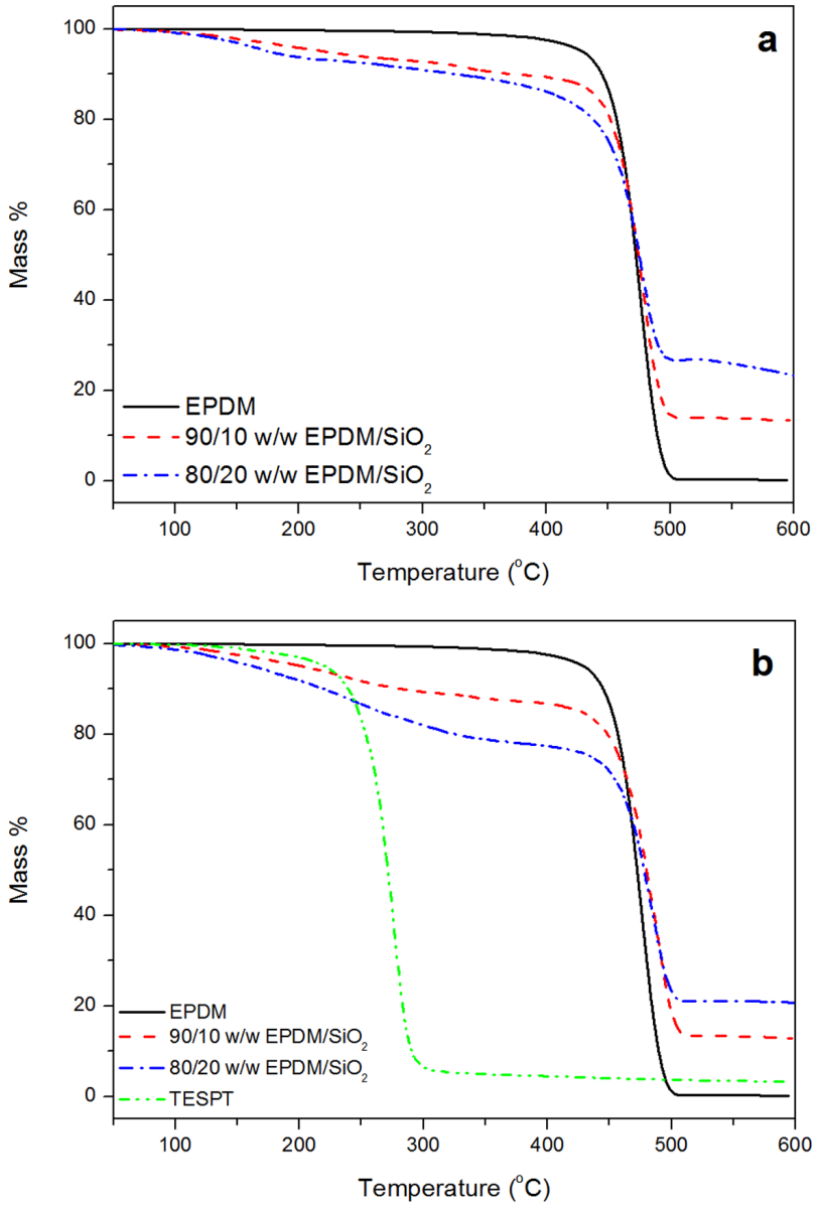

Figure 5.3 TGA curves for a) EPDM and silica filled EPDM composites and b) EPDM and silica filled EPDM composites in the presence of TESPT

The onset of thermal degradation looks very similar for all the investigated samples, and the temperatures at maximum degradation rate (T_{max}) are also very similar within experimental error. However, the actual rate of degradation is lower for the silica-containing samples (slopes of second degradation step less steep, Figure 5.3). The decrease in the rate of degradation is more pronounced for the composites prepared in the presence of TESPT (Figure 5.3b). The most probable explanation is that the well dispersed silica particles found for samples prepared in the presence of TESPT, reduced the polymer chain mobility and retarded the diffusion of volatile products from the sample.

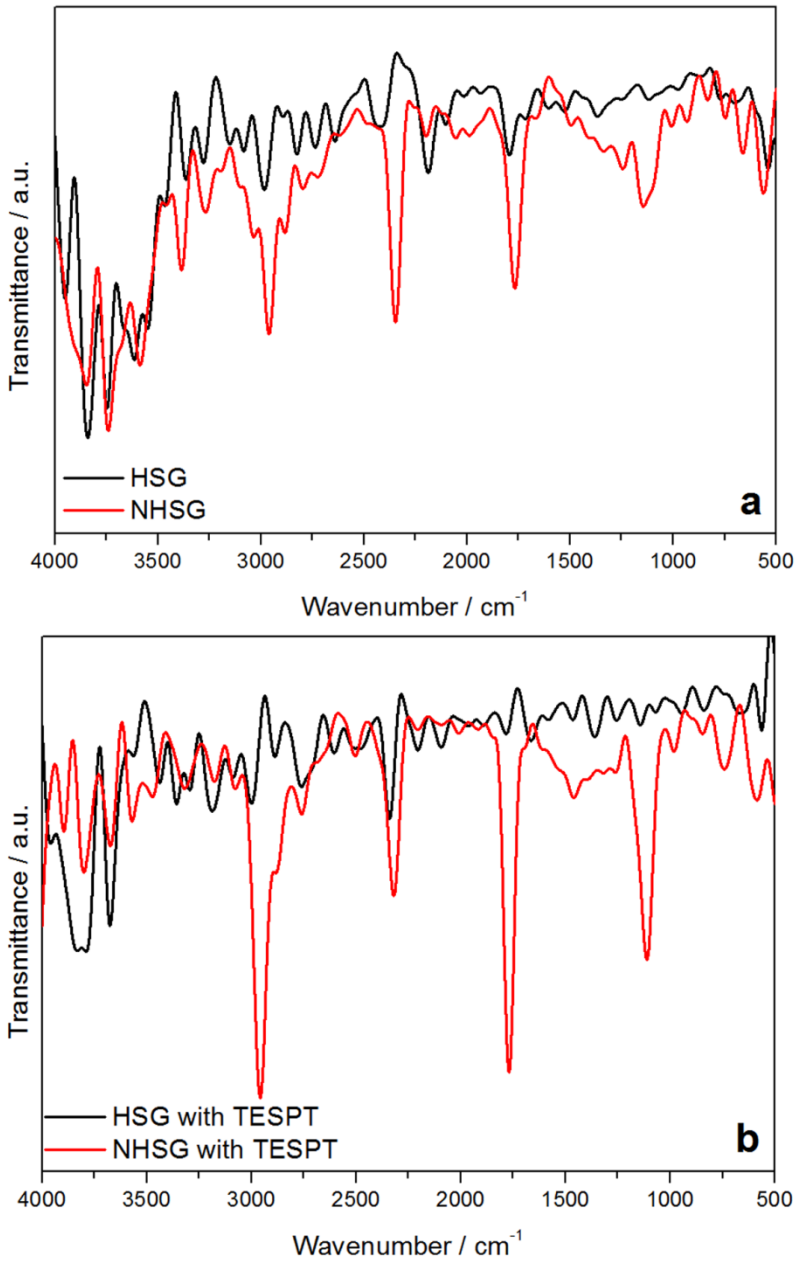

Figure 5.4 FTIR spectra of 80/20 w/w EPDM/SiO_2 during the thermal degradation in a TGA at a heating rate of 10 °C min^{-1}taken at 250 °C for (a) NHSG and HSG without TESPT and (b) NHSG and HSG with TESPT

Table 5.2 Summary of TGA results of EPDM and EPDM/SiO_2 composites

Samples	$M_{300\ ^oC}$ / %	T_{max} / °C	Char content / %	% SiO_2
EPDM	99.4 ± 0.04	475 ± 4.9	0	0
Unmodified composites				
90/10 w/w EPDM/SiO_2	92.4 ± 0.5	480 ± 1.4	12.9 ± 0.6	12.9 ± 0.6
80/20 w/w EPDM/SiO_2	91.2 ± 0.3	476 ± 2.1	22.6 ± 0.5	22.6 ± 0.8
TESPT modified composites				
TESPT	6.5 ± 0.0	277 ± 1.4	3.3 ± 0.0	-
90/10 w/w EPDM/SiO_2	89.3 ± 0.1	481 ± 4.9	13.7 ± 1.1	12.8 ± 0.6
80/20 w/w EPDM/SiO_2	81.8 ± 0.5	482 ± 7.8	22.0 ± 1.6	21.9 ± 1.6

$M_{300\ °C}$, T_{max} and % SiO_2 are the mass loss at 300 °C, the temperature at maximum degradation rate, and the silica content after normalization taking into account the char content of TESPT

Table 5.2 shows that the char content at 600 °C increases with increasing silica content for the composites prepared in the absence and presence of TESPT. The values are slightly higher than what is theoretically expected, and an FTIR analysis of the char (Figure 5.5) shows the presence of carbon (C-O bending at 1615 cm^{-1}). This could explain the higher than expected char content. The other observed peaks are the Si-O-Si stretching and Si-O-C bending at 1055 and 802 cm^{-1} respectively. The composites prepared in the absence and presence of TESPT show char spectra with similar peaks.

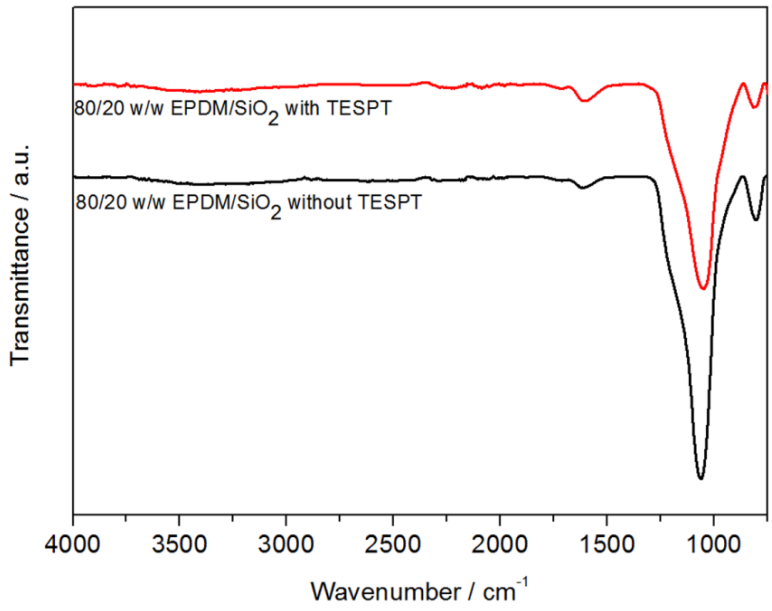

Figure 5.5 FTIR spectra of the char taken at 600 °C of two of the investigated composites

5.3.5 Tensile testing

The Young's modulus as function of volume fraction of neat EPDM and its silica filled composites are shown in Figure 5.6 together with its predicted Nielsen theoretical model fitting [11,28-31]. The values for Young's modulus, stress and elongation at break are summarized in Table 5.3. For composite materials consisting of spherical particles in the matrix, the Nielsen equation has the form given in Equations 5.8 and 5.9.

$$E = E_1 \left[\frac{1+AB\phi_2}{1-B\psi\phi_2}\right] \quad (5.8)$$

$$B = \frac{{}^{E_2}/_{E_1} - 1}{{}^{E_2}/_{E_1} + A} \quad (5.9)$$

Where E, E_2 and E_1 are the modulus values of the composite, filler and matrix respectively, and ϕ_2 is the volume fraction of the filler. The theoretical modulus used for the silica particles was E_2 = 70 GPa [32]. The factor ψ takes into account the values of ϕ_m of the dispersed phase and it is given by Equation 5.10.

$$\psi = 1 + \left[\left(\frac{1-\phi_m}{\phi_m^2}\right)\phi_2\right] \quad (5.10)$$

where ϕ_m is the maximum packing fraction. The constant B takes into account the relative moduli of the filler and matrix phases, and its value is 1.0 for very large E_2/E_1 ratios (the values for E_2 and E_1 are 70 GPa and 2.0 MPa, respectively, and therefore we could confidently use a value of 1.0). The constant A is related to the Einstein coefficient given by Equation 5.11 and is determined by the morphology of the system. For strong aggregates, the value of A can become quite large while ϕ_m of the dispersed phase will decrease.

$$A = k_E - 1 \quad (5.11)$$

Figure 5.6 represents the Young's modulus of all the investigated samples, together with Nielsen's model fittings. The values of the A and ϕ_m used to predict the relationship between the experimental and theoretical moduli were 2.0 and 0.35 respectively for the composites prepared in the absence of TESPT. For the composites prepared in the presence of TESPT,

the values of A and ϕ_m were 3.5 and 0.2. The *in situ* generation of silica particles by a NHSG route obviously reduced the silica particle size and improve its dispersion in EPDM compared to our previous work using the HSG route [16,17]. The non-hydrolytic route seems to overcome the typical problems related to hydrolytic route, in which the low miscibility of the sol-gel aqueous system limits the dispersion and distribution of the filler in the matrix. The low value of ϕ_m indicates the presence of agglomerated silica particles, but the aggregates are small enough for the value of A to be fairly small. The composites prepared in the presence of TESPT shows a better Nielsen's model fit and higher Young's modulus values than the composites prepared in absence of TESPT. This is in line with the smaller particles and better dispersion observed in the TEM images in Figure 5.1. Smaller particles and better dispersion will improve the matrix-filler interaction and increase the rubber reinforcement, giving rise to higher tensile modulus values.

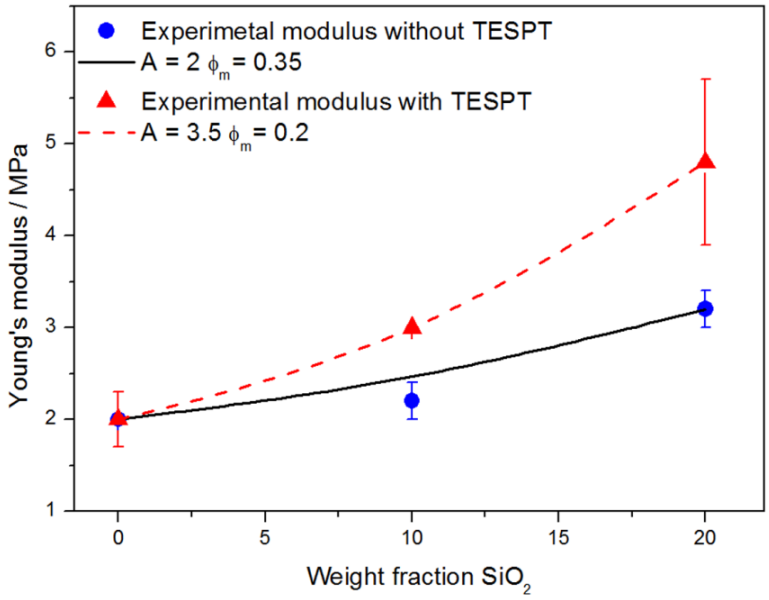

Figure 5.6 Young's modulus as a function of weight fraction of SiO_2 in EPDM/SiO_2 composites (Δ) with TESPT and (●) without TESPT: experimental modulus and Nielsen's model fittings

The stress and elongation at break values observably increase with increasing silica content for all the EPDM/SiO_2 composites compared to those of the neat EPDM (Table 5.3). This indicates good reinforcement and is the result of improved adhesion between the filler and the matrix giving rise to effective stress transfer. For 10 wt.% of filler the stress and elongation at break values increased, but for 20 wt.% filler these values decreased, but they are still higher

than that of pure EPDM. The reason for this observation is the agglomeration of the silica particles in the 20 wt.% filled composite. The composites prepared in the presence of TESPT have significantly higher stress at break, but lower elongation at break, values than the comparable composites prepared in the absence of TESPT. The most probable explanation for the lower elongation at break for the samples prepared in the presence of TESPT is that TESPT probably settled on the interface between the silica particles and EPDM and did not form part of the network. Table 5.4 shows the percentage differences between the stress and elongation at break values of samples prepared according to the HSG and NHSG routes, and in the absence and presence of TESPT. The change in the reaction route from HSG to NSHG shows increased σ_b and ε_b values as a result of smaller particles and better particle matrix interactions. However, when TESPT was present, the same change in reaction route only improved the stress at break, but reduced the elongation at break. The reason for this is the fact that during the HSG route the TESPT takes part in the sol-gel reaction and becomes part of the crosslinked network, while during the NHSG route it does not take part in the sol-gel reaction and only sits on the EPDM-silica interface.

Table 5.3 Summary of tensile results of EPDM and EPDM/SiO_2 composites

Samples	E/ MPa	σ_b / MPa	ε_b / %
EPDM	2.0 ± 0.3	1.6 ± 0.3	589 ± 43
Unmodified composites			
90/10 w/w EPDM/SiO_2	2.2 ± 0.2	4.9 ± 2.1	2863 ± 101
80/20 W/W EPDM/SiO_2	3.2 ± 0.2	3.4 ± 0.3	1865 ± 35
TESPT modified composites			
90/10 w/w EPDM/SiO_2	3.0 ± 0.0	10.0 ± 1.6	1570 ± 14
80/20 W/W EPDM/SiO_2	4.8 ± 0.9	4.4 ± 2.1	963 ± 10

E, σ_b and ε_b, are the modulus, stress at break and elongation at break

Table 5.4 Percentage change in stress and elongation at break with change in reaction route and with addition of TESPT

Changes in the reaction route (80/20 w/w EPDM/SiO_2)	% change in σ_b	% change in ε_b
HSG→NHSG in the absence of TESPT	17	95
HSG→NHSG in the presence of TESPT	19	-9
Presence of TESPT for HSG	28	11
Presence of TESPT for NHSG	29	-48

5.3.6 Dynamic mechanical analysis (DMA)

Values obtained from dynamic mechanical analysis (DMA) are summarized in Table 5.5. The filler effectiveness (Factor C) in the rubber matrix can be evaluated from the values of the storage modulus obtained in the glassy and rubbery regions by using Equation 5.12 [33].

$$Factor\ C = \frac{(E'_g/E'_r)composites}{(E'_g/E'_r)matrix} \qquad (5.12)$$

where, E'_g and E'_r are the storage moduli determined in the glassy and rubbery regions, respectively. The state of filler dispersion in the rubber matrix was determined by calculation of the damping reduction (DR) from the damping values obtained from the normalized tan δ peaks ($(\tan\delta)_{EPDM}$ and $(\tan\delta)_{composite}$) and is given by Equation 5.13 [33].

$$DR = \frac{(\tan\delta)_{EPDM} - (\tan\delta)_{composite}}{(\tan\delta)_{EPDM}} \times 100\% \qquad (5.13)$$

The storage modulus values in the glassy region increase with increasing silica content (see $E'_{T=-80^oC}$ values in Table 5.5). There is also a significant increase in the storage modulus with increasing silica content in the rubbery region (see $E'_{T=20^oC}$ values in Table 5.5). These modulus values depend on (i) the degree of crosslinking of the rubber, (ii) the content of the rigid dispersed phase, and (iii) the sizes of the filler particles. All these factors will contribute to an increase in the modulus. As can be seen from Table 5.1, the degree of crosslinking decreased with increasing silica content. However, the presence of the rigid dispersed silica particles and their interaction with EPDM reduced the chain mobility and increased the stiffness of the rubber to such an extent that the effect of the reduced crosslinking was not

observable. The increase in agglomeration at higher silica content may also have contributed to the increase in modulus. Furthermore, the modulus values of the composites prepared in the presence of TESPT are significantly higher than those of the comparable composites prepared in the absence of TESPT. This is in line with the already discussed Young's modulus values.

Table 5.5 Summary of DMA results of EPDM and EPDM/SiO_2 composites with and without TESPT

Samples (w/w)	$E'_{-80\,°C}$ / MPa	$E'_{20\,°C}$ / MPa	$(\tan\delta)_{max}$	T_g / °C	DR^{Norm} / %	Factor C
EPDM	4.1	1.7	0.5188	- 41.0	-	1
Unmodified composites						
90/10 EPDM/SiO_2	9.1	4.2	0.5197	-46.7	- 0.17	1.21
80/20 EPDM/SiO_2	5.9	6.8	0.4405	-42.1	15.1	0.38
TESPT modified composites						
90/10 EPDM/SiO_2	6.6	6.9	0.4378	-44.3	15.6	0.45
80/20 EPDM/SiO_2	11.8	9.9	0.3958	-42.5	23.7	0.57

$E'_{-80\,°C}$, $E'_{20\,°C}$, $(\tan\delta)_{max}$, T_g, Factor C and DR^{Norm} are the modulus values at -80 °C and 20 °C, maximum tan δ (normalised to the amount of rubber in the nanocomposites), glass transition temperature, filler effectiveness and the damping reduction (calculated from $(\tan\delta)_{max}$)

Table 5.6 Storage modulus at 40 °C of EPDM/SiO_2 nanocomposites prepared according to the HSG and NHSG routes in the absence and presence of TESPT

$E'_{T=40°C}$ / MPa	
Hydrolytic sol-gel (HSG) route without TESPT	
90/10 w/w EPDM/SiO_2	80/20 w/w EPDM/SiO_2
6.7	12.3
Hydrolytic sol-gel (HSG) route with TESPT	
90/10 w/w EPDM/SiO_2	80/20 w/w EPDM/SiO_2
8.2	8.8
Non-hydrolytic sol-gel (NHSG) route without TESPT	
90/10 w/w EPDM/SiO_2	80/20 w/w EPDM/SiO_2
4.2	6.8
Non-hydrolytic sol-gel (NHSG) route with TESPT	
90/10 w/w EPDM/SiO_2	80/20 w/w EPDM/SiO_2
6.7	9.9

$E'_{40\ °C,}$ storage modulus value at 40 °C

Table 5.6 shows the storage modulus values in the rubbery region at 40 ^{o}C for the EPDM/SiO_2 composites prepared according to the HSG and NHSG routes in the absence and presence of TESPT. Generally, comparable composites prepared according to the HSG route show higher storage modulus values than the composites prepared according to the NHSG route. The reasons for this is probably (i) that larger silica particles formed for the samples prepared according to the HSG route, and that these larger particles add more stiffness to the EPDM matrix than the smaller particles, and (ii) that the TESPT formed part of the network structure for the samples prepared according to the HSG route, while it sat on the EPDM-silica interface for the samples prepared according to the NHSG route, to some extent acting as a plasticizer.

The filler effectiveness (Factor C) can be used to indicate the composite reinforcing capacity. By definition an unfilled rubber matrix has a Factor C equal to 1, and a Factor C lower than 1 indicates a mechanical stiffening effect as well as a thermal stability contribution of the used filler [33]. The values in Table 5.5 show that the silica particles improved the stiffness of

EPDM. However, the 90/10 w/w EPDM/SiO_2 composite shows values that are not in line with the rest of the values. This is the result of the high storage modulus values obtained at temperatures below the glass transition temperature. This result was found to be reproducible, and therefore it is not possible to offer an explanation at this point in time.

The normalized tan δ values in Table 5.5 clearly decrease with increasing silica content for the composites prepared in the absence and presence of TESPT, and they are lower for the samples prepared in the presence of TESPT. This is attributed to good adhesion between the filler and the matrix, which resulted in a restriction in the rubber chain mobility in the composites. The damping reduction (DR^{Norm}) values, which increased with both increasing silica content and with TESPT treatment, confirm the stronger interaction of EPDM with smaller and well dispersed silica particles which led to a reduction in the polymer chain mobility. However, the glass transition temperature (T_g) decreased for the 10 wt.% silica-containing samples (Table 5.5), but again increased for the 20 wt.% silica-containing samples. Reduced crosslinking should decrease the value of T_g, while the presence of the silica particles and their interaction with EPDM should reduce the mobility of the rubber chains and increase the value of T_g. In the case of the 10 wt.% silica containing samples the reduced crosslinking seems to have a dominant effect, while the effect of chain immobilization by the silica particles is more dominant in the case of the 20 wt.% silica containing samples.

5.4 Conclusions

NHSG synthesis of EPDM-silica composites prepared in the absence and presence of a coupling agent was investigated. The TEM results showed that in the absence of TESPT the silica particles were homogeneously and fairly well dispersed, but with clear evidence of particle agglomeration and much larger agglomerates were visible at high silica content (20 wt.%). The introduction of TESPT reduced the particle-particle interaction, and gave rise to much reduced agglomeration and observably better dispersion. The presence of silica particles inhibited the crosslinking density of the vulcanized EPDM matrix for all the composites prepared in the absence and presence of TESPT. The reduced crosslinking density of the composites prepared in the absence of TEST was caused by reduced amounts of DCP available to initiate crosslinking, because the DCP was partially utilised in the grafting of silanol groups onto the rubber chains. In the case of the composites prepared in the presence of TESPT, the decline was due to the coupling agent that probably settled on the interface

between the silica particles and EPDM and did not form part of the network. This caused enough free volume between the chains to accommodate the toluene molecules during swelling, and resulted in an increase in the swelling ratio.

The thermal stability of the EPDM/SiO_2 composites showed two mass loss steps for all the composites. The mass loss in the range 100-400 ^oC was caused by the evaporation of t-butyl chloride and other acid chlorides present in the composites, as well as the evaporation of TESPT that settled on the interface between the silica particles and EPDM for composites prepared in the presence of TESPT.

The Nielsen fitting of the Young's modulus indicated smaller and better dispersed filler particles for the NSHG route, and this further improved when the preparation was done in the presence of TESPT. Improved stress at break was observed as a result of improved EPDM-silica interactions that led to better stress transfer. However, the elongation at break was lower for the samples prepared in the presence of TESPT, probably because TESPT settled on the interface between the silica particles and EPDM and did not form part of the network. The DMA results supported the observations and conclusions from the other techniques.
In summary, the NHSG route generally gave rise to smaller and better dispersed filler particles than the HSG route, and this was reflected in the investigated thermal and mechanical properties of the composites. However, the presence of TESPT during the sol-gel preparation had a much smaller influence in the NHSG route. This is probably because TESPT did not take part in the sol-gel reaction and only settled on the interface between EPDM and the silica particles, as was established from a thermal degradation analysis of the samples.

5.5 References

1. D. Morselli, F. Bondioli, M. Fiorini,M. Messori. Poly(methyl methacrylate)-TiO_2 nanocomposites obtained by non-hydrolytic sol-gel synthesis: The innovative tert–butyl alcohol route. Journal of Materials Science 2012; 47:7003-7012.
   DOI: 10.1007/s10853-012-6651-4
2. D. Morselli, M. Messori, F. Bondioli. Poly(methyl methacrylate)-TiO_2 nanocomposite obtained by non-hydrolytic sol-gel synthesis. Journal of Materials Science 2011; 46:6609-6617.

DOI:10.1007/s10853-011-5610-9

3. D. Morselli, F. Bondioli, M. Sangermano, M. Messori. Photo-cured epoxy networks reinforced with TiO_2 *in-situ* generated by means of non-hydrolytic sol-gel process. Polymer 2012; 53:283-290.
   DOI: 10.1016/j.polymer.2011.12.006
4. P.H. Mutin, A. Vioux. Nonhydrolytic processing of oxide-based materials: Simple routes to control homogeneity, morphology, and nanostructure. Chemistry of Materials 2009; 21: 582–596.
   DOI: 10.1021/cm802348c
5. D.P. Debecker, P.H. Mutin. Non-hydrolytic sol–gel routes to heterogeneous catalysts. Chemical Society Reviews 2012; 41:3624-3650.
   DOI: 10.1039/C2CS15330K
6. V. Lafond, P.H. Mutin, A. Vioux. Non-hydrolytic sol–gel routes based on alkyl halide elimination: Toward better mixed oxide catalysts and new supports: Application to the preparation of a SiO_2–TiO_2 epoxidation catalyst. Journal of Molecular Catalysis A: Chemical 2002; 182–183:81–88.
   DOI: S1381-1169(01)00487-3
7. M. Niederberger. Nonaqueous sol-gel routes to metal oxide nanoparticles. Accounts of Chemical Research 2007; 40:793–800.
   DOI: 10.1021/ar600035e
8. C. Lind, S.D. Gates, N.M. Pedoussaut, T.I. Baiz. Novel materials through non-hydrolytic sol-gel processing: Negative thermal expansion oxides and beyond. Materials 2010; 3:2567-2587.
   DOI:10.3390/ma3042567
9. P. Arnal, R.J.P. Corriu, D. Leclercq, P.H. Mutin, A. Vioux. A solution chemistry study of non-hydrolytic sol-gel routes to titania. Chemistry of Materials 1997; 9:694-698.
   DOI:10.1021/cm960337t
10. J.N. Hay, H.M. Raval. Synthesis of organic-inorganic hybrids via the non-hydrolytic sol-gel process. Chemistry of Materials 2001; 13:3396–3403.
11. Y.-P. Wu, Q.-X. Jia, D.-S. Yu, L.-Q. Zhang. Modeling Young's modulus of rubber-clay nanocomposites using composite theories. Polymer Testing 2004; 23:903-909.
    DOI: 10.1016/j.polymertesting.2004.05.004

12. T.K. Jayasree, P. Predeep. Effect of filler on mechanical properties of dynamically crosslinked styrene butadiene rubber/high density polyethylene blends. Journal of Elastomers and Plastics 2008; 40:127-146.
DOI: 10.1177/0095244307083865
13. S. Ahmed, F.R. Jones. A review of particulate reinforcement theories for polymer composites. Journal of Materials Science 1990; 25:4933-4942.
14. L.E. Nielsen. Morphology and elastic modulus of block polymers and polyblends. Rheological Acta 1974; 13:86-92.
15 L.E. Nielsen, R.F. Landel. Mechanical Properties of Polymers and Composites. Marcel Dekker, Inc.: New York (1994)
ISBN: 0 8247 8964 4
16. T.H. Mokhothu, A.S. Luyt, D. Morselli, F. Bondioli, M. Messori. Influence of *in situ* generated silica nanoparticles on EPDM morphology, thermal, thermomechanical and mechanical properties. Polymer Composites (submitted).
17. T.H. Mokhothu, A.S. Luyt, M. Messori. Reinforcement of EPDM rubber with *in situ* generated silica particles in the presence of a coupling agent *via* a sol-gel route. Polymer Testing 2014; 33:97-106.
DOI:10.1016/j.polymertesting.2013.11.009
18. M. Messori, F. Bignotti, R. De Santis, R. Taurino. Modification of isoprene rubber by *in situ* silica generation. Polymer International 2009; 58:880-887.
DOI: 10.1002/pi.2606
19. Y. Ikeda, Y. Kemeda. Preparation of “green” composites by the sol-gel process: *In situ* filled natural rubber. Journal of Sol-Gel Science and Technology 2004; 31:137-142.
DOI: 10.1023/B:JSST.0000047975.48812.1b
20. S. Prasertsri, N. Tattanasom. Mechanical and damping properties of silica/natural rubber composites prepared from latex system. Polymer Testing 2011; 30:515-526.
DOI: 10.1016/j.polymertesting.2011.04.001
21. H. Wang, W. Zhong, P. Xu, Q. Du. Polyimide/silica/titania nanohybrids via a novel non-hydrolytic sol-gel route. Composites Part A: Applied Science and Manufacturing 2005; 36: 909–914.
DOI:10.1016/j.compositesa.2004.12.008
22. D. Zhu, W.J. van Ooij. Structural characterization of bis-[triethoxysilylpropyl] tetrasulfide and bis-[trimethoxysilylpropyl]amine silanes by Fourier-transform infrared

spectroscopy and electrochemical impedance spectroscopy. Journal of Adhesion Science and Technology2002; 16:1235–1260.
DOI: 10.1163/156856102320256873

23. T.E. Motaung, A.S. Luyt, S. Thomas. Morphology and properties of NR/EPDM rubber blends filled with small amounts of titania nanoparticles. Polymer Composites 2011; 32:1289-1296.
DOI:10.1002/pc.21150

24. Q. Ji, X. Wang, Y. Zhang, Q. Kong, Y. Xia. Characterization of poly(ethylene terephthalate)/SiO_2 nanocomposites prepared by sol-gel method. Composites Part A 2009; 40:878-882.
DOI: 10.1016/j.compositesa.2009.04.010

25. K. Chrissafis, D. Bikiaris. Can nanoparticles really enhance thermal stability of polymers? Part I: An overview on the thermal decomposition of addition polymers. Thermochimica Acta 2011; 523:1-24.
DOI: 10.1016/j.tca.2011.06.010

26. D. Bikiaris. Can nanoparticles really enhance thermal stability of polymers? Part II: An overview on the thermal decomposition of polycondensation polymers. Thermochimica Acta 2011; 523:25-45.
DOI: 10.1016/j.tca.2011.06.012

27. T.K. Dey, M. Tripathi. Thermal properties of silicon powder filled high-density polyethylene composites. Thermochimica Acta 2010; 502:35-42.
DOI: 10.1016/j.tca.2010.02.002.

28. G.M.O. Barra, J.S. Crespo, J.R. Bertolino, V. Soldi, A.T.N. Pires. Maleic anhydride grafting on EPDM: Qualitative and quantitative determination. Journal of the Brazilian Chemical Society 1999; 10:31-34.

29. A.I. Hussain, M.L. Tawfic, A.A. Khalil, T.E. Awad. High performance emulsified EPDM grafted with vinyl acetate as compatibilizer for EPDM with polar rubber. Nature and Science 2010; 8:348-357.
No DOI: only (ISSN: 1545-0740)

30. T.K. Jayasree, P. Predeep. Effect of filler on mechanical properties of dynamically crosslinked styrene butadiene rubber/high density polyethylene blends. Journal of Elastomers and Plastics 2008; 40:127-146.
DOI: 10.1177/0095244307083865

31. S. Ahmed, F.R. Jones. A review of particulate reinforcement theories for polymer composites. Journal of Materials Science 1990; 25:4933-4942.
32. T.H. Hsieh, A.J. Kinloch, K. Masania, J.S. Lee, A.C. Taylor, S. Sprenger. The toughness of epoxy polymers and fibre composites modified with rubber microparticles and silica nanoparticles. Journal of Materials Science 2010; 45:1193-1210.
DOI: 10.1007/s10853-009-4064-9
33. A. Gregorova, M. Machovsky, R. Wimmer. Viscoelastic properties of mineral-filled poly(lactic acid) composites. International Journal of Polymer Science 2012; 2012:1-6.
DOI: 10.1155/2012/252981

Chapter 6

EPDM rubber reinforced with titania generated by non-hydrolytic sol-gel process

This chapter has been published as:
K. Paderni, M. Messori, D. Morselli, F. Bondioli, A.S. Luyt, T.H. Mokhothu. EPDM rubber reinforced with titania generated by non-hydrolytic sol-gel process. Polymer Engineering & Science (in press).

Abstract

EPDM rubber was reinforced with titania *in situ* generated by using a non-hydrolytic sol-gel (NHSG) process starting from $TiCl_4$ as titania precursor and *tert*-butanol as oxygen donor. Titania particles in anatase form and with average diameter of 6 nm were synthesized via NHSG route and then the same procedure was adopted in presence of EPDM rubber to obtain composites containing up to 30 wt% of filler. Extraction and equilibrium swelling tests suggested an interfering effect of the NHSG reaction on the vulcanization process of the rubber resulting to a crosslink density which decreased in the presence of titania. Quasi-static and dynamic-mechanical characterizations indicated that the presence of titania as rigid filler in both the unvulcanized and vulcanized EPDM matrix led to a significant increase in stiffness and stress at break. The experimental values of modulus were systematically higher than the values predicted by classical equations suggesting an additional stiffening contribution deriving from the molecular interaction between the rubber and the filler.

6.1 Introduction

Organic-inorganic hybrid nanocomposites represent not only a new field of basic research but also, thanks to their remarkable new properties and multifunctional nature, hybrids offer prospects for many new applications in extremely different technological fields. Today the very large set of accessible hybrid materials span a wide spectrum of properties which yield the emergence of innovative industrial applications in various domains such as transportation, health, energy, housing, optics, micro-electronics, and the environment among others [1].

Concerning the specific case of polymer matrices modified/reinforced with nano-fillers, it is well known that metal oxide nano-particles arising from flame pyrolysis or aqueous syntheses cannot be easily dispersed in organic oligomers or polymers by means of conventional physical mixing processes, due to their hydrophilic character and strong tendency to agglomeration. In this respect, organic-inorganic hybrid materials based on *in situ* generation of nanoparticles represent a possible alternative to design new composite materials [2]. Among the different synthetic procedures, sol-gel chemistry represents one of the preferred ways for the bottom-up approach for the preparation of organic-inorganic hybrids thanks to its mild conditions particularly suited for thermally unstable organic polymers. The sol-gel process is a chemical method to prepare inorganic materials, initially employed to synthesize high purity inorganic networks such as glasses and ceramic materials. Typical precursors are metal alkoxides which, when reacting with water, lead to nano-particles having narrow grain size distribution with dimensions ranging from 5 to 100 nm.

The most used method is based on the so-called aqueous (or hydrolytic) sol-gel process, which is generally divided into two steps: the first one named hydrolysis, which produces hydroxyl groups, and the second one named condensation, that involves the polycondensation of hydroxyl groups and residual alkoxyl groups to form a three-dimensional network [3]. The presence in the reactive system of an organic oligomer or polymer (bearing or not bearing suitable groups reactive towards the sol-gel process) leads to the formation of organic-inorganic hybrid structures composed of metal oxide and organic phases intimately mixed with each other.

Alternative to the aqueous route, the so-called non-hydrolytic sol-gel (NHSG) reaction can be used to obtain metal oxides with high purity and crystallinity [4]. As in the case of the aqueous route, the NHSG process is divided in two steps. The first step involves the reaction of a metal halide or a metal alkoxide with an organic oxygen donor (such as an alcohol, ether, etc.). The second step (condensation) can follow different pathways depending on the alkoxide employed. One of the most used condensation reactions occurs through alkyl halide elimination and/or ether elimination as schematically indicated:

Step 1	$MX_m + n\ ROH \rightarrow M(X)_{m-n}(OR)_n + n\ HX$
Step 2	$\equiv M\text{-}OR + RO\text{-}M\equiv \rightarrow \equiv M\text{-}O\text{-}M\equiv + R\text{-}O\text{-}R$
and/or	$\equiv M\text{-}OR + X\text{-}M\equiv \rightarrow \equiv M\text{-}O\text{-}M\equiv + R\text{-}X$

In general terms, compared to the hydrolytic counterpart, it is recognized that the NHSG process is potentially solvent-free, without problems with hydrophobic substances and particularly suitable for water-sensitive species [5]. On the other hand, the formation of alkyl halide and/or alkyl ethers as by-products and the potential incompatibility with oxygen-containing species have to be taken into account as possible negative aspects.

The possibility of preparing rubbers, modified with metal oxides generated *in situ* by a sol-gel process, has already been reviewed by several authors in recent publications [6,7]. Authors recently published several papers on the *in situ* generation of inorganic oxides into isoprene, epoxy and ethylene-propylene-diene-monomer (EPDM) rubbers by using a hydrolytic sol-gel process reporting detailed studies on the interrelation between preparation conditions, structure and mechanical reinforcement [8-12].

Concerning the specific case of EPDM-based materials modified by *in situ* generation of silica, Das *et al.* [13] swelled triethoxysilyl-grafted EPDM in tetraethoxysilane and activated the sol-gel process by adding *n*-butyl amine as a basic catalyst. After rubber vulcanization, mechanical characterization showed that *in situ* sol-gel derived fillers had superior reinforcing efficiency, compared with the externally added silica at the same concentration of these fillers in an EPDM matrix. The main limitation of the proposed synthetic method was the relative low value of the maximum concentration of *in situ* generated silica, which appeared limited by diffusion phenomena of TEOS within the unvulcanized rubber matrix during the swelling step. In order to overcome this drawback, an alternative solution process was proposed to ensure a highly homogeneous dispersion of the *in situ* generated filler in the rubbery matrix, also for high reinforcing metal oxide contents [12].

On the other hand, the use of the NHSG processes to prepare filled polymers is not widely reported in literature even if authors already reported some applications limited to rigid thermoplastics [14,15] and thermosets [16].The NHSG method is here proposed as an alternative synthetic way with respect to the hydrolytic route. The conventional hydrolytic route has two intrinsic drawbacks, such as the poor crystallinity of the synthesized oxides and the great sensitivity on various reaction parameters. Another remarkable drawback related to this route is the immiscibility between the polymeric phase and the aqueous oxygen donor, which usually leads to the formation of particles agglomerates if no coupling agent is employed.

A very simple procedure (few parameters to control), significantly higher crystallinity and the absence of water can be mentioned as major advantages of the NHSG. Moreover, the in situ synthesis should improve the compatibility between filler and matrix thanks to the presence of an organic layer on the particles' surface. On this basis, in the present work titania nano-particles were *in situ* generated by using an NHSG process from $TiCl_4$ as titania precursor and *tert*-butanol as oxygen donor in the presence of EPDM rubber dissolved in toluene. The obtained filled elastomers were thus characterized in terms of physical and mechanical properties.

6.2 Experimental

6.2.1 Materials

EPDM rubber (Polimeri Europa Dutral TER 4038, density ρ_{EPDM} = 0.91 g·cm^{-3}) was kindly provided by ATG Italy (Castel d'Argile, BO, Italy). Titanium(IV) chloride ($TiCl_4$), *tert*-butanol (*t*-BuOH), toluene, ethanol (EtOH), and dicumyl peroxide (DCP) were purchased from Sigma Aldrich (Milan, Italy). All materials were high purity reactants and were used as received without any further purification.

6.2.2 Preparation of EPDM-titania composites

EPDM rubber was dissolved in toluene (about 3 g in 100 mL) at room temperature. After complete dissolution, the sol-gel system was prepared as follows: a given amount of $TiCl_4$ was added drop-wise to t-BuOH under vigorous stirring at room temperature. After stirring for 15 min, the resulting sol was mixed with a previously prepared EPDM solution in a round-bottom flask and heated in an oil bath at 70°C for 24 h in order to complete the NHSG reaction in the presence of the organic matrix. The t-BuOH/$TiCl_4$ molar ratio was maintained at 25; therefore the amount of $TiCl_4$ was varied in order to obtain composites having a nominal content of TiO_2 (i.e. considering the complete conversion of $TiCl_4$ to TiO_2) of 0, 10, 20, and 30 wt% with respect to EPDM rubber. The obtained suspensions were concentrated by rotary evaporation at 50°C in order to eliminate about 90% of the volatile substances (toluene, unreacted t-BuOH and by-products of the NHSG reaction). For all the samples, DCP (in toluene solution) was also added at a concentration of 4 phr (with respect to EPDM) as

vulcanizing agent and mechanically mixed before the end of the solvent elimination step, when the viscosity of the suspension was not too high to inhibit the mixing.

The high viscous suspensions were then cast in a Petri dish (10 min of dynamic vacuum was applied for removing all possible bubbles) and the volatiles were completely eliminated by leaving the systems under an aspiration hood overnight. The slow solvent evaporation (at room temperature and under atmospheric pressure) permitted the production of specimens without the presence of bubbles. Bubbles formation was not observed neither in unvulcanized and vulcanized samples. Some of the films (about 0.5 mm thick) were vulcanized by hot-pressing at 160^{o}C for 20 min. The vulcanization conditions were optimized on the basis of preliminary tests carried out on unfilled EPDM. The hot plate press used for the vulcanization was rapidly cooled by cooling system working by tap water and specimens were quickly cooled at room temperature immediately after the curing step.

Unfilled reference EPDM sample was prepared in the same conditions used for filled EPDM. In particular, EPDM was previously dissolved in toluene and the evaporation step was subsequently applied in order to produce specimens with as much as possible similar preparation procedure of the filled ones.

The unvulcanized and vulcanized materials were coded as EPDM_x and EPDM_x_V, respectively, in which x represents the nominal final weight percent of titania. In order to characterize the powders embedded in the EPDM, the NHSG reaction was performed following the same procedure described above, except for the presence of EPDM in the reaction media. The synthesized powder was carefully washed and centrifuged (15 min and 4000 rpm), twice with 15 mL of chloroform, twice with 15 mL of acetone and once with 15 mL of diethyl ether. Finally it was dried overnight under an aspiration hood at room temperature. The obtained powder was coded as TiO_2_tert.

6.2.3 Characterization

The synthesized dried TiO_2 particles were analyzed with a computer-assisted conventional Bragg-Brentano diffractometer using the Ni-filtered CuK_α monochromatic radiation (λ = 1.5418 Å) (PANalytical, X'Pert PRO difractometre) to identify the crystalline phase. The X-ray diffraction (XRD) patterns were collected at room temperature in a 2θ range of 10-90°,

with a scanning rate of 0.005 °·s^{-1} and a step size of 0.02 °. In addition, the crystallite size were estimated from X-ray reflection broadening measurements by evaluating the full width at half maximum of the TiO2 (1,0,1) diffraction line at 25^{o}(2θ), according to the Scherrer equation [17].

In order to evaluate the amount of organic phase on the particles' surfaces and calculate the reaction yields of the NHSG, thermogravimetric analysis (TG) was performed by a Perkin-Elmer TGA7 thermogravimetric analyzer under nitrogen flow, from 30 up to 700 °C at a heating rate of 10 °C·min^{-1}.

Density of the synthesized powder was determined by a picnometer (Accupic 1330 apparatus, Micromeritics).

Particle morphologies and particle sizes were examined by transmission electron microscopy (TEM) using a JEM 2010 TEM Jeol instrument. A drop of the suspensions in methanol (previously sonicated for 30 min) was placed on a copper grid covered with a transparent polymer, followed by drying under vacuum. TEM Images were analyzed and processed by ImageJ open-source software.

The composites, both unvulcanized and vulcanized, were broken in liquid nitrogen and the cross-sections were analyzed by scanning electron microscopy (SEM, TESCAN VEGA3) by the application of an accelerating voltage of 25 kV. The samples (cross section) were coated with gold (thickness 150 nm) by an electrodeposition method to impart electrical conduction before the SEM analysis.

Thermogravimetric analysis (TG) was performed on the composites using the same instrument and experimental conditions used for the powders.

Swelling experiments were carried out by the immersion of punch-cut specimens (size 10×10×0.5 mm^3) in 15 mL of toluene at room temperature for several hours in order to eliminate all uncross-linked fractions, such as unvulcanized EPDM chains, which would lead to wrong values of the swelling ratio. When the swollen mass (m_s) reached a constant value, the sample was dried to a constant mass (i.e., the dried mass m_d), and the absolute swelling ratio (q) was evaluated according to the following equation:

$$q = \frac{m_s}{m_d} \quad (6.1)$$

The absolute extractable fraction (f) was determined as follows:

$$f = \frac{m_o - m_d}{m_o} \times 100 \quad (6.2)$$

where m_0 is the mass of the sample before its immersion in toluene.

The values of q and f were also normalized to the actual EPDM weight (i.e., the swellable phase and, in the case of incomplete vulcanization, the extractable phase), and these values were called q_{EPDM} and f_{EPDM}, respectively. Their values were calculated as follows:

$$q_{EPDM} = \frac{q}{W_{EPDM}} \quad (6.3)$$

$$f_{EPDM} = \frac{f}{W_{EPDM}} \quad (6.4)$$

where w_{EPDM} is the weight fraction of EPDM present in the composite.

Dynamic-mechanical analysis (DMA) was carried out using a Perkin-Elmer Diamond DMA; punch-cut specimens (40×10×0.5 mm^3) were tested in tensile mode at a constant frequency of 1 Hz, while heated from -100 to 100 °C at a rate of 3 °C·min^{-1} under nitrogen gas.

Uniaxial tensile tests were performed by a Hounsfield dynamometer (model H5KS). The experiments were run at room temperature, on strips 32×13×0.5 mm^3 in size, using a gauge length of 10 mm and a crosshead speed of 100 mm·min^{-1}.

6.3 Results and discussion

6.3.1 Characterization of titania powders

All the characterizations performed on the titania powder are summarized in Table 6.1 and the XRD pattern of the synthesized powder is reported in Figure 6.1. All peaks show the presence of anatase (ICCD 00-021-1272) as main crystalline phase while the shoulder at about 31° (2θ) can be attributed to the presence of brookite (ICCD 00-029-1360) as secondary phase.

Furthermore, using Scherrer's equation [17] to determine the crystallites size by peak broadening analysis, the average crystal size of powder was calculated to be about 5 nm.

Table 6.1 Properties of titania powders obtained from the corresponding suspensions

Material code	Average crystal size from XRD /nm	Average crystal size from TEM / nm	Residue at 700 °C /wt.%	NHSG reaction yield / %	ρ_{exp} / g·cm^{-3}	ρ_{TiO2} / g·cm^{-3}
TiO_2_tert	5 ± 2	6 ± 1	71.4 ± 0.6	92 ± 5	2.7 ± 0.3	3.5 ± 0.4

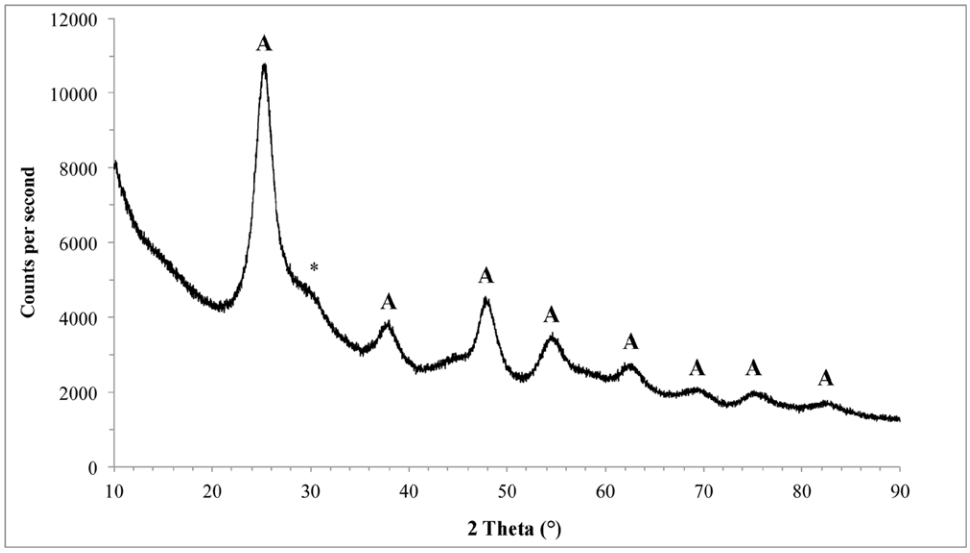

Figure 6.1 XRD pattern of the synthesized TiO2-tert powder (A: anatase, * brookite)

The shape and the dimensions of the primary particles were also evaluated by TEM. The obtained images (Figure 6.2a) show that the synthesized powder is nanostructured and presents crystals having particle sizes in the range from 3 to 12 nm, as reported in Figure 6.2b showing an average value of 6 ± 1 nm, in good agreement with that obtained by Scherrer's equation.

TG analysis, carried out to evaluate the presence of organic substances strongly absorbed and/or covalently linked to the titania particles, show the presence of a significant amount of organic substance, which leads to an average mass loss of 29 wt%. Moreover, the NHSG reaction yield was calculated taking into account the mass loss found by TG analysis. The average yield was 92%, in good agreement with the results obtained by TG analysis on the

unvulcanized composites that showed actual titania amounts between 89 and 91% if compared to the nominal ones.

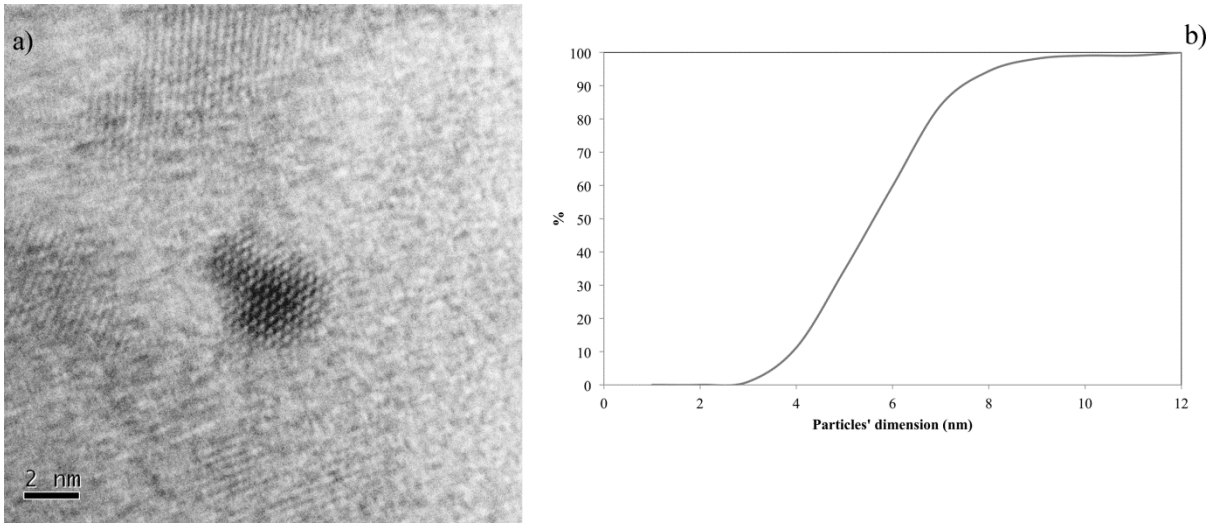

Figure 6.2 TEM micrograph (a) and particles' size distribution (b) of the synthesized powder

On the basis of this evidence, the experimental density (ρ_{exp}) value of the powder (Table 6.1) is relatively low if compared to the literature value of 3.9 g·cm^{-3} for pure anatase, and can be considered as deriving from hybrid materials comprised of titania and organic substances presumably covering the surface of the inorganic particles, as confirmed by TG analysis. In order to determine the actual density of the titania particles without the contribution of the organic component, density value was corrected by assuming *t*-BuOH as main component of the organic phase (density $\rho_{t\text{-BuOH}}$ = 0.775 g·cm^{-3}) and the density additivity rule, according to the following equation:

$$\rho_{exp} = \rho_{TiO2} \cdot w_{TiO2} + \rho_{t\text{-BuOH}} \cdot w_{t\text{-BuOH}} \qquad (6.5)$$

in which w_{TiO2} and $w_{t\text{-BuOH}}$ are the weight fractions of titania and *t*-BuOH, respectively. This corrected value was used for the calculation of the volume composition of the prepared EPDM-titania nanocomposites.

6.3.2 Characterization of EPDM-titania composites

6.3.2.1 Scanning electron microscopy (SEM)

SEM characterization of the composites allowed the evaluation of the distribution and aggregation of titania particles in the rubber matrix. Typical SEM micrographs of unvulcanized rubber with a nominal titania content of 10, 20 and 30 wt% are reported in Figure 6.3. The picture for EPDM_10 in Figure 6.3a shows a fairly good dispersion of the titania particles in the rubber matrix, although there is also clear evidence of particle agglomeration. The TEM analysis of the titania particles showed that they had diameters around 6 nm, while the aggregates in the composites seem to have dimensions around 300 nm. By increasing the titania content (EPDM_20 in Figure 6.3b), the particle distribution remained good enough, but a significant increase in particle sizes was observed. The average aggregate dimension was around 1.4 μm.

The sample with the highest titania content (EPDM_30 in Figure 6.3c) showed an increase in the particle size and in the size distribution. In particular, large particles having diameters higher than 15 μm were present together with smaller particles (about 1 μm in size), meaning that higher filler content causes higher particle aggregation, as already observed and reported by other authors for similar systems [9,18] and can be tentatively explained taking into account that by increasing the amount of *in situ* formed dispersed phase an increase in the coalescence of the growing particles and of both the average dimensions of the dispersed particles and aggregation are expected. The SEM micrographs showed no relevant differences between the vulcanized material (EPDM_20_V in Figure 6.3d) and the unvulcanized materials, meaning that the vulcanization process does not affect the composite morphologies.

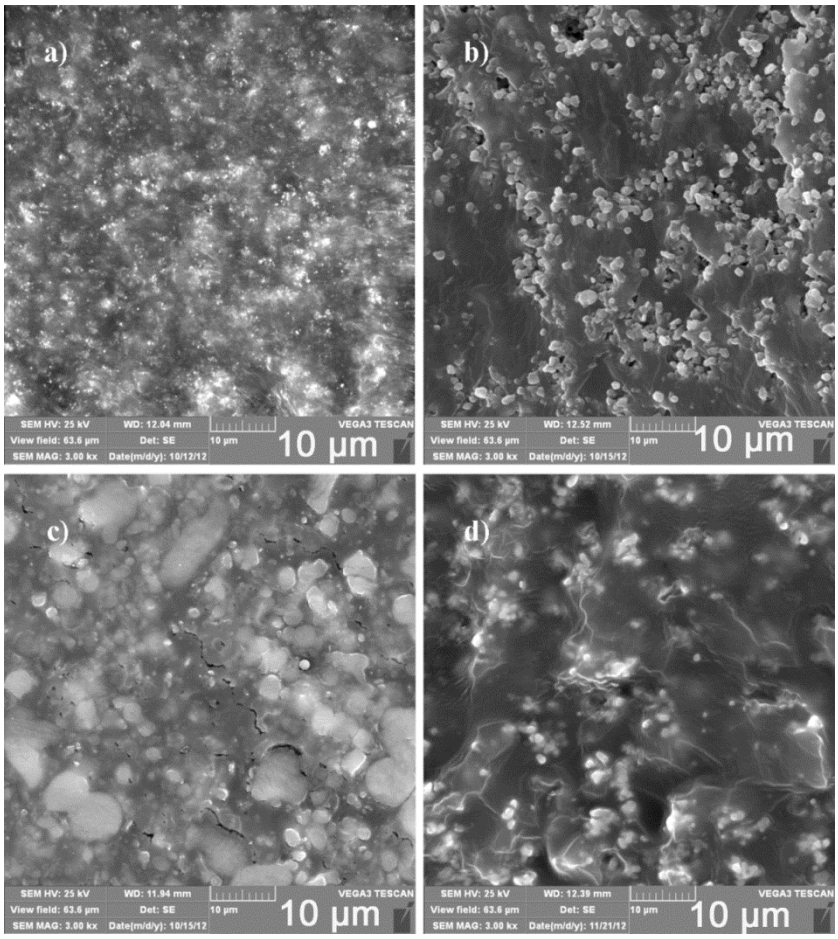

Figure 6.3 SEM micrographs of (a) EPDM_10, (b) EPDM_20, (c) EPDM_30, and (d) EPDM_20_V

6.3.2.2 Thermogravimetric analysis (TGA)

TG analysis was used to determine the actual content of titania and to investigate the thermal oxidative stability of the composites. The actual filler content values are reported in Table 6.2 for unvulcanized and vulcanized composites. In all the cases, the actual filler contents were very near to the expected values, indicating that the experimental conditions used were appropriate to induce an almost complete conversion of $TiCl_4$ to titania. Other recently reported rubber-matrix composites obtained by *in situ* generation of titania through a hydrolytic sol-gel process showed conversion values of titania precursors (titanium *iso*-propoxide) in the range 80-84% [11] suggesting a higher reactivity of NHSG with respect to the hydrolytic counterpart. As expected, the vulcanization process carried out at high temperature induced a slight increment in the yield of titania.

Table 6.2 Thermogravimetric analysis: actual titania content (mass residue at 700 °C) and onset temperature (T_{ONSET}) of the main degradation step of EPDM_x and EPDM_x_V composites

Material code	Actual TiO_2 content / %	T_{ONSET} / °C	Material code	Actual TiO_2 content / %	T_{ONSET} / °C
EPDM_0	0.0 (-)	435	EPDM_0_V	0.0 (-)	431
EPDM_10	9.1 (91)	435	EPDM_10_V	9.6 (96)	441
EPDM_20	17.7 (89)	358	EPDM_20_V	18.8 (94)	433
EPDM_30	27.2 (91)	327	EPDM_30_V	28 (93)	375

Representative TG curves of unvulcanized EPDM_x are reported in Figure 6.4 and the T_{ONSET} values of the main degradation step are reported in Table 6.2. The weight losses occurred in three distinct steps. In the first step, the weight loss in the range 50-200 °C was probably due to the evaporation of strongly absorbed solvents and/or condensation by-products of the reaction of $TiCl_4$ to titania. Interestingly, this degradation step was significantly delayed in the case of unfilled EPDM_0. The second step corresponding to the maximum weight loss in the range of 250-500 °C was ascribed to the decomposition of the polymer chain and its onset was strongly affected by the titania content. In the third step, the weight loss observed up to 650 °C was presumably due to the elimination of char residues formed in the previous step.

Comparing the sample containing 10 wt% of filler content with the pristine EPDM, the decomposition temperature didn't change for the unvulcanized materials or slightly increased for the vulcanized ones as indicated by the T_{ONSET} values reported in Table 6.2. The slight increase in resistance to thermal decomposition resulted for the fact that TiO_2 particles were able to sustain high temperature and to retard the heat to diffuse into EPDM matrix.

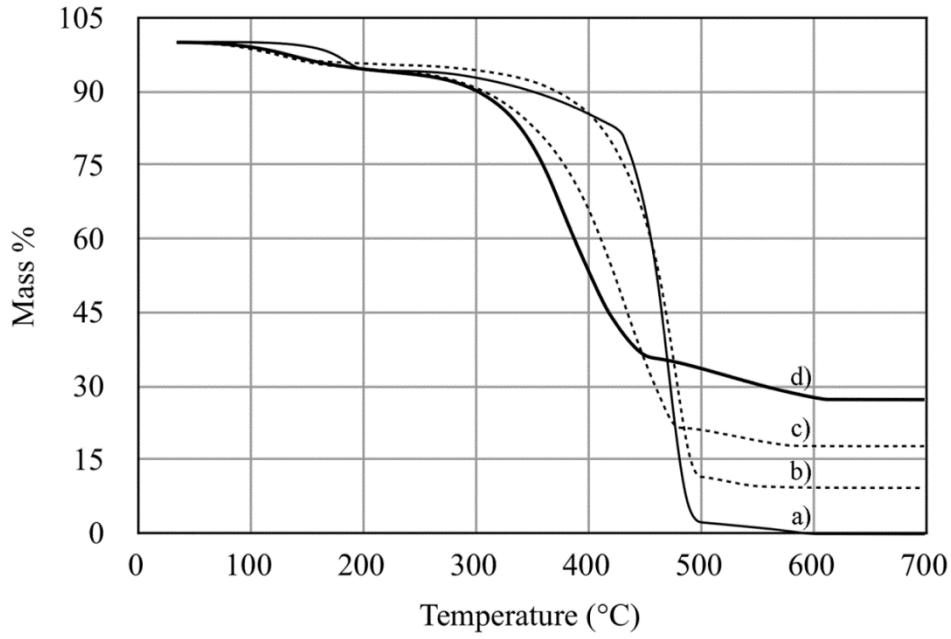

Figure 6.4 TG curves of (a) EPDM_0, (b) EPDM_5, (c) EPDM_15, and (d) EPDM_30

With further increment of filler loadings (20 and 30 wt%), a worsening or no further increases in thermal resistance of composites were observed, in accordance to Haitao *et al.* [19]. One possibility is that with higher titania content particles aggregated more seriously in EPDM matrix, which made the decline in thermal resistance, furthermore it could probably be attributed to metal-catalyzed oxidative decomposition pathways in the polymer/titania composite, as already observed and discussed for similar materials [20].

6.3.2.3 Equilibrium swelling analysis and extractable fraction

The values of q, q_{EPDM}, f *and* f_{EPDM} in toluene are reported in Table 6.3. For the unfilled rubber, equilibrium swelling analysis is a well-known method to evaluate the number of effective network chains per volume unit (i.e., the cross-linking density) of an elastomer after vulcanization. In the case of the filled vulcanized rubber, the swelling behavior depends on complex and different phenomena, such as the crosslinking degree of the rubber matrix, the solvent absorption contribution of the titania phase, the ability of the titania particles to act as crosslinking points (i.e., density of polymer-filler attachments), and so on. Taking into account that conversion of $TiCl_4$ to titania can be considered almost quantitative, the extractable fraction in toluene was mainly derived from the uncrosslinked fraction of EPDM.

In other words, it could be considered an indicator of the progress of the vulcanization process of EPDM.

In principle, the presence of inorganic fillers should lead to a reduction of the swelling ratio with respect to the unfilled vulcanized rubber, because of the fact that the filler does not absorb toluene during the experiment. In the present case an opposite trend was observed: both values (q and q_{EPDM}) of unfilled rubber are lower than those of the filled samples. In particular, the increment of q_{EPDM} (i.e., the swelling ratios referring only to the organic rubber phase) for the filled systems compared to the unfilled ones was attributable to the decreased crosslink density of the rubber phase after vulcanization. This hypothesis is also supported by the observation that f_{EPDM} in toluene increased with increasing titania content (and thus the initial $TiCl_4$ concentration); this clearly indicates an interfering effect of the sol-gel reaction of $TiCl_4$ to titania on the vulcanization process of the rubber. The same behaviour has already been observed for EPDM modified with silica generated *in situ* by a hydrolytic sol-gel process [12].

Table 6.3 Swelling/extraction tests: absolute extractable fraction (f), swelling ratio (q) and values normalized with respect to the EPDM content (f_{EPDM} and q_{EPDM})

Material code	f (%)	f_{EPDM} (%)	q (-)	q_{EPDM} (-)
EPDM_0_V	0	0	9.4	9.4
EPDM_10_V	29.7	32.6	24.7	27.1
EPDM_20_V	31.7	38.5	20.7	25.2
EPDM_30_V	47.4	65.1	16.7	22.9

6.3.2.4 Quasi-static mechanical properties

In order to differentiate the effects due to presence of titania (hydrodynamic effect of a rigid filler) and to the vulcanization of the EPDM matrix (crosslink density), quasi-static and dynamic-mechanical properties were determined before and after the vulcanization step of EPDM-based composites. The results obtained by mechanical characterization (tensile tests) for unvulcanized and vulcanized composites are summarized in Tables 6.4 and 6.5.

The data shown in Table 6.4 indicate that the presence of titania as rigid filler in the unvulcanized EPDM matrix led to a significant increase in stiffness (both initial and secant moduli) and of the ultimate properties such as stress at break (σ_b). Concerning the low deformation range, the initial modulus increased monotonically by increasing the titania content with an average value for EPDM_30 (8.43 MPa) almost 6 times higher than that of the unfilled unvulcanized EPDM_0 (1.47 MPa). Stiffening and reinforcing effects due to the presence of titania were also observed over a large deformation range with values of secant modulus $E_{sec,\varepsilon=1}$, $E_{sec,\varepsilon=2}$ and $E_{sec,\varepsilon=3}$ and of stress at break σ_b being systematically higher than those of the unfilled rubber. Also for these parameters, a monotonic increase by increasing the titania content was observed indicating that the concentration of titania particles represent the main parameter for controlling the mechanical properties of these composite materials.

Comparing the stress at break and deformation at break of the filled composites, it is evident that the material EPDM_10 has the highest value of deformation at break and a good value of stress at break only with 9.1 wt% of titania content, thanks to a good dispersion and the lowest particle aggregation in the rubber matrix.

Das *et al.* [13] proposed a ‘‘reinforcing efficiency’’ (R.E.) parameter to evaluate the reinforcing effect due to the presence of rigid filler with respect to the unfilled rubber matrix. R.E. is defined as the quotient of the difference of the secant moduli at 100% elongation of filled and unfilled vulcanized rubber ($(E_{sec,\varepsilon=1})_{filled}$ and $(E_{sec,\varepsilon=1})_{unfilled}$, respectively), with reference to the amount of filler (wt %TiO_2). The reinforcing efficiency is thus defined by:

$$RE = \frac{(E_{100\%})_{filled} - (E_{100\%})_{unfilled}}{wt\%\ TiO_2} \qquad (6.6)$$

Table 6.4 Mechanical characterization of unvulcanized composites: initial modulus (E_{in}), secant modulus at an elongation ε = 1, 2, 3 ($E_{sec,\varepsilon=1}$, $E_{sec,\varepsilon=2}$, $E_{sec,\varepsilon=3}$), stress at break (σ_b), deformation at break (ε_b) and reinforcing efficiency parameter (R.E.)

Material code	E_{in} / MPa	$E_{sec,\varepsilon=1}$ / MPa	$E_{sec,\varepsilon=2}$ / MPa	$E_{sec,\varepsilon=3}$ / MPa	σ_b / MPa	ε_b / %	RE / MPa.wt%$^{-1}$
EPDM_0	1.47 ± 0.09	0.81 ± 0.06	0.47 ± 0.03	0.33 ± 0.02	2.03 ± 0.35	1322 ± 216	-
EPDM_10	2.13 ± 0.10	0.97 ± 0.04	0.56 ± 0.03	0.42 ± 0.02	3.11 ± 0.57	1425 ± 218	0.018
EPDM_20	3.53 ± 0.18	1.40 ± 0.10	0.75 ± 0.08	0.60 ± 0.04	2.82 ± 0.30	854 ± 140	0.033
EPDM_30	8.43 ± 0.18	2.85 ± 0.08	1.67 ± 0.05	1.23 ± 0.04	5.16 ± 0.70	896 ± 182	0.075

Table 6.5 Mechanical characterization of vulcanized composites: initial modulus (E_{in}), secant modulus at an elongation ε = 1, 2, 3 ($E_{sec,\varepsilon=1}$, $E_{sec,\varepsilon=2}$, $E_{sec,\varepsilon=3}$), stress at break (σ_b), deformation at break (ε_b) and reinforcing efficiency parameter (R.E.)

Material code	E_{in} / MPa	$E_{sec,\varepsilon=1}$ / MPa	$E_{sec,\varepsilon=2}$ / MPa	$E_{sec,\varepsilon=3}$ / MPa	σ_b / MPa	ε_b / %	RE / MPa.wt%$^{-1}$
EPDM_0_V	1.40 ± 0.10	0.89 ± 0.08	0.61 ± 0.03	-	1.12 ± 0.21	171 ± 48	-
EPDM_10_V	1.69 ± 0.16	0.91 ± 0.12	0.53 ± 0.07	0.39 ± 0.04	2.51 ± 0.47	1148 ± 95	0.002
EPDM_20_V	2.56 ± 0.35	1.17 ± 0.12	0.67 ± 0.07	0.49 ± 0.05	2.90 ± 0.13	1144 ± 153	0.015
EPDM_30_V	3.58 ± 0.16	1.42 ± 0.08	0.83 ± 0.03	0.62 ± 0.02	3.90 ± 0.46	1256 ± 167	0.019

R.E. values varied from 0.018 to 0.075, showing the maximum value for the highest titania content (EPDM_30) as already discussed for the above reported mechanical properties. Interestingly, the present values are of the same order of magnitude as those observed by Das *et al*. [13] (in the range 0.03-0.12) for composite materials prepared by generating silica particles through a hydrolytic sol-gel process and by using triethoxysilyl-grafted EPDM as rubber matrix which ensured a very good interfacial interaction between the silica particles and the rubber matrix. This comparison, even if concerning different filler particles, can suggest that the generation of titania particles by NHSG in the presence of the rubber matrix was able to enhance the mechanical properties typical of filled systems in the presence of coupling agents, that is a strong filler-matrix interface was created due to the NHSG process.

Concerning the effect of the vulcanization process, the data reported in Table 6.5 indicate an unexpected generalized slight decrement of properties. The values of initial modulus (E_{in}), secant moduli ($E_{sec,\varepsilon=1}$, $E_{sec,\varepsilon=2}$, $E_{sec,\varepsilon=3}$) and stress at break (σ_b) were systematically lower than those determined before vulcanization. This decrease of moduli (strongly remarkable for EPDM_20_V and EPDM_30_V compared with the unvulcanized ones) can be mainly ascribed to some degradative effect due to the vulcanization step at high titania contents. Accordingly, the R.E. parameter also decreased significantly. However, the trend of reinforcement for increased amount of titania was confirmed also in the case of vulcanized composites.

A very significant difference of elongation at break after vulcanization is clearly evident. This behaviour can be explained taking into account that the vulcanization process seems to be inhibited in the presence of titania generated by NHSG process (see swelling/extraction data reported in Table 3). In other words, an efficient vulcanization of EPDM_0_V resulted in a relatively high crosslinking degree (which results in a lower elongation at break) while the opposite for EPDM_10_V, EPDM_20_V and EPDM_30_V samples.

Concerning the initial modulus, the effect due to the inclusion of rigid filler particles is known as hydrodynamic reinforcement and can be quantitatively predicted by using the Smallwood-Guth-Einstein equation: [20]

$$E = E_0(1 + 2.5\phi + 14.1\phi^2) \qquad (6.7)$$

in which ϕ represents the filler volume fraction. Notwithstanding the strict assumptions of this equation (the filler particles are spherical, completely wetted by the rubber and interact only pair-wise), it could be a useful preliminary evaluation of the expected hydrodynamic reinforcement due to the addition of a rigid filler. The initial elastic modulus E_{in} of unvulcanized and vulcanized EPDM-based composites predicted by the Smallwood-Guth-Einstein equation is reported in Figure 6.5, together with the experimental data obtained with tensile tests.

The figure clearly shows significantly higher modulus values with respect to the theoretical calculation based only on a hydrodynamic effect. As already pointed out, this effect increased by increasing the titania content and it was particularly important in the case of unvulcanized materials even if significantly present also after vulcanization. This behavior (mechanical properties of the rubber are enhanced more than what would be expected from a mere addition of rigid particles to a soft elastomeric matrix) was already observed for EPDM reinforced with silica *in situ* generated by a hydrolytic sol-gel process [12] and it was tentatively explained as an additional contribution arising from the molecular interaction between the rubber and the filler.

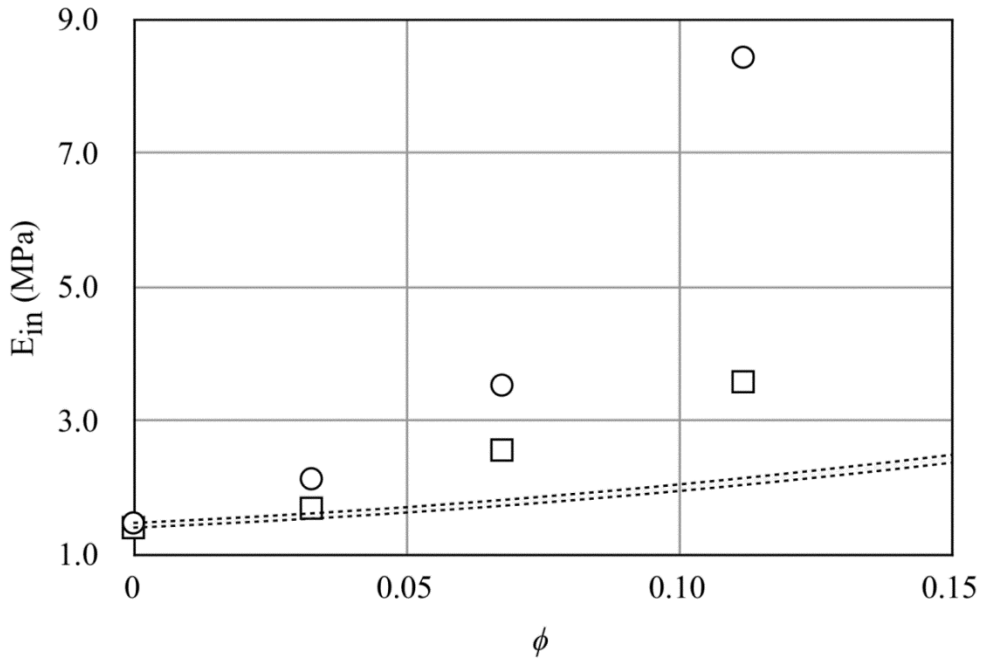

Figure 6.5 Initial elastic modulus as a function of filler volume fraction for EPDM_x and EPDM_x_V: predicted values from the Smallwood-Guth-Einstein equation (upper and lower dashed lines, respectively) and experimental data (○ and □, respectively)

6.3.2.5 Dynamic-mechanical properties

Storage modulus (E') and loss factor (tan δ) as a function of temperature are reported in Figures 6.6 and 6.7 for the EPDM_x and EPDM_x_V composites, respectively. The values of storage modulus measured in the glassy region (at a temperature of -70 °C, E'_{-70C}) and in the rubbery region (at a temperature of 25 °C, E'_{25C}), damping (expressed as maximum value of loss factor, tan δ_{max}) and glass transition temperature (T_g, determined as the peak temperature value of the loss factor) are reported in Table 6.6.The DMA results show that dynamic-mechanical properties of the vulcanized rubber were significantly affected by the presence and content of titania particles. According to the results obtained with quasi-static tensile properties, the storage modulus values measured in the glassy region (E'_{-70C}) and in the rubbery region (E'_{25C}) increased significantly by increasing the titania content in the case of unvulcanized rubber. The same trend is not clearly visible for vulcanized rubbers due to the lower crosslink density of the rubber phase after vulcanization. Furthermore, it is usually expected that in particulate filled polymers, the addition of rigid fillers to the polymer matrix restricts the movement of the polymer chains leading to a reduction in damping and a shift in T_g values to higher temperatures [22].

In this study, a significant reduction of damping (here evaluated as the maximum value of the loss factor, tan δ_{max}) was observed by increasing the titania content in both unvulcanized and vulcanized EPDM rubber. The glass transition temperature was slightly affected by the presence of *in situ* generated titania in the case of unvulcanized materials with values monotonically increasing from -38.7 °C for unfilled EPDM (EPDM_0) up to -31.8 °C for the composite with the highest titania content (EPDM_30).

In the case of the vulcanized composites, the increase in T_g by increasing the titania content was less evident and not strictly correlated with the filler concentration. In previous papers, a hindering effect towards the vulcanization process due to the presence of *in situ* generated inorganic oxides (silica) was observed resulting in a reduction in the cross-linking degree of the vulcanized EPDM rubber [12]. Also in the present case the vulcanization of EPDM in the presence of fillers generated by sol-gel processes produced a crosslinked rubber matrix with lower crosslink densities. Taking into account that both the quasi-static and dynamic-mechanical properties of the vulcanized rubber derive from different contributions such as filler amount and crosslink density of the matrix [22], the lack of strict correlation between

filler concentration and ultimate properties can be tentatively attributed to the less efficient vulcanization of the rubber matrix.

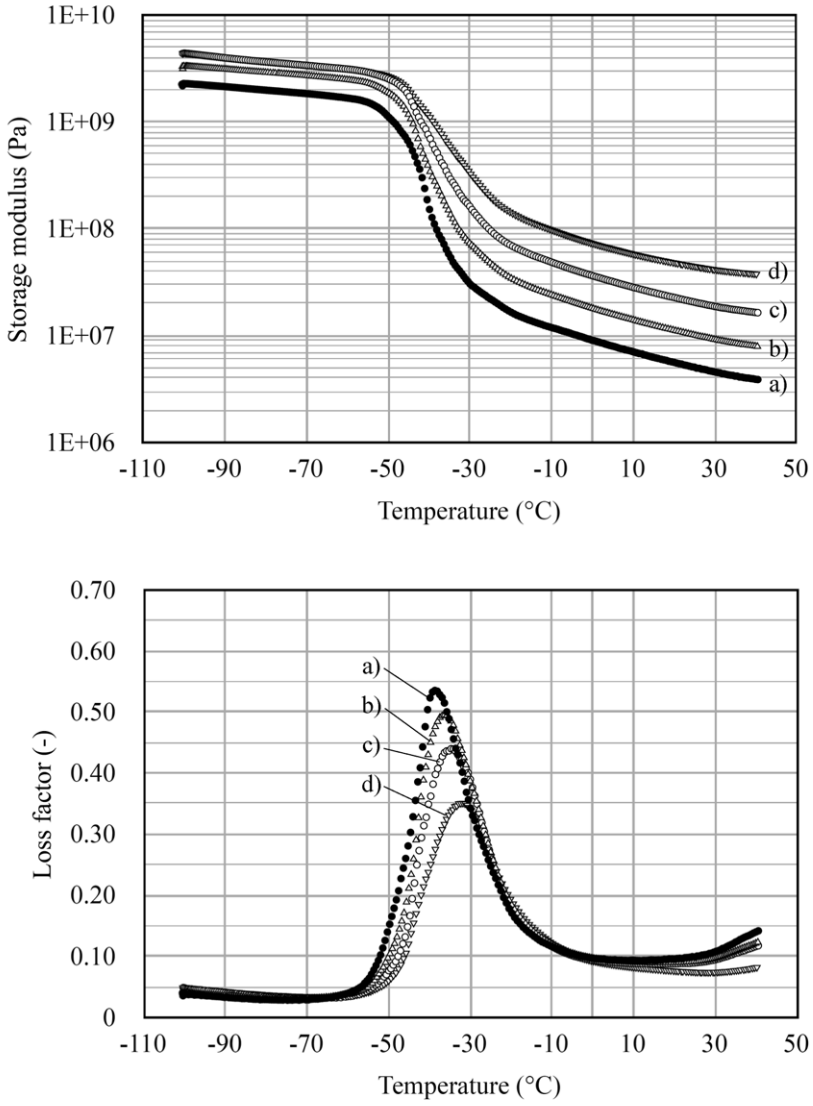

Figure 6.6 Dynamic–mechanical analysis of unvulcanized composites: storage modulus (E') and loss factor (tanδ) as a function of temperature for (a) EPDM_0, (b) EPDM_10, (c) EPDM_20, and (d) EPDM_30

Table 6.6 Dynamic-mechanical characterization of composites: storage modulus measured in the glassy region (at a temperature of -70 °C, E'_{-70C}) and in the rubbery region (at a temperature of 25 °C, E'_{25C}), damping (maximum value of tan δ, tan δ_{max}) and glass transition temperature (T_g) (the values after vulcanization are reported in bracket)

Material code	E'_{-70C} / GPa	E'_{25C} / MPa	tan δ_{max}	T_g / °C
EPDM_0	1.84 (1.46)	5.07 (3.07)	0.535 (0.610)	-38.7 (-34.1)
EPDM_10	2.70 (2.91)	10.13 (10.33)	0.495 (0.541)	-36.4 (-33.1)
EPDM_20	3.38 (2.53)	20.66 (11.86)	0.440 (0.474)	-34.7 (-31.8)
EPDM_30	3.40 (3.98)	44.49 (22.77)	0.351 (0.458)	-31.8 (-32.6)

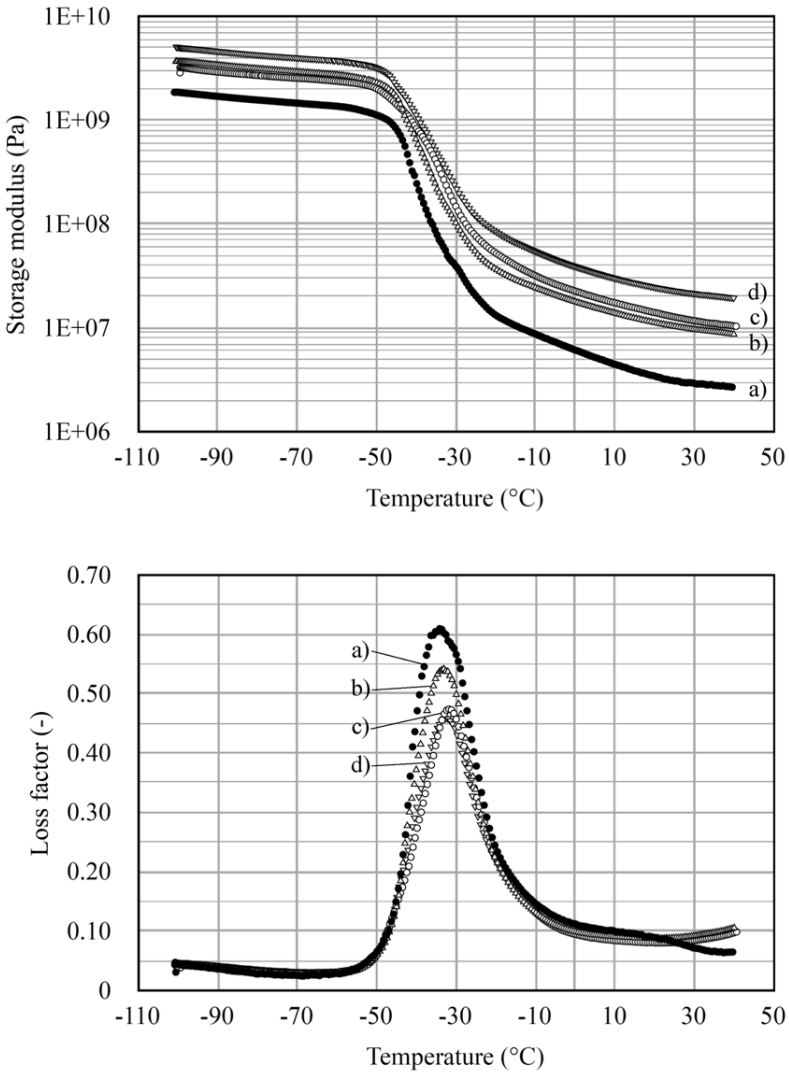

Figure 6.7 Dynamic–mechanical analysis of vulcanized composites: storage modulus (E') and loss factor (tanδ) as a function of temperature for (a) EPDM_0_V, (b) EPDM_10_V, (c)EPDM_20_V, and (d) EPDM_30_V

6.4 Conclusions

EPDM rubber reinforced with titania in situ generated by using a NHSG process was successfully prepared with a titania content ranging from 0 to 30 wt%. Anatase was the main crystalline phase of titania having nanometric sizes, but forming submicrometric and micrometric agglomerate particles in the composites. Thermogravimetric analysis showed that the introduction of titania caused a strong decrease in thermal stability of the polymer/titania composites compared with the pristine EPDM probably due to the activation of a metal-catalyzed oxidative decomposition mechanism.

Extraction and equilibrium swelling tests and mechanical characterization indicated an interfering effect of the sol-gel reaction of $TiCl_4$ to titania on the vulcanization process of the rubber. Quasi-static and dynamic-mechanical characterizations indicated that the presence of titania as rigid filler in both the unvulcanized and vulcanized EPDM matrix led to a significant increase in glass transition temperature, stiffness and of the ultimate properties such as stress at break, while elongation at break improved only up to a point (10 wt%), then diminished at higher titania concentrations. The experimental values of modulus were systematically higher than the values theoretically predicted by the classical Smallwood-Guth-Einstein equation and this enhanced stiffness was tentatively attributed to an additional contribution arising from the molecular interaction between the rubber and the filler due to its in situ generation.

6.5 References

1. C. Sanchez, P. Belleville, M. Popall, L. Nicole. Applications of advanced hybrid organic-inorganic nano-materials: from laboratory to market. Chemical Society Reviews 2011; 40:696-753.
   DOI: 10.1039/C0CS00136H
2. C. Sanchez, B. Julian, P. Belleville, M. Popall. General strategies for the design of functional hybrid materials. Journal of Materials Chemistry 2005; 15: 3559.
3. C.J. Brinker, G.W. Shrerer. Sol-Gel Science: The Physics and Chemistry of Sol-Gel Processing. New York: Academic Press (1990).
4. Bilecka, M. Niederberger. New developments in the non-aqueous and/or non-hydrolytic sol-gel synthesis of inorganic nanoparticles. Electrochimica Acta 2010; 55:7717-7725.

DOI: 10.1016/j.electacta.2009.12.066

5. J.N. Hay, H.M. Raval. Synthesis of organic-inorganic hybrids via the non-hydrolytic sol-gel process.Chemistry of Materials 2001; 13:3396‑3403.
   DOI:10.1021/cm011024n
6. M. Messori. In Situ Synthesis of Rubber Nanocomposites. In: Mittal V, Kim JK, and Pal K, editors. Recent Advances in Elastomeric Nanocomposites, vol. 9. Berlin Heidelberg: Springer, 2011.pp. 57.
7. A. Bhowmick, A. Bandyopadhyay. Rubber-Silica Hybrid Nanocomposites. Current Topics in Elastomers Research: CRC Press, 2008.
8. F. Bignotti, S. Borsacchi, R. de Santis, M. Geppi, M. Messori, U.P. Sudhakaran. Interrelation between preparation conditions, structure, and mechanical reinforcement in isoprene rubber filled with *in situ* generated silica. Journal of Applied Polymer Science 2012; 125:E398–E412.
   DOI: 10.1002/app.36337
9. M. Messori, F. Bignotti, R. De Santis, R. Taurino. Modification of isoprene rubber by in situ silica generation. Polymer International 2009: 58:880–887.
   DOI 10.1002/pi.2606
10 M. Messori, M. Fiorini. Isoprene rubber filled with silica generated *in situ.* Journal of Applied Polymer Science 2011; 119:3422-4328.
   DOI: 10.1002/app.32992
11. F. Bondioli, M.E. Darecchio, A.S. Luyt, M. Messori. Epoxy resin modified with *in situ* generated metal oxides by means of sol–gel process. Journal of Applied Polymer Science 2011; 122:1792–1799.
   DOI: 10.1002/app.34264
12. D. Morselli, F. Bondioli, A.S. Luyt, T.H. Mokhothu, M. Messori. Preparation and characterization of EPDM rubber modified with *in situ* generated silica. Journal of Applied Polymer Science 2013; 128:2525–2532.
   DOI: 10.1002/app.38566
13. A. Das, R. Jurk, K.W. Stockelhuber, G. Heinrich.Silica-ethylene propylene diene monomer rubber networking by in situ sol-gel method. Journal of Macromolecular Science, Part A: Pure and Applied Chemistry 2008; 45:101-106.
   DOI: 10.1080/10601320701683447

14. D. Morselli, F. Bondioli, M. Fiorini, M. Messori. Poly(methyl methacrylate)-TiO_2 nanocomposites obtained by non-hydrolytic sol– gel synthesis: the innovative tert–butyl alcohol route. Journal of Material Science, 2012; 47:7003-7012.
DOI: 10.1007/s10853-012-6651-4
15. D. Morselli, M. Messori, F. Bondioli. Poly(methyl methacrylate)-TiO_2 nanocomposite obtained by non-hydrolytic sol-gel synthesis. Journal of Materials Science 2011; 46:6609-6617.
DOI: 10.1007/s10853-011-5610-9
16. D. Morselli, F. Bondioli, M. Sangermano, M. Messori. Photo-cured epoxy networks reinforced with TiO_2 *in-situ* generated by means of non-hydrolytic sol-gel process. Polymer 2012; 53:283-290.
DOI:10.1016/j.polymer.2011.12.006
17. J.I. Langford, A.J.C. Wilson. Scherrer after sixty years: A survey and some new results in the determination of crystallite size. Journal of Applied Crystallography, 1978; 11:102-113.
DOI:10.1107/S0021889878012844
18. Y. Ikeda, Y. Kameda. Preparation of "Green" composites by the sol-gel process: *in situ* silica filled natural rubber. Journal of Sol-Gel Science and Technology 2004; 31:137-142.
DOI: 10.1023/B:JSST.0000047975.48812.1b
19. S. Haitao, C. Juqing, Z. Qiang, Z. Wei, H. Qihui, H. Baixing, S. Jian. Preparation and properties of EPDM/TiO_2 composites. Journal of Applied Polymer Science 2007; 106:314–319.
DOI: 10.1002/app.26614
20. C.-C. Wu, S.L.-C. Hsu. The Journal of Physical Chemistry C 2010; 114:2179.
21. G. Kraus. In: Kraus G, editor. Reinforcement of Elastomers. New York: Wiley (1965).
22. L.E Nielsen, R.F. Landel. Mechanical Properties of Polymers and Composites. Marcel Dekker, Inc.: New York (1994).
ISBN: 0 8247 8964 4

Chapter 7

CONCLUSIONS

The properties of rubber/inorganic oxide nanocomposites prepared by *in situ* hydrolytic and non-hydrolytic sol-gel routes were investigated. For the hydrolytic sol-gel (HSG) process, tetraethoxysilane (TEOS) was used as precursor in toluene in the absence and presence of bis-[-3-(triethoxysilyl)-propyl]-tetrasulfide (TESPT) as coupling agent. In the non-hydrolytic sol-gel (NHSG) synthesis the EPDM-silica composites were prepared with silicone tetrachloride ($SiCl_4$) as a precursor and tert-butanol as an oxygen donor. The effect of filler amount, in the range of 5-30 wt.%, was also investigated.

The results generally showed homogeneously dispersed silica and titania particles in the EPDM matrix, with the presence of agglomeration at high filler contents. The particle size distribution progressively increased with increasing filler content as a result of increased coalescence of the growing silica and titania particles when increasing the amount of the dispersed phase. It was observed that for the composites prepared according to the non-hydrolytic route, reduced particles size and agglomeration, better filler dispersion and improved interactions between the silica and titania particles and the rubber matrix were observed, which further improved for silica containing samples prepared in the presence of TESPT. The non-hydrolytic route was able to overcome the typical problems related to the hydrolytic route, in which the low miscibility of the sol-gel aqueous system limits the dispersion and distribution of the filler in the matrix.

The presence of silica and titania particles reduced the extent of crosslinking of the vulcanized EPDM for both the HSG and NHSG, and in the absence and presences of TESPT. Reasons offered for this observation were that (i) more DCP was utilised for the grafting of silanol or ethoxysilane groups onto the rubber chains so that less DCP was available to initiate crosslinking of the rubber chains, and (ii) for the composites prepared in the presence of TESPT according to the NHSG route the coupling agent settled on the interface between the silica particles and EPDM and did not form part of the network. This caused enough free volume between the chains to accommodate the toluene molecules during swelling, and resulted in an increase in the swelling ratio. Although the gel content decreased with longer

reaction times (HSG route), a more extensive crosslinked network was formed when grafted and/or unreacted fractions of TEOS reacted further to form more crosslinks between the rubber chains. In the case of the composites prepared in the presence of TESPT, the networks were still extensive enough to maintain a high gel content. This was due to the TEOS and TESPT reacting to form silica containing crosslinks between the rubber chains.

The introduction of the coupling agent in the HSG route improved the interaction of the silica particles with and dispersion in the EPDM matrix, which gave rise to an increased thermal stability of the EPDM compared to the composites prepared in the absence of a coupling agent. The reason for this observation was the improved interaction and good dispersion of the silica particles in the EPDM matrix in the presence of a coupling agent. This gave rise to reduced polymer chain mobility and retarded diffusion of the volatile products from the sample, which increased the temperature at which the EPDM showed a mass loss. The introduction of titania through the NHSG route caused a strong decrease in thermal stability of the composites compared with the neat EPDM due to a metal oxide-catalyzed decomposition mechanism. In the case of silica there was a mass loss step in the temperature range 100-400 °C, caused by the evaporation of t-butyl chloride and other acid chlorides present in the composites, as well as the evaporation of TESPT that settled on the interface between the silica particles and EPDM. This observation confirmed that TESPT did not take part in the sol-gel reaction according to the NHSG route.

Improved stress at break was observed as a result of improved EPDM, silica and titania interactions that led to better stress transfer. The longer crosslink chains formed in the presence of the coupling agent for the samples prepared according to the HSG route gave rise to larger elongation at break values, and the polysulfidic linkage from the TESPT caused a strong reinforcement between the rubber and the filler, which gave rise to the larger stress at break values. However, larger amounts of filler led to agglomeration of the filler particles, which resulted in a decrease in the stress and elongation at break, which was seen for all the samples prepared in the absence of TESPT. The composites prepared according to the NHSG route in the presence of TESPT showed a decrease in elongation at break because of the TESPT which did not form part of the network but settled on the interface between the silica particles and EPDM.

The Young's modulus predicted by the Smallwood-Guth-Einstein equation for silica filled composites prepared according to the HSG route at short reaction times, and for titania composites prepared according to NHSG route, showed significantly higher modulus values compared to the theoretical calculation based only on a hydrodynamic effect. The enhanced stiffness was attributed to (i) an additional contribution arising from the molecular interaction between the rubber and the filler due to its *in situ* generation, and (ii) to structural effects and the introduction of additional crosslinks into the network by the filler. For the other investigated samples the Young's modulus was modelled by the Nielsen equation, with changes in the parameters A and ϕ_m related to changes in filler particle size and dispersion. This analysis indicated smaller and better dispersed filler particles for the samples prepared according to the NSHG route in the presence of TESPT. There was a good correlation between the storage modulus and Young's modulus values, and the values increased significantly with increasing filler content for all the silica and titania composites. The increased stiffness and thermal stability were confirmed by the filler effectiveness factor values, while the damping reduction values confirmed that the EPDM interacted strongly with the well dispersed silica particles, indicating a mechanical stiffening effect as well as a thermal stability contribution by the filler.

It is clear from this research that the type and amount of filler, the method used for the *in situ* sol-gel preparation of the composites, the type of precursor used, and whether a coupling agent was used, to a large extent determines the thermal and mechanical properties of the EPDM nanocomposites. The way these variables are combined will also significantly influence these properties. Generally the NHSG route gave rise to smaller filler particles and improved dispersion, while the presence of coupling agent further improved the morphology for both routes. Whether these morphologies gave rise to improved thermal and mechanical properties also depended on other factors like the extent of crosslinking and whether the coupling agent took part in the sol-gel reaction.